UNIVERSITÉ PARIS 13 - SORBONNE PARIS CITÉ

THÈSE

pour obtenir le grade de

DOCTEUR DE L'UNIVERSITÉ PARIS 13

Discipline : **SIGNAUX ET IMAGES**

pésentée et soutenue publiquement

par

Cong Luong NGUYEN

le 28/05/2014

Titre :

Robust Time and Frequency Synchronization in 802.11a Communication Wireless System

Directeur de thèse : **M. Jean-Pierre ASTRUC**

Co-Directeurs de thèse : **Mme. Anissa MOKRAOUI**

M. Pierre DUHAMEL

JURY

M. Michel KIEFFER	*Prof. à l'Université Paris 11*	**Rappoteur**
M. Yannis POUSSET	*Prof. à l'Université de Poitiers*	**Rappoteur**
Mme. Anissa MOKRAOUI	*Prof. à l'Université Paris 13*	**Examinatrice**
M. Pierre DUHAMEL	*Directeur de recherches CNRS*	**Examinateur**
M. Nguyen-Linh TRUNG	*Prof. à l'Univ. Nat. du Vietnam*	**Examinateur**
M. Jean-Pierre ASTRUC	*Prof. à l'Université Paris 13*	**Examinateur**

Remerciements

Il me sera très difficile de remercier tout le monde car c'est grâce à l'aide de nombreuses personnes que j'ai pu mener cette thèse à son terme.

Je voudrais tout d'abord remercier profondément ma codirectrice de thèse, Mme. Anissa Mokraoui, qui a su se montrer disponible et compétente pour me permettre de mener à bien ces travaux, qui m'a encouragé, soutenu et qui a cru en moi. Sa rigueur et sa conscience professionnelle font d'elle un exemple à mes yeux, un exemple que je tacherai de suivre.

Un grand merci à mon codirecteur de thèse, M. Pierre Duhamel, qui m'a d'abord fait confiance et puis conseillé tout au long de ces années. J'ai pu bénéfcier de ses compétences techniques et théoriques, ainsi que de son aptitude à déceler les orientations susceptibles de mener à des résultats scientifiques intéressants.

Ensuite, un grand merci aussi à mon directeur de thèse M. Jean Pierre Astruc pour m'avoir permis de faire cette thèse et pour m'avoir conseillé pour les présentations.

Je tiens à exprimer ma profonde reconnaissance à M. Nguyen Linh Trung, qui m'a toujours encouragé et m'a aidé à développer des compétences et des méthodes de recherche afin d'obtenir la meilleure performance.

Je suis très honoré que M. Michel KIEFFER et M. Yannis POUSSET aient accepté de rapporter mon manuscrit. Je leur suis extrêmement reconnaissant pour leurs commentaires et remarques constructives qui m'ont permis d'améliorer mon rapport. C'est par erreur si j'oublie les personnels du laboratoire L2TI de l'institut Galilée. Je vous remercie de votre accueil et de votre humeur quotidienne. Avec vous, j'ai passé des moments bien agréables. Vous allez me manquer.

RÉSUMÉ

Le problème de la synchronisation en temps et en fréquence dans un système de transmission OFDM (Orthogonal Frequency Division Multiplexing) sans fil de type IEEE 802.11a est étudié. Afin d'améliorer la synchronisation de trame entre les stations mobiles, bien que des solutions aient déjà été proposées pour compenser les décalages en temps et en fréquence, nous avons développé une nouvelle approche conforme à la norme IEEE 802.11a. Cette approche exploite non seulement les informations habituellement spécifiées par la norme à savoir les séquences d'apprentissage mais également d'autres sources d'informations disponibles au niveau de la couche physique et par ailleurs connues par l'émetteur et le récepteur qui les exploitera. Tenant compte des informations fournies par les protocoles réseaux, nous avons montré que les différents sous-champs du champ SIGINAL de la trame physique, identifié comme séquence de référence, sont connus ou prédictibles à partir des deux trames de contrôle RtS (Request to Send) et CtS (Clear to Send) lorsque le mécanisme de réservation de support CSMA/CA (Transporteur Sense Multiple Access avec évitement de collision) est activé conjointement à des algorithmes d'adaptation de débit binaire sur le canal. De plus, la trame RtS reçue permet au récepteur d'estimer le canal avant d'entamer l'étape de synchronisation. Tenant compte de la connaissance sur le champ SIGNAL et de l'information sur le canal de transmission, nous avons développé plusieurs algorithmes conjoints de synchronisation temporelle et fréquentielle et d'estimation de canal compatible avec la norme 802.11a. Les résultats de simulation montrent une amélioration conséquente des performances en termes de probabilité d'échec de synchronisation en comparaison avec les algorithmes existants.

Mots clés- IEEE 802.11a, Communications, OFDM, CSMA/CA, RtS, CtS, Synchronisation temporelle, Synchronisation fréquentielle.

ABSTRACT

Time and frequency synchronization problem in the IEEE 802.11a OFDM (Orthogonal Frequency Division Multiplexing) wireless communication system is investigated. To enhance the frame synchronization between mobile stations, although solutions to compensate time and frequency offsets have already been proposed, we developed a new approach conform to the IEEE 802.11a standard. This approach exploits not only the reference information usually specified by the standard such as training sequences but also additional sources of information available at the physical layer further known by both the transmitter and receiver to be then exploited. According to the knowledge protocol, we showed that the parts of the identified SIGNAL field considered as a reference sequence of the physical frame are either known or predictable from the RtS (Request to Send) and CtS (Clear to Send) control frames when the CSMA/CA (Carrier Sense Multiple Access with Collision Avoidance) mechanism is triggered jointly to bit-rate adaptation algorithms to the channel. Moreover the received RtS control frame allows the receiver to estimate the channel before synchronization stage. According to the knowledge of the SIGNAL field and the channel information, we developed multistage joint time/frequency synchronization and channel estimation algorithms conform to the standard. Simulation results showed a strongly improved performance in terms of synchronization failure probability in comparison with the existing algorithms.

Index Terms- IEEE 802.11a, Communications, OFDM, CSMA/CA, RtS, CtS, Time Synchronization, Frequency Synchronization.

Contents

List of Figures

List of Tables

List of abbreviations

Symbol	Description
ACF	Auto-Correlation Function
AGC	Automation Gain Control
ARQ	Automatic Repeat-Request
AWGN	Additive White Gaussian Noise
BPSK	Binary Phase Shift Keying
BER	Bit Error Rate
CSMA/CA	Carrier Sense Multiple Access with Collision Avoidance
CCF	Cross-Correlation Function
CE	Channel Estimation
CEE	Channel Estimation Error
CFS	Coarse Frequency Synchronization
CFO	Carrier Frequency Offset
CIR	Channel Impulse Response
CP	Cyclic Prefix
CSP	Correlation Sequence of the Preamble
CtS	Clear To Send
CTS	Coarse Time Synchronization
DA	Data-Aided
DAB	Digital Audio Broadcasting
DAC	Digital-to-Analogue Converter
DFT	Discrete Fourrier Transform
DVB-T	Digital Video Broadcasting - Terrestrial
FDT	Frequency Division Multiplexing
FFT	Fast Fourrier Transform
FFS	Fine Frequency Synchronization
FFO	Fractional Frequency Offset
FTS	Fine Time Synchronization
GI	Guard Interval

Symbol	Description
ICI	Inter-Carrier Interference
IDFT	Inverse Discrete Fourrier Transform
IFFT	Inverse Fast Fourrier Transform
IFO	Integer Frequency Offset
ISI	Inter-Symbol Interference
JTS-CE	Joint Time Synchronization and Channel Estimation
LS	Least Square
LOS	Line Of Sight
LTF	Long Training Field
MAP	Maximum A Posteriori
MIMO	Multiple-Input Multiple-Output
MMSE	Minimum Mean-Square Error
ML	Maximum Likelihood
M-PSK	M-ary Phase Shift Keying
M-QAM	M-order Quadrature Amplitude Modulation
MSE	Mean-Square Error
NDA	Non-Data-Aided
OFDM	Orthogonal Frequency Division Multiplexing
PDP	Power Delay Profile
PDF	Probability Density Function
PSF	Probability of Synchronization Failure
PAPR	Peak-to-Average Power Ratio
RtS	Request to Send
SER	Symbol Error Rate
SISO	Soft-Input Soft-Output
SNR	Signal to Noise Ratio
STF	Short Training Field
STO	Symbol Timing Offset
WIFI	Wireless Fidelity
WIMAX	Worldwide Interoperability for Microwave Access
WLAN	Wireless Local Area Networks
WMAN	Wireless Metropolitan Area Networks

CHAPTER 1

Introduction

Contents

1.1 Introduction

In wireless digital communication systems, data physical packets are transmitted via a wireless channel from the transmitter to the receiver. At the reception station, the packet is detected and then demodulated. Many novel technologies have been investigated to support high rate applications such as multimedia services. GSM (Global System for Mobile communication), bluetooth, WLAN (Wireless Local Area Networks), WIFI (Wireless Fidelity) are some examples. In these systems, the spectrum efficiency is always important because the frequency resource is limited while high rate applications require a wide bandwidth. On the other hand, wireless channels are often frequency selective and Inter-Symbol Interference (ISI) which impair the received signal. To deal with this problem, full band channel equalization has been introduced. However, it is quite complex because the multipath spans many symbols, and Orthogonal Frequency Division Multiplexing (OFDM) was proposed as a promising technology for reducing the effects of multipath distortions. OFDM is a parallel data transmission technique. Specifically, the OFDM divides the wideband channel into many narrowband subchannels wherein each subchannel is considered as being flat fading. OFDM is thus a multicarrier technique.

Multicarrier techniques have been used for a long time. The Frequency Division Multiplexing (FDM), for example, use a lot of non-overlapping frequency sub-bands, each of which is used to carry a separate signal. An optimal version of multicarrier transmission is OFDM technique. In OFDM, the subcarriers overlap each other in frequency domain and this reduces the bandwidth requirement compared with the FDM technique. Nevertheless, to get such advantage, orthogonality between the subcarriers is required. It means that a lot of sinusoidal generators and demodulators with the high precision is required and this is very difficult when the number of subcarriers increases. In order to avoid using the banks of subcarrier oscillators, a Discrete Fourier Transform (DFT) and Inverse Discrete Fourier Transform (IDFT) [25] were proposed as an efficient implementation strategy for OFDM. By using a set of related sinusoidal and cosinusoidal functions that contain frequencies that are integer multiple of the basic frequency, the DFT is to generate the orthogonal subcarriers for the OFDM signal. In addition, to compute the same result but more quickly, the Fast Fourier Transform (FFT)/Inverse Fast Fourier Transform (IFFT) algorithm have been applied [24].

Thanks to its high spectral efficiency, the OFDM satisfies the growing demand for higher data rates and therefore has been widely used in many wired and wireless

communication applications as well as standards [79], [89]. Some wired systems are listed as Asymmetric Digital Subscriber Lines (ADSL), Very-High-speed Digital Subscriber Lines (VHDSL) [34] that is capable to support applications such as high-definition television over a single flat untwisted of twisted pair of copper wires, Digital Video Broadcasting - Cable (DVB-C, a European standard) for broadcast transmission of digital television via cable. And some examples of wireless systems such as Wireless LAN (WLAN) with the standards IEEE 802.11a, g [2], n [3] and HIPERLAN/2 [28], Wireless Metropolitan Area Networks (WMANs) IEEE 802.16 [1], the terrestrial digital TV DVB-T [73], the terrestrial mobile TV systems DVB-H [50], 3GPP-LTE [12], [56] and 4G-LTE-Advanced [31].

Although the OFDM technique has been exploited in a wide range of high data rate communication systems, it has two main disadvantages. The first problem concerns the Peak-to-Average Power Ratio (PAPR) or crest factor that is higher than that of full band techniques employing traditional modulations (M-PSK, M-QAM...). This results in a system that either transmits less bits per second with the same hardware or transmits the same bits per second with higher-power hardware. Especially, it becomes a very big problem if the crest factor reduction techniques (CFR) are not used [15]. This problem has been mentioned and solved in the literature.

1.2 Scope of the thesis

This thesis focuses on the other disadvantage, namely that OFDM systems are very sensitive to synchronization errors at the receiver. The errors are known as Carrier Frequency Offset (CFO) and Symbol Timing Offset (STO). Both errors introduce Inter-Carrier Interference (ICI) [36], [82], [86] and Inter-Symbol Interference (ISI) [21] that destroy the orthogonality of the adjacent subcarriers and degrade the performance of the OFDM receiver [9], [88], [45], [39].

In order to combat ICI and ISI, several synchronization algorithms have been developed in the literature. Synchronization schemes can be classified in two groups: Non-Data-Aided (NDA) and Data-Aided (DA) [35]. For the NDA techniques which are also denoted as blind techniques, no training sequences is required to be sent to the receiver. The receiver thus exploits some statistical information to estimate the synchronization parameters. NDA techniques save bandwidth and power but they usually have high computational complexity and slower convergence rate. In addition, a common problem for most NDA approaches is that they are not robust to multipath distortion which makes them a difficult choice for transmission in

multipath fading channels. On the contrary, for the DA techniques, it is required to insert known data sequences such as repeated OFDM symbols, pilots...The receiver exploits the known sequence for its synchronization process. These techniques allow an easy implementation in the receiver via such functions as auto-correlation, cross-correlation.... However, because part of the packet is reserved for carrying the known sequence, some power and bandwidth are used for synchronization purposes.

To enhance the consistency for the systems, some IEEE wireless standards such as 802.11a/g/n have been developed. They have been widely applied in the wireless communication systems. The preamble used to perform the DA synchronization facilitates the receivers task. Moreover, the accuracy of the synchronization algorithms based on the standard is much higher than that of the NDA techniques. The exploitation of the preamble for synchronization has been studied in the literature and the corresponding performance has been analyzed. This thesis investigates time and frequency synchronization algorithms in the IEEE 802.11a standard wireless communication system based mainly on the Carrier Sense Multiple Access with Collision Avoidance (CSMA/CA) mechanism.

1.3 Organization of the thesis

This thesis provides new time and frequency synchronization algorithms in SISO wireless communication systems. The outline of the thesis is summarized in Figure 1.1 and briefly described below.

Chapter 2 introduces the wireless communication system model using OFDM technique. Tapped delay lines are used to represent the wireless channels. The physical data packet is generated according to the IEEE 802.11a standard. The mathematical equations are also used to present the various steps of the packet modulation/demodulation.

Chapter 3 expresses mathematically the effects of synchronization errors as STO and CFO on the performance of the system. We then classify and review conventional synchronization methodologies in OFDM systems. Simulation results are also given in this section to evaluate the algorithms.

Chapter 4 investigates novel time synchronization algorithms. In addition to the training sequence specified by the standard, we propose to exploit the SIGNAL field of the physical frame for the time synchronization process with the support of CSMA/CA mechanism. Next, we take into account channel information to improve the performance of the proposed algorithms. Based on the relationship between the time offset and the accuracy of channel estimation, we develop both a joint

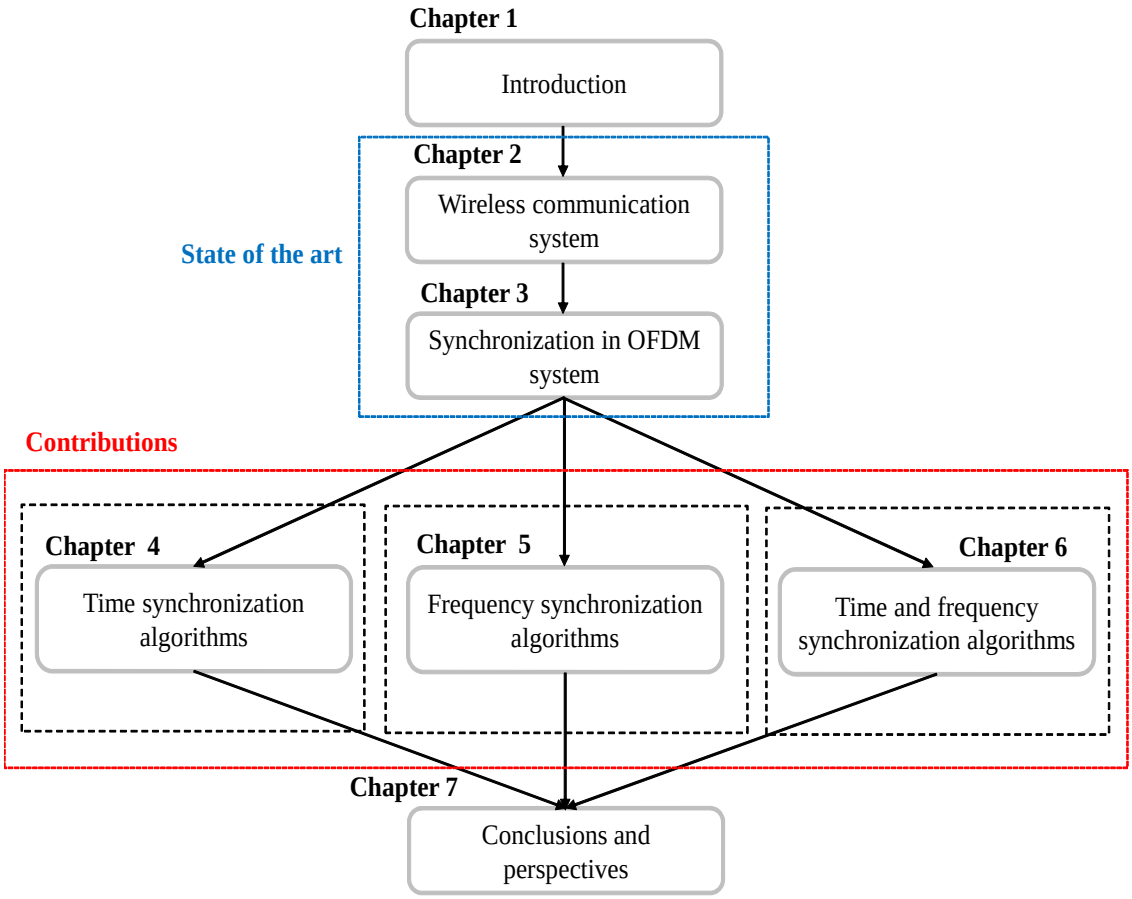

Figure 1.1. Thesis outline.

fine time synchronization and a channel estimation algorithm. We suggest a new metric taking into account all channel estimations errors. Performance analysis and simulation results of the various algorithms are then presented and discussed.

Chapter 5 introduces synchronization algorithms for CFO estimation. Similar to the algorithms mentioned in Chapter 4, we employ the information of the SIGNAL and channel via the RtS (Request to Send) control frame to improve the accuracy of frequency synchronization.

Chapter 6 presents the combination of timing and frequency estimations. The hybrid scheme is introduced to provide a complete synchronization process. The appropriate combination of algorithms of time and frequency synchronizations proposed in chapters 4 and 5 is generated to achieve the best performance.

Chapter 7 concludes this thesis by summarizing the original contributions. It reviews the algorithms that we proposed and their important role in solving the synchronization problems for OFDM based-systems. We finally discuss future works.

1.4 Contributions of the thesis

The purpose of this thesis is to investigate totally robust symbol timing and frequency synchronization schemes for the IEEE 802.11a wireless communication system by providing accurate estimation parameters over frequency selective fading channels while respecting the specifications of the standard.

It is well known that a synchronization process is required as a first stage of the receiver in order to enable correct demodulation of a data packet. Playing a very important role in OFDM systems, the synchronization topic has been addressed in many papers. Many synchronization algorithms have been studied with the purpose to give the best solutions for the packet detection as well as frequency offset determination. These proposals were adapted to either a common system or the standards

In this thesis, we consider time and frequency synchronization problems in the IEEE 802.11a wireless communication systems based on OFDM. Our work is divided in three parts (see Figure 1.1, Contribution). The common feature of the proposed algorithms is to make use of information brought by upper layers of the protocol stack.

In the first part, four robust time synchronization algorithms are proposed. The first algorithm exploits the SIGNAL field specified by the IEEE 802.11a standard when the CSMA/CA (Carrier Sense Multiple Access with Collision Avoidance) mechanism is triggered (Section 1.5, reference [1]). The SIGNAL field can be used at the receiver since its parts (its subfields) are known or predictable via the frame controls of the CSMA/CA mechanism. To enhance the time synchronization, in the second part, the proposed algorithm performs joint time synchronization and channel estimation based on Maximum *a Posteriori* (MAP) criterion (Section 1.5, reference [2]). This algorithm is based on the fact that there is a relationship between the time offset and a channel estimation process and that the MAP algorithm is considered as a good estimation. In both algorithms above, in the coarse time synchronization stage, we use a cross-correlation function between the received signal and the training sequence. Due to the multipath fading channel, the correlation between two identical sequences is reduced, this makes us to think of getting the channel information before of the synchronization process. From the observation that in the CSMA/CA mechanism, the control frame RtS is sent before the DATA frame, we take advantage the channel estimation from the RtS frame reception as an additional information to improve the performance of the synchronization pro-

cess of the DATA frame. This is also the idea of the third algorithm (Section 1.5, reference [4]). Additionally, for the fourth algorithm, we build a new metric for the time synchronization by taking average of the error transmission function employing the integral function over all channel estimation errors (Section 1.5, reference [3]). The proposed techniques have shown superior performance compared with other well-established algorithms in the literature.

In the second part, we address frequency synchronization problem to estimate the CFO. Relying on the CSMA/CA mechanism, we suggest two strategies taking account the SIGNAL field and channel estimation. Furthermore, the MAP technique is also applied to obtain the smallest mean squared error.

In the last part, we investigate efficient symbol timing and frequency offset recovery algorithms in the IEEE 802.11a standard based system by combining the approaches developed in the two previous parts. First, the SIGNAL field and channel information are used to reduce the deviation between the true symbol timing and its estimation of the coarse time synchronization stage. Then, along with the preamble specified by the standard, the additional information is exploited for a joint MAP fine time, frequency synchronization and channel estimation (Section 1.5, reference [5]). Furthermore, to achieve the highest remaining time offset estimate, we implement the last stage by applying the timing metric in presence of all channel estimation errors (Section 1.5, references [6] and [7]).

1.5 Publications

[1] **C. L. Nguyen**, A. Mokraoui, P. Duhamel, and N. Linh-Trung, "Time Synchronization Algorithm in IEEE802.11a Communication System", *EUSIPCO 2012*, pp. 1628-1632, Aug. 2012.

[2] **C. L. Nguyen**, A. Mokraoui, P. Duhamel, and N. Linh-Trung, "Enhanced Time Synchronization for IEEE802.11a System Using SIGNAL Field And MAP Channel Estimation", *IEEE ATC 2012*, pp. 46-49, Oct. 2012.

[3] **C. L. Nguyen**, A. Mokraoui , P. Duhamel, N. Linh-Trung, Improved Time Synchronization in Presence of Imperfect Channel State Information, *IEEE ICASSP 2013*, May 26-31, 2013 Vancouver, Canada.

[4] **C. L. Nguyen**, Mokraoui A, Duhamel P., N. Linh-Trung, Algorithme conjoint de synchronisation temporelle et d'estimation de canal compatible avec la norme

IEEE 802.11a, *GRETSI 2013*, vol. p.1-5.

[5] **C. L. Nguyen**, Mokraoui A, Duhamel P., N. Linh-Trung, Improved Time and Frequency Synchronization Algorithm for IEEE 802.11a Wireless Standard Based on SIGNAL field, *REV Journal on Electronics and Comm.*, vol. 3, pp. 40-49, January-June 2013.

[6] **C. L. Nguyen**, A. Mokraoui , P. Duhamel, N. Linh-Trung, A Joint MAP Time and Frequency Synchronization in Presence of Imperfect Channel State Information, *IEEE ICASSP 2014*, May 4-9, 2014, Florence, Italy.

[7] **C. L. Nguyen**, Mokraoui A, Duhamel P., N. Linh-Trung, Novel joint MAP Time, Frequency Synchronization and Channel Estimation for IEEE 802.11a standard based-system, Preparing for Submission in *EURASIP Journal on Wireless Communications and Networking*.

CHAPTER 2

Wireless communication system

Contents

This chapter describes the structure of the IEEE 802.11a standard physical packet, the system model recommended by the standard as well as the wireless channel model.

We first introduce the fields of the IEEE 802.11a physical packet and explain to which functions these fields are associated. The modulation and demodulation structure for the packet are shown via block diagram as well as the corresponding mathematical expressions which will allow to analyze the problem in the rest of the thesis.

In addition, we introduce the wireless channel models. It is well known that when a packet is transmitted via a wireless channel, it is not only carried by one path but also by multipaths. Each path is characterized by two main parameters, namely the delay time and gain power. The number of paths of the channel in theory is infinite but in practice, it is considered as a channel of finite length. More precisely, the multipath wireless channel is usually modeled by a tapped delay line.

On the whole, there are two common types of channel models in wireless communication corresponding to indoor and outdoor scenarios. To evaluate our algorithms in both scenarios, we select two channel models that have been recommended in the literature.

2.1 System model

This section introduces the structure of the physical packet and the system model recommended by the IEEE 802.11a standard.

2.1.1 IEEE 802.11a physical packet structure

Figure 2.2 shows the structure of the IEEE 802.11a physical packet containing the PREAMBLE training field, SIGNAL field (header field) and DATA field [2].

The PREAMBLE field is composed of the Short Training Field (STF) and Long Training Field (LTF):

(i) The STF consists of ten short repetitions, each of length 16 samples ($\sim 0.8\mu s$). They are used for Automation Gain Control (AGC) convergence, diversity selection, signal detection and Coarse Frequency Synchronization (CFS).

(ii) The LTF contains two long repetitions, each one composed of 64 samples of length ($\sim 3.2\mu s$), reserved for channel estimation and fine frequency synchronization. Note that the two LTF repetitions are preceded by a Guard Interval 2 (GI2) that has the double length of the GI of the SIGNAL and DATA symbols. This ensures the LTF repetitions to be subject to ISI even in a deep fading environment.

The PREAMBLE field is followed by the SIGNAL field which is illustrated in Figure 2.1. The four bits from 0 to 3 are dedicated to encode the RATE field which conveyes information about the transmission rate in Mbits/s and the type of modulation while bits 5-16 encode the LENGTH field used to provide information about the length in octets of the DATA field. The fourth bit is reserved for future, the seventeenth bit is even parity check and the last 6 bits are added as tail bits. The physical modulated SIGNAL field is represented by one OFDM symbol of 80

Figure 2.1. SIGNAL field

samples in which 16 samples are reserved for GI and 64 samples for the useful part. The DATA field carries the payload and can be represented by many OFDM symbols. The maximum length of the DATA field is fixed to 4096 octets.

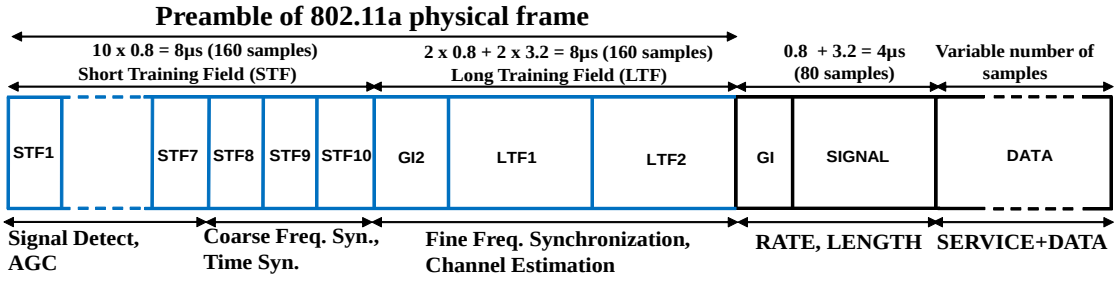

Figure 2.2. Structure of the IEEE 802.11a physical packet

2.1.2 IEEE 802.11a wireless communication system

The physical packet modulation recommended by the IEEE 802.11a standard is summarized in Figure 2.3 which consists of three parts: transmitter, channel and receiver.

At the transmitter, before being fed to an IFFT transform, the symbols in frequency domain of the fields (PREAMBLE, SIGNAL and DATA) must be generated. For the PREAMBLE field, the symbols of the STF and LTF are taken from the IEEE 802.11a standard. Specifically, the STF symbols contain 12 subcarriers distributed as follows [2]:

$$\begin{aligned} X_{STF} = &\sqrt{13/6} \times \{0,0,1+j,0,0,0,-1-j,0,0,0,1+j,0,0,0,-1-j, \\ &0,0,0,-1-j,0,0,0,1+j,0,0,0,0,0,0,0,-1-j,0,0,0,-1-j,0,0,0, \\ &1+j,0,0,0,1+j,0,0,0,1+j,0,0,0,1+j,0,0\}, \end{aligned}$$

the factor $\sqrt{13/6}$ is used to normalize the average power of the resulting OFDM symbol, which employs 12 out of 52 subcarriers. The LTF symbols consist of 53 subcarriers (including a zero value at DC), as follows [2]:

$$X_{LTF} = \{1, 1, -1, -1, 1, 1, -1, 1, -1, 1, 1, 1, 1, 1, 1, -1, -1, 1, 1, -1, 1, -1, 1, 1, 1, 1, 0, 1, \\ -1, -1, 1, 1, -1, 1, -1, 1, -1, -1, -1, -1, -1, 1, 1, -1, -1, 1, -1, 1, -1, 1, 1, 1, \\ 1\}.$$

For the SIGNAL field, based on the information from the DATA field, 24 bits are generated as shown on Figure 2.1. The SIGNAL bits stream is used as an input of the convolutional encoder (with constraint length $K = 7$, polynomial generator $[171, 133]$, and code rate $R = 1/2$). Its outputs are then interleaved (by a known interleaver) and then BPSK (Binary Phase Shift Keying) modulated to get the SIGNAL symbols X_{SIGNAL}. This is followed by pilots insertion. Note that the contents of the SIGNAL field are not scrambled.

Similar to the SIGNAL field modulation, however, the DATA field bits are scrambled before the convolutional encoder. Furthermore, the variable code rates (with $R = 1/2,\ 2/3$ or $3/4$) and various modulations (as M-PSK or M-QAM) are available depending on the desired data rate and channel quality.

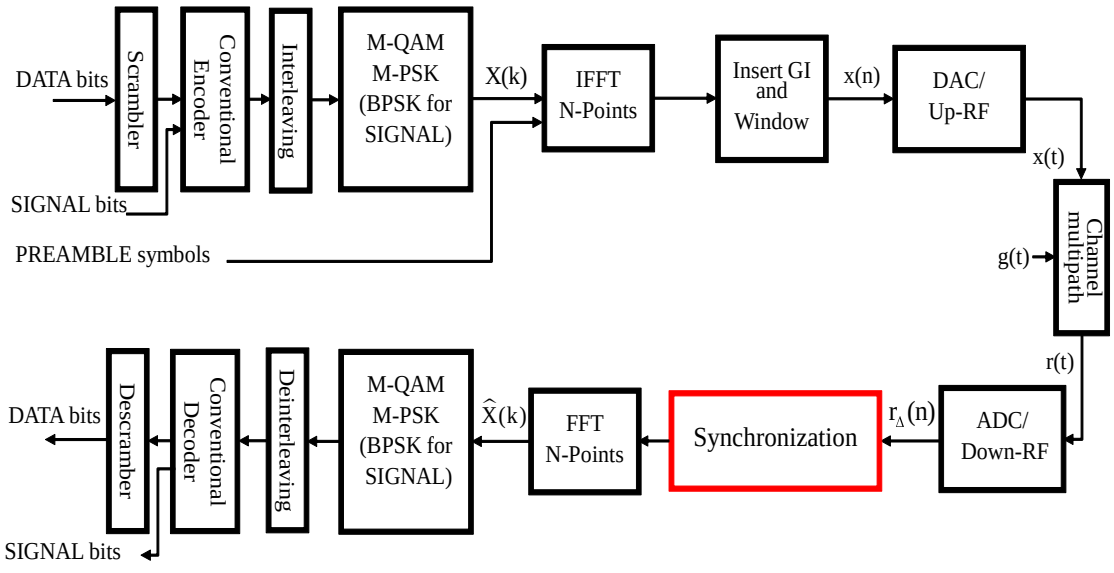

Figure 2.3. Wireless communication system using OFDM

Let $X(k)$, $k = 0 : N - 1$, be the symbol in the frequency domain. Here $X(k)$ denotes the STF, LTF, SIGNAL or DATA field symbols. The symbols are first fed

into the N points IFFT. The output of the IFFT of length N is given by

$$x(n) = \frac{1}{N} \sum_{k=0}^{N-1} X(k) e^{j2\pi k \frac{n}{N}}, \tag{2.1}$$

where $x(n)$ is the time-domain sample at the output of the IFFT transform, N is the number of the FFT/IFFT points and k is the subcarrier index. The sample is then multiplied by a windowing function in discrete-time domain to shape one OFDM symbol, this function in discrete domain is expressed by

$$W_{N_W}(n) = \begin{cases} 1 \text{ if } 0 \leq n \leq N_W \\ 0.5 \text{ if } n = 0, N_W \\ 0 \text{ otherwise,} \end{cases} \tag{2.2}$$

where N_W is the window length, depending on the field it is applied to. For example, if the field is the STF or the LTF $N_W = 160$ while $N_W = 80$ for the SIGNAL or DATA field [2].

After passing by a digital to analog converter, the signal in analog domain, $x(t)$ is expressed by [2]

$$x(t) = W_{T_W}(t) \frac{1}{N} \sum_{k=0}^{N-1} X(k) e^{j2\pi k \Delta f t}, \tag{2.3}$$

where Δf is the subcarrier spacing. Let B be the total passband bandwidth, then $\Delta f = B/N$, $W_{T_W}(t)$ is the analog form of $W_{N_W}(n)$ given by [2]

$$W_{T_W}(t) = \begin{cases} \sin^2(\frac{\pi}{2}(0.5 + \frac{t}{T_{TR}})) & \texttt{if } -\frac{T_{TR}}{2} < t < \frac{T_{TR}}{2} \\ 1 \quad \texttt{if } \frac{T_{TR}}{2} < t < T - \frac{T_{TR}}{2} \\ \sin^2(\frac{\pi}{2}(0.5 - \frac{t-T}{T_{TR}})) & \texttt{if } T - \frac{T_{TR}}{2} < t < T + \frac{T_{TR}}{2} \end{cases}, \tag{2.4}$$

where T_{TR} is the transition time between two OFDM symbols, T is the duration of the OFDM symbol and T_W corresponds to N_W.

Before being transmitted, the signal $x(t)$ is modulated with a carrier frequency f_c as follows:

$$x(t) e^{j2\pi f_c t}. \tag{2.5}$$

This signal is transmitted via the multipath channel which will be described in more detail in the next section. At the receiver, the signal is then brought back to the baseband by multiplying with $e^{-j2\pi f_c t}$. The basedband signal is expressed by [71]

$$r(t) = \sum_{i=0}^{L-1} h(\tau_i) x(t - \tau_i - \tau) e^{j2\pi \Delta F_c (t-\tau)} + g(t), \tag{2.6}$$

where $h(\tau_i)$ is the coefficient of path i; τ_i is the delay of path i; τ is the unknown symbol timing; L is the number of paths. In theory, L can be infinite, but it is actually represented by a certain number that depends on the type of channel model; $g(t)$ is the complex AWGN; ΔF_c is the Carrier Frequency Offset (CFO) which is the carrier frequency difference between the transmitter and receiver caused by the tolerance on the oscillator frequencies.

The baseband signal $r(t)$ is then converted into discrete-time domain with a sampling time T_s as follows (note that $\tau_i = i\frac{1}{B} = iT_s$):

$$\begin{aligned} r(nT_s) &= r(t) \sum_{n=-\infty}^{\infty} \delta(t - nT_s) \\ &= \{\sum_{i=0}^{L-1} h(\tau_i)x(t - \tau_i - \tau)e^{j2\pi\Delta F_c(t-\tau)} + g(t)\} \sum_{n=-\infty}^{\infty} \delta(t - nT_s) \\ &= \sum_{i=0}^{L-1} h(\tau_i)x(t - \tau_i - \tau)e^{j2\pi\Delta F_c(t-\tau)} \sum_{n=-\infty}^{\infty} \delta(t - nT_s) + g(t) \sum_{n=-\infty}^{\infty} \delta(t - nT_s) \\ r(nT_s) &= \sum_{i=0}^{L-1} h(iT_s)x(nT_s - iT_s - \theta T_s)e^{j2\pi\Delta F_c(nT_s-\theta T_s)} + g(nT_s). \end{aligned} \tag{2.7}$$

The index T_s can be removed in the terms $r(.), h(.), x(.), g(.)$ and by replacing $T_s = \frac{T}{N}$ into $e^{j2\pi\Delta F_c(nT_s-\theta T_s)}$. Therefore the expression of $r(nT_s)$ becomes

$$r(n) = \sum_{i=0}^{L-1} h(i)x(n - i - \theta)e^{j\frac{2\pi\epsilon(n-\theta)}{N}} + g(n), \tag{2.8}$$

where $\epsilon = \Delta F_c T_s$ is the normalized CFO while θ is the normalized symbol timing. The parameters ϵ and θ have to be estimated so that the packet is recovered correctly at the receiver. $h(i)$ denotes the slowly time-varying discrete complex Channel Impulse Response (CIR) with $\sum_{i=0}^{L-1} E\{|h(i)|^2\} = 1$ (E is the expectation operator).

2.2 Channel model

In this section, we introduce the wireless communication channels. Two channel models corresponding to the indoor and outdoor typical environments are selected. Let us first briefly introduce the multipath fading.

2.2.1 Multipath fading

A fading channel is a communication channel comprising fading caused by the multipath propagation or by shadowing from obstacles affecting the signal propagation. Due to the presence of the multipath propagation, the receiver gets multiple copies

of the transmitted signal, each one following a different path. It means that the signal at the receiver is a summation of multiple signals with differences in gain, delay and phase shift. These parameters can be variable in time, however, in this thesis, they are considered as changing slowly in time. In general, it can be classified into two types of model that correspond to the outdoor and indoor environments. In the indoor environments, the distance to the obstacles is usually shorter than that in outdoor environments and correspondingly the channel spread that is the time interval between the first and last delay of path is smaller. Depending on the phase shift, the received signal can be either boosted or attenuated.

The effect of multipath fading channel can be modeled by a tapped delay as shown in Figure 2.4 [76], where $\tilde{x}(t)$ is the received signal at the output of the

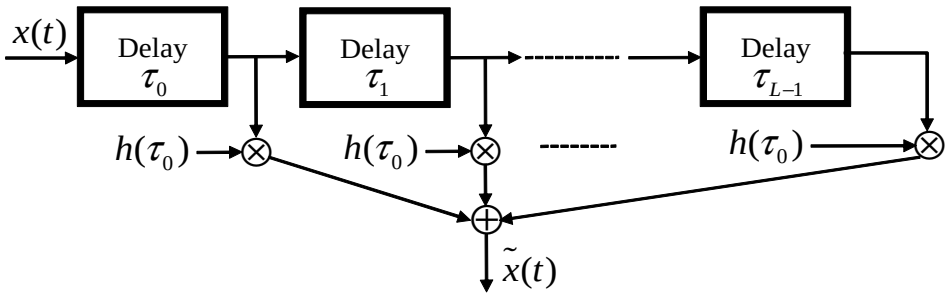

Figure 2.4. Multipath channel model

multipath channel model, without the CFO, symbol timing as well as noise, $\tilde{x}(t)$ is expressed as

$$\tilde{x}(t) = \sum_{i=0}^{L-1} h(\tau_i)x(t - \tau_i). \tag{2.9}$$

As mentioned above, the parameter $h(\tau_i)$ can be variable in time and thus we should write $h(\tau_i, t)$, therefore implying that the value of this parameter is time varying. Nevertheless, here we consider a slow fading, therefore, the time parameter can be omitted for simplicity. The terms slow and fast fading are used to imply the rate at which the channel coefficient (i.e. $h(\tau_i)$) changes. To consider if a channel is slow fading or fast fading, one bases on the coherence time. The coherence time, is inversely proportional to the maximum Doppler frequency as follows [100]:

$$T_c = \frac{1}{D_s}, \tag{2.10}$$

where T_c is the coherence time, D_s is the Doppler spread (Doppler shift) given by the difference between the maximum and minimum Doppler frequency.

A channel is considered as slow fading when the coherence time of the channel is large relative to the variation of the channel. In this case, the amplitude, phase

change imposed by the channel can be considered constant over the period of use. In contrast, fast fading occurs when the coherence time of the channel is small relative to the variation of the channel. In this case, the amplitude and phase change imposed by the channel varies considerably over the period of use. For rigorous treatment on channel modeling, the reader can be referred to [72], [40].

2.2.2 Wireless channel models

This section mentions briefly two wireless channel models denoted as COST-207 RA [65] and BRAN A [30].

In 1984, the European working group COST-207 was created. The group developed channel models suitable for the outdoor propagation environments. The typical environments are classified into areas: RA (Rural Area), TU (Typical Urban, areas typical for cities and suburbs), BU (Bad Urban, built urband areas with bad propagation conditions) and HT (Hilly Terrain). Later, the group COST-207 developed specifications known as COST86 and COS89 [65]. In this thesis, we consider the model COST-207 RA as being the channel model characterizing the outdoor environment. The Power Delay Profile (PDP) that contains the necessary parameters of the COST-207 RA model is listed in Table 2.1.

Table 2.1. PDP of the COST-207 RA model with LOS and average delay spread $0.1\mu s$

Path order	Propagation delay (τ_i) (ns)	Path power (dB)	Doppler spectral density
0	0	0	"Rice"
1	200	-2	"Jakes"
2	400	-10	"Jakes"
3	600	-20	"Jakes"

As can be seen from the table, this model has 4 paths. Each path is characterized by a relative delay (with respect to the first path delay), a relative power, and a Doppler spectrum type. There are some possible Doppler categories as CLASS, RICE, GAUS1, and GAUS2. The CLASS category refers to the "classical" spectrum, which is also often denoted as the Jakes spectrum. The RICE Doppler spectrum is equivalent to the CLASS Doppler spectrum, but with an impulse at the frequency corresponding to the Doppler shift of the Line-of-Sight (LOS) component. The GAUS1 and GAUS2 Doppler categories are the sum of two Gaussian functions in frequency.

Another model that is commonly used in the indoor scenarios is BRAN. It can be BRAN A, B, C, D or E. Model A corresponds to a typical office environment while B is for an office environment with large delay spread. Model D corresponds to the LOS conditions in a large open space indoor or an outdoor environment.

Models C and E are dedicated to the typical large open space indoor and outdoor environments with large delay spread.

In this thesis, the models COST-207 RA and BRAN A are selected. Similar to COST-207 RA, the BRAN A is also characterized by its PDP listed in Table. 2.2.

Table 2.2. PDP of the BRAN A model with NLOS and average delay spread $50ns$

Path order	Propagation delay (τ_i) (ns)	Path power (dB)	Doppler spectral density
0	0	0	"Class"
1	10	-0.9	"Class"
2	20	-1.7	"Class"
3	30	-2.6	"Class"
4	40	-3.5	"Class"
5	50	-4.3	"Class"
6	60	-5.2	"Jakes"
7	70	-6.1	"Class"
8	80	-6.9	"Class"
9	90	-7.8	"Class"
10	110	-4.7	"Class"
11	140	-7.3	"Class"
12	170	-9.9	"Class"
13	200	-12.5	"Class"
14	240	-13.7	"Class"
15	290	-18	"Class"
16	340	-22.4	"Class"
17	390	-26.7	"Class"

2.3 Conclusion

In this chapter, we described the IEEE 802.11a physical packet structure, OFDM-based wireless communication system and channel model. The IEEE 802.11a physical packet contains three fields, the function of each field were explained clearly. The modulation and demodulation of the packet at the transmitter and receiver was also shown via both block and mathematical models. Finally, two wireless channel models COST-207 and BRAN A for the outdoor and indoor environment respectively presented by their PDP.

CHAPTER 3

Synchronization in OFDM system

Contents

3.1 Introduction

As discussed in Chapter 1, in the OFDM system, the data is carried via parallel transmissions on orthogonal subcarriers in order to decrease the distortion caused by the frequency-selective channel caused by the ISI in the multipath channel environment. However, this equivalent parallel transmission is based on the orthogonality of the subcarriers and, in presence of Symbol Time Offset (STO) and Carrier Frequency Offset (CFO), this orthogonality disappears. In fact, ISI and ICI appear when the received signal is transformed in the frequency domain [38], [64] and as a result, this does not allow orthogonality between subcarriers, and the performance of the system is degraded [69], [19], [86], [46]. To estimate and compensate STO and CFO, some synchronization process is always required at the receiver. In practical wireless communication systems, it is usually difficult to define exactly the STO value due to the multipath channel, noise and CFO. Although, by using Cyclic Prefix (CP) that is placed at the beginning of every OFDM symbol, the system actually allows to be insensitive to small values of STO, the allowed range depends on the relative values of the channel delay spread and the CP length [63].

Depending on the target of the synchronization (STO, CFO estimation or both of them), we classify the algorithms into time, frequency or time and frequency synchronization algorithms respectively. For each category, we further categorize them into time and frequency domain ones.

In this chapter, we study the effect of the STO and CFO that closely follows the explanations in [22] and review some synchronization algorithms to estimate them.

3.2 Time synchronization techniques in OFDM system

The main purpose of time synchronization process is to determine the starting point of the OFDM symbol (i.e. symbol timing θ). The difference between the true symbol timing and its estimation creates the STO. In the ideal case, the STO value is zero and this allows to extract exactly the set of useful samples (the actual DATA symbols) used to calculate the FFT transform. In the opposite, depending on the value of the estimated symbol timing, the effect of the STO on the performance is different and analyzed in the next section.

3.2.1 Effect of STO

Let δ be the normalized time offset that remains after synchronization (which is not always performed perfectly at the receiver). To study the effects of the STO, the terms of channel, frequency offset and noise in equation (2.8) are ignored. The

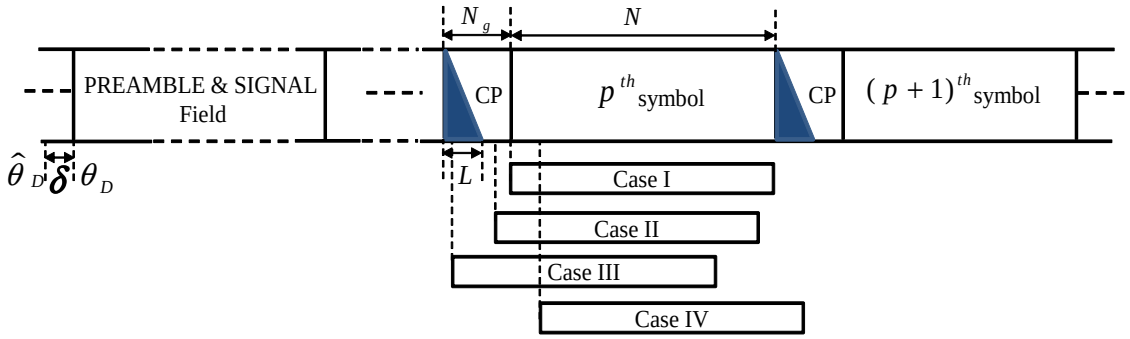

Figure 3.1. Possible cases of estimated starting positions corresponding to the STO

received baseband signal in presence of STO reads

$$r(n) = x(n + \delta), \tag{3.1}$$

where $x(n)$ and $r(n)$ are respectively the transmitted and received signals corresponding to the p^{th} considered symbol as shown in Figure 3.1, $\delta = \theta_D - \hat{\theta}_D$ with $\hat{\theta}_D$ being the estimated starting position of the OFDM symbol and θ_D being the true one that implies the starting point of the actual OFDM symbol (without the CP). The index D denotes the data OFDM symbols. Note that in equation (3.1), we assume that $\delta = \theta_D - \hat{\theta}_D$ takes a positive value, which simplifies the analysis.

Table 3.1 presents the effect of the STO on the received signal in time and frequency domain. According to the FFT/IFFT transform property, the STO included in the time-domain signal causes a phase offset $2\pi k\delta/N$ in frequency domain. Depending on the estimated symbol timing (i.e. $\hat{\theta}_D$), the effect of the STO (i.e. δ) is different. There are four possible cases as shown in Figure 3.1. Theses cases are: exact (ideal) symbol timing (Case I); a little earlier symbol timing (Case II); too early symbol timing (Case III); and a little later compared to the exact symbol timing (i.e. θ_D) (Case IV).

Table 3.1. The effect of Symbol Time Offset (STO)

	Received signal	STO
Time domain	$r(n)$	$x(n+\delta)$
Frequency domain	$R(k)$	$e^{j2\pi k\delta/N}X(k)$

i) **Case I**: This case occurs when the estimated position of OFDM symbol corresponds to the true position (i.e. $\theta_D = \hat{\theta}_D$). In this case, the orthogonality among subcarriers is maintained and the OFDM symbol can be correctly recovered without any interference.

ii) **Case II**: This case is the situation where the estimated starting point of OFDM symbol is earlier than the true position (i.e. $\theta_D > \hat{\theta}_D$ or $\delta > 0$) but the difference does not reach a very large value. More specifically, the ISI introduced by the previous symbol $(p-1)^{th}$ does not interfere with the current one p^{th}. The effect of the STO is studied via taking the FFT of the current received OFDM signal as follows:

$$\begin{aligned} R_p(k) &= \frac{1}{N}\sum_{n=0}^{N-1} x_p(n+\delta)e^{-j2\pi nk/N} \\ &= \frac{1}{N}\sum_{n=0}^{N-1}\{\sum_{l=0}^{N-1} X_p(l)e^{j2\pi(n+\delta)l/N}\}e^{-j2\pi nk/N} \\ &= \frac{1}{N}\sum_{l=0}^{N-1} X_p(l)e^{j2\pi\delta l/N}\sum_{n=0}^{N-1} e^{j2\pi(l-k)kn/N}. \end{aligned} \tag{3.2}$$

At the receiver, assuming that l is chosen to be equal to k, then

$$R_p(k) = X_p(k)e^{j2\pi\delta k/N}, \tag{3.3}$$

Equation (3.3) expresses that in this case, the recovered symbol is with the transmitted symbols but its phase is rotated by an amount of $2\pi\delta k/N$. To estimate this phase, in the IEEE 802.11a standard, for each OFDM symbol, four symbol pilots are inserted at positions $k = -21, -7, 7$ and 21. It means that $X_p(-21), X_p(-7), X_p(7)$ and $X_p(21)$ are known at the receiver. Based on these pilots, the estimation of δ can be realized as follows:

$$R_p(21) \times R_p^*(7) = \{X_p(21)e^{-j2\pi\delta 21/N}\} \times \{X_p^*(7)e^{j2\pi\delta 7/N}\} \tag{3.4}$$

and δ is calculated by

$$\hat{\delta} = -\frac{N}{2\pi \times 14}(\varphi_{R_p^{(21,7)}} - \varphi_{X_p^{(21,7)}}), \tag{3.5}$$

where $\varphi_{R_p^{(21,7)}} = \arg\{R_p(21)\} - \arg\{R_p(7)\}$ and $\varphi_{X_p^{(21,7)}} = \arg\{X_p(21)\} - \arg\{X_p(7)\}$, with $\arg\{\}$ being angle operator. By this way, we can consider this case (i.e. little earlier) as correct synchronization one.

iii) **Case III**: This case is similar to Case II but the beginning point of the OFDM symbol belongs to the ISI area. Therefore, the orthogonality between subcarriers is reduced by the ISI.

iv) **Case IV**: This case corresponds to the estimated beginning point of the OFDM symbol after the true point (i.e. $\theta_D < \hat{\theta}_D$ or $\delta > 0$). Therefore, the FFT

transform window consists of a part of the current OFDM symbol and a part of the next one $(p+1)^{th}$ (i.e. the cyclic prefix of the next symbol) as follows:

$$r_p(n) = \begin{cases} x_p(n+\delta) \ \texttt{if} \ 0 \leq n \leq N-1-\delta \\ x_{p+1}(n+\delta-N_g) \ \texttt{if} \ N-\delta \leq n \leq N-1, \end{cases} \tag{3.6}$$

where x_{p+1} is the transmitted sample of the next OFDM symbol and N_g is the CP length. Taking the FFT of $r_p(n)$ as follows:

$$\begin{aligned} R_p(k) &= \frac{1}{N}\sum_{n=0}^{N-1-\delta} x_p(n+\delta)e^{-j2\pi nk/N} + \frac{1}{N}\sum_{n=N-\delta}^{N-1} x_{p+1}(n+\delta-N_g)e^{-j2\pi nk/N} \\ &= \frac{1}{N}\sum_{n=0}^{N-1-\delta}\{\sum_{l=0}^{N-1} X_p(l)e^{j2\pi(n+\delta)l/N}\}e^{-j2\pi nk/N} + \\ &+ \frac{1}{N}\sum_{n=N-\delta}^{N-1}\{\sum_{l=0}^{N-1} X_{p+1}(l)e^{j2\pi(n+\delta-N_g)l/N}\}e^{-j2\pi nk/N} \\ R_p(k) &= \frac{N-\delta}{N}X_p(k)e^{j2\pi\delta k/N} + \underbrace{\frac{1}{N}\sum_{l=0,l\neq k}^{N-1} X_p(l)e^{j2\pi\delta l/N}\sum_{n=0}^{N-1-\delta} e^{j2\pi(l-k)n/N}}_{\text{ICI}} + \\ &+ \underbrace{\frac{1}{N}\sum_{l=0}^{N-1} X_{p+1}(l)e^{j2\pi(\delta-N_g)l/N}\sum_{n=N-\delta}^{N-1} e^{j2\pi(l-k)n/N}}_{\text{ISI}}. \end{aligned} \tag{3.7}$$

It can be seen from equation (3.7) that its second term consists of the ICI element from the others subcarriers at indexes different from k of the current symbol while the third term of (3.7) is identified as the ISI caused by the next symbol. The interference power of these two elements (i.e. ISI and ICI) degrades seriously the system performance [62].

3.2.2 Time synchronization techniques

This section reviews time synchronization techniques developed in literature. We classify them into time-and frequency-domain synchronization algorithms.

3.2.2.1 Time-domain time synchronization algorithms

Two type of time synchronization algorithms can be considered: Non-Data Aided (NDA) (i.e. blind techniques) and Data Aided (DA). For the first one, the CP of an OFDM symbol is usually exploited while the latter one uses training sequences (either proposed by authors or recommended by standards as described in Subsection

(b)) sent along with the packet. In what follows, the performance will be evaluated in terms of percentage of time the exact synchronization has been obtained, even if we shall see later that this criterion is too strict when dealing with practical situations.

(a) Time synchronization using NDA based on Cyclic Prefix

To achieve a high spectral efficiency, blind synchronization algorithms exploit the CP without requiring the use of training sequences. Recall that a CP is a copy of the data part of the OFDM symbol and placed before the OFDM symbol. Each OFDM symbol is preceded by a CP to reduce the ISI effect in multipath channel environment. The basic idea of the time synchronization algorithms exploiting the CP is based on the correlation property between the CP and its copy in the OFDM symbol.

Indeed, at the receiver, one uses two sliding windows each has the CP length and spaced by actual OFDM symbol length. The general idea is to find the maximum similarity between two blocks and thus determine the beginning point of the OFDM symbol.

Specifically, in [90] the beginning point can be found by searching the index at which the difference between the two sliding windows is minimum as follows:

$$\widehat{\theta} = \arg\min_{\theta}\{\sum_{n=0}^{N_g-1} |r(n+\theta) - r(n+\theta+N)|\}, \tag{3.8}$$

where N_g is the CP length, $r(n)$ denotes the received signal and N is the length of an OFDM symbol (without the CP part).

For this algorithm, when the CFO exists, the similarity between the received signals corresponding to the two blocks is reduced and thus the estimate accuracy can be degraded.

Another technique to deal with CFO is to minimize the squared difference between the first block and the conjugate of the second one [85] given by

$$\widehat{\theta} = \arg\min_{\theta}\{\sum_{n=0}^{N_g-1} (|r(n+\theta)| - |r(n+\theta+N)|)^2\}. \tag{3.9}$$

Usually, the Auto-Correlation Function (ACF) is used for measuring the similarity of those two blocks. The start point is then defined via maximizing the ACF as follows [22]:

$$\widehat{\theta} = \arg\max_{\theta}\{|\sum_{n=0}^{N_g-1} r(n+\theta)r^*(n+\theta+N)|\}. \tag{3.10}$$

To evaluate the performance of time synchronization algorithms exploiting the CP mentioned as in [85] and [22], we provide some numerical results given by Figure 3.2. The curves illustrate the Probability of Synchronization Failure (PSF) versus Signal Noise Ratio (SNR) with no time deviation between the estimated symbol timing with respect to its true time position, i.e. $\hat{\theta} = \theta$. For convenience to compare with the rest of this thesis, the simulation parameters are selected as specified by the IEEE 802.11a standard and listed in Table 3.2 where the OFDM symbol duration $T = N \times T_s = 3.2\mu s$ and the length of the CP (GI) is 16. The normalized frequency offset ϵ is set to zero while the symbol timing θ is selected as a uniformly distributed random variable. Simulations are performed in presence of multipath channel COST207-RA following the Rice model with a LOS (see Chapter 2) and Gaussian noise.

Table 3.2. Simulation parameters

Parameters	*Values*
Bandwidth (B)	20 MHz
Sampling time (T_s)	50 ns
Number of subcarriers (N_c)	52
Length of CP (N_g)	16
Number of points FFT/IFFT (N)	64
Subcarrier spacing (ΔF)	0.3125 MHz
Data rate	6 Mbps

It can be observed from the figure that the PSF of these algorithms is still quite high even for realistic SNR (the operating region of WiFi, depicted in the figure) or for high SNR. This is related to Figure 3.3 showing magnitude of metrics (3.9) and (3.10) at $SNR = 15$dB when for example, the true timing symbol selected randomly is $\theta = 20$. It exists a flat interval next to the true timing symbol (here 20). This results in an excess of false detection and thus in high PSF.

Based on the CP, the Maximum Likelihood (ML) algorithm can be derived to estimate both the symbol timing and frequency offset, as proposed in [92]. First the log-likelihood function of the time and frequency offsets is given by

$$\ell(\theta, \epsilon|\mathbf{r}) = \log\{p(\mathbf{r}|\theta, \epsilon)\}, \tag{3.11}$$

where $\ell(\theta, \epsilon|\mathbf{r})$ is the log-likelihood function and $p(\mathbf{r}|\theta, \epsilon)$ is the Probability Density Function (PDF) of the observed signal vector $\mathbf{r}$ given the parameters θ, ϵ with ϵ being the normalized CFO and θ being the symbol timing. The estimate of θ is given by the index at which the function obtains maximum, shown as

$$\widehat{\theta} = \arg\max_{\theta}\{|\gamma(\theta)| - \rho\Phi(\theta)\}, \tag{3.12}$$

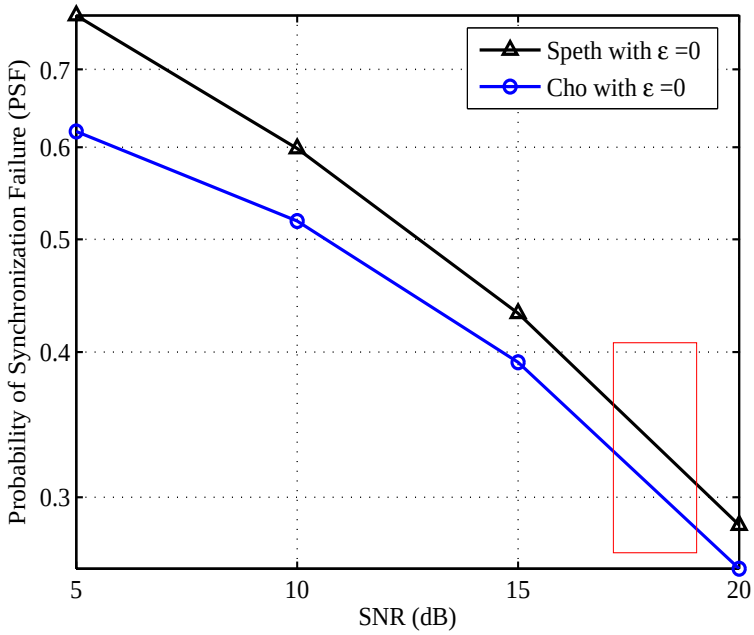

Figure 3.2. PSF of algorithms [85] (Speth), [22] (Cho) with no time deviation (the rectangular box is considered as the operating mode of the standard)

where

$$\gamma(\theta) = \sum_{n=0}^{N_g-1} r(n+\theta) r^*(n+\theta+N),$$

$$\Phi(\theta) = \frac{1}{2} \sum_{n=0}^{N_g-1} \{|r(n+\theta)|^2 + |r(n+\theta+N)|^2\}$$

and $\rho = \frac{\sigma_s^2}{\sigma_s^2+\sigma_g^2}$ with σ_s^2, σ_g^2 are variances of signal and noise, respectively.

In [92], the synchronization algorithm works directly on the complex received samples and it is quite hard to compute. In [91], the authors still use the ML function based on the CP of OFDM symbol, however the received samples are quantized into new ones according to the relationship $c(n) = \text{sign}(\Re\{r(n)\}) + j\text{sign}(\Im\{r(n)\})$, where $r(n)$ is the received signal and the operator "sign" is defined as follows:

$$\text{sign}(x) = \begin{cases} +1 \ \texttt{if} \ x \geq 0 \\ -1 \ \texttt{if} \ x < 0. \end{cases} \tag{3.13}$$

This means that the new complex samples actually consist of the real and imagine parts equal to ± 1. Despite such quantization, the new complex samples still contain information about the symbol timing while the computation becomes simpler because of the limitation of received values.

(b) Time synchronization using DA based on training sequence

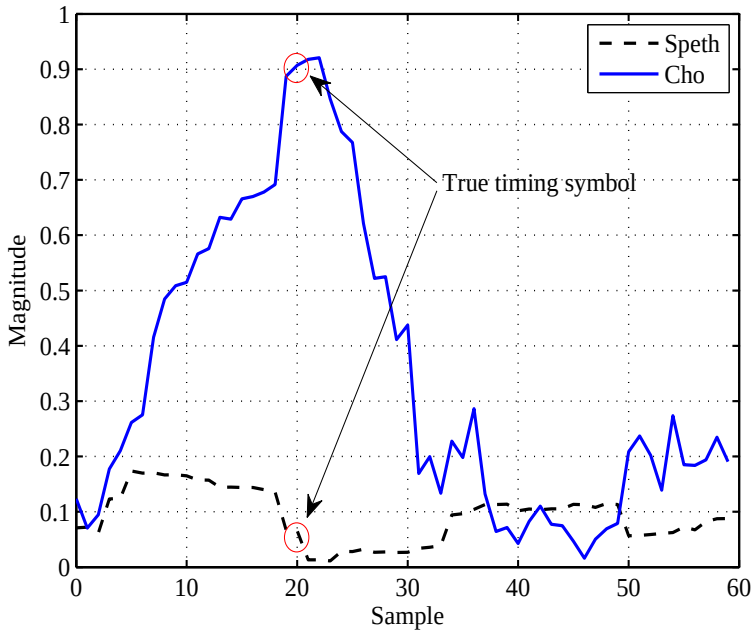

Figure 3.3. Magnitude of metrics (3.9) and (3.10) at $SNR = 15$dB when $\theta = 20$

Training symbols can be transmitted along with data symbols for the time synchronization at the receiver. This process thus requires more bandwidth in order to send the training sequence. However, compared with the CP-based algorithms, these algorithms are more accurate because they are based on the exact knowledge of what has been sent, instead of relying on some property enforced at the transmitter, but observed at reception, after the signals have been impaired by the channel.

In [80] and [81], the training sequence is composed of a CP (or GI) and two OFDM symbols as shown in Figure 3.4. The time synchronization algorithms using

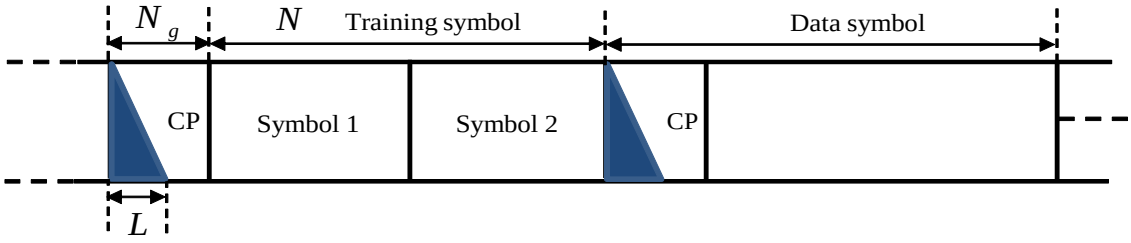

Figure 3.4. Training sequence of two repetitions

the CP can be also applied in this case. For example, the symbol timing can be estimated by minimizing the squared difference between two OFDM symbols [80] or by maximizing the ACF [81] that takes the advantage of well performing

synchronization without being effected by CFO. However, with these algorithms, it still exists a flat interval with the length of CP and this makes the receiver difficult to determine the symbol timing. This problem can be solved by taking the average of ACF values over the length of the CP [58] as follows:

$$\widehat{\theta} = \arg\max_{\theta} \Big(\frac{1}{N_g} \sum_{m=0}^{N_g-1} \Big| \sum_{n=0}^{N/2-1} r(n+m+\theta) r^*(n+m+\theta+N/2) \Big|^2 \Big), \tag{3.14}$$

where $N/2$ is the period of the training sequence.

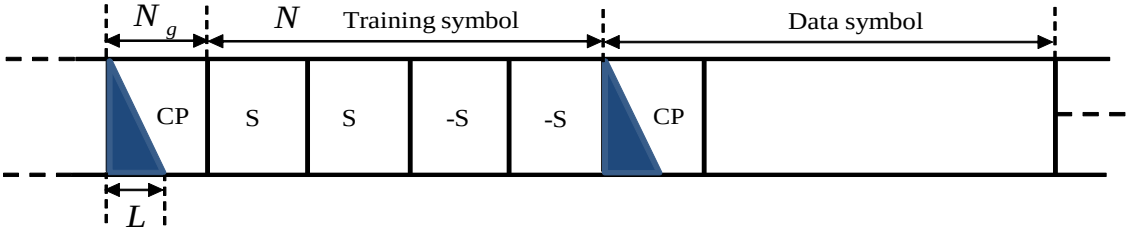

Figure 3.5. Training sequence with four repetitions

Based on two-symbols training sequence and the ML criterion, the authors of [27] and [20] proposed to use a timing metric given by

$$M(\theta) = \frac{E(\theta) - 2|P(\theta)|}{N}, \tag{3.15}$$

where

$$E(\theta) = \sum_{n=0}^{N-1} (|r(n+\theta)|^2 + |r(n+\theta+N)|^2) \tag{3.16}$$

and

$$P(\theta) = \sum_{n=0}^{N-1} (r(n+\theta) r^*(n+\theta+N). \tag{3.17}$$

The estimation of time shift is then given by

$$\hat{\theta} = \arg\min_{\theta} M(\theta). \tag{3.18}$$

It is observed from equation (3.15) that in the noiseless case, $M(\theta)$ becomes a minimum value when θ is at the correct timing symbol and a higher value when θ does not corresponds to the correct position. However, in presence of noise or in deep fading, false detection may occur since $E(\theta)$ gives also some values close to the minimum value. This can be reduced by using the timing metric mentioned in [59] as follows:

$$\hat{\theta} = \arg\max_{\theta} M_{minn}(\theta), \tag{3.19}$$

with

$$M_{minn}(\theta) = \frac{2|P(\theta)|}{E(\theta)}, \tag{3.20}$$

where $P(\theta)$ and $E(\theta)$ are given by equations (3.17) and (3.16), respectively. The notation *minn* only implies the name of the author proposing this metric.

Indeed, under a noiseless condition, $M_{minn}(\theta)$ will give a maximum value of one when θ is at the correct symbol timing and approximately a minimum value of zero for incorrect symbol timing. For a noise case, the metric would be approximately equal to zero. Consequently, the false detection can be avoided. The square form is also considered in practice i.e. $M^2_{minn}(\theta)$.

The timing metric of equation (3.20) is introduced in the context of two identical parts. It can be further built for a training symbol containing L_{minn} identical parts of M samples each. In this case, the timing metric to be maximized is expressed as follows [59]:

$$M_{minn}(\theta) = \Big(\frac{L_{minn}}{L_{minn}-1}\frac{|P(\theta)|}{E(\theta)}\Big)^2, \tag{3.21}$$

where

$$P(\theta) = \sum_{m=0}^{L_{minn}-2}\sum_{n=0}^{M-1} r(n+mM+\theta)r^*(n+\theta+(m+1)M) \tag{3.22}$$

and

$$E(\theta) = \sum_{i=0}^{M-1}\sum_{n=0}^{L_{minn}-1} (|r(i+\theta+nM)|^2), \tag{3.23}$$

where M is the number of samples of an identical part.

To reduce the training symbols, authors in [70] proposed to use only one symbol which is copied from the first symbol of the data symbols. The symbol timing estimate is then achieved via minimizing the ML function i.e. the last deployment of which is given by

$$M(\theta) = \sum_{n=0}^{N-1}\Big[|r(n+\Delta\theta)|^2+|r(n+\Delta\theta+N)|^2-2|r^*(n+\Delta\theta)r(n+\Delta\theta+N)|\Big], \tag{3.24}$$

where N is the length of the training symbol.

In comparison to the algorithms using the ACF and ML criterion, the Cross-Correlation Function (CCF) between the training symbol and the received signal can be considered if the training sequence is known at the receiver. In [26], the author proposed a training sequence composed of two repetitions. The CCF between the received signal and the known sequence is performed as follows:

$$Q_\theta = \mathbf{g}^H\mathbf{r}, \tag{3.25}$$

where $\mathbf{g}$ is one of two repetitions and $\mathbf{r}$ is the received signal vector. As a result of the CCF for this proposal, there are two peaks (at the beginning positions of the first repeated sequence and the second one). The beginning of frame is defined by the first index that satisfies:

$$|Q_\theta|^2 - \beta|\mathbf{g}|^2|\mathbf{r}|^2 > 0, \tag{3.26}$$

where β is a threshold which, in this reference, is suggested as 0.8. Indeed, when the frame does not arrive, the value of $|Q_\theta|$ is small and the subtraction is negative. In the opposite case, the subtraction becomes positive.

Likewise, however, in [43] the authors use the CCF between the received signal and special preamble sequence (which is called in the paper the "Correlation Sequence of the Preamble (CSP)"). This preamble sequence is built from the whole products available from given preamble for its correlation. Specifically, for a given preamble vector $\mathbf{C} = [C(0), C(1), ..., C(N-1)]$, with N being the length of the given preamble. Then the CSP is generated by the Hadamard product as follows:

$$\mathbf{B} = \mathbf{C}^* \circ \mathbf{C}_{\Xi_z}, \tag{3.27}$$

where $\circ$ is the Hadamard product that performs element by element multiplication of the two vectors, $\mathbf{C}^*$ is the conjugation of $\mathbf{C}$ and $\mathbf{C}_{\Xi_z}$ is obtained using circular shift of the vector $\mathbf{C}$ by an amount z as follows:

$$\mathbf{C}_{\Xi_z} = [C(z), C(z+1), ..., C(N-1), C(0), ..., C(z-1)]. \tag{3.28}$$

Note that z is known at both transmitter and receiver. From (3.27), we get the CSP given by

$$\begin{aligned}\mathbf{B} =&[C^*(0)C(z), C^*(1)C(z+1), ..., C^*(N-1-z)C(N-1), C^*(N-z)C(0)\\ &, ..., C^*(N-1)C(z-1)].\end{aligned} \tag{3.29}$$

From (3.29), if changing z, we will get a new CSP sequence. It means that for a given preamble we can obtain many different CSP sequences. Therefore the timing estimator can use one of these CSP preambles to perform time synchronization. In equation (3.29), the vector $\mathbf{C}_{\Xi_z}$ is changeable while $\mathbf{C}$ is fixed, to increase the available products, in [4] and [5], the vector $\mathbf{C}$ is adjustable as $\mathbf{C}_{\Xi_z}$.

On the whole, the performance of the CCF is better than the ACF if the CFO is small. However, in the presence of large CFO, its performance is degraded. Mathematical comparison between them is provided in Appendix A of this thesis.

(c) Time synchronization using DA based on IEEE 802.11a preamble structure

The IEEE standards has chosen appropriate synchronization algorithms that allow the receiver to perform better time synchronization than the above mentioned algorithms, by an appropriate definition of training sequences as preamble. In this section, we describe the algorithms exploiting the preamble. Recall that the IEEE 802.11a standard preamble contains ten Short Training Field (STF) repetitions, each one of length 16 samples and two Long Training Field (LTF) repetitions of 64 samples each. A Guard Interval 2 (GI2) of 32 samples is inserted between the STF and the LTF fields.

Based on the structure of IEEE 802.11a physical packet, the proposed time synchronization algorithm in [16] proceeds in two main steps: the Coarse Time Synchronization (CTS) step followed by the Fine Time Synchronization (FTS) step to estimate the remaining time offset. The CTS uses the ACF relying on 160 samples of the STF as specified by the standard as follows:

$$\overline{R}(\theta) = |R(\theta)|/P(\theta), \tag{3.30}$$

where

$$R(\theta) = \sum_{n=0}^{143} r^*(n+\theta)r(n+\theta+16)$$

and

$$P(\theta) = \sum_{n=0}^{143} |r(n+\theta)|^2.$$

The estimation of the beginning of physical frame is determined by

$$\hat{\theta} = \arg\max_{\theta}\{\overline{R}(\theta)\}. \tag{3.31}$$

The fine estimation is then carried out using the CCF between the received signal and a part of the LTF (32 out of 128 samples) of the standard as follows:

$$\Delta\hat{\theta}_f = \arg\max_{\Delta\theta\in\Lambda}\{|C(\Delta\theta)|^2\}, \tag{3.32}$$

where $\Delta\theta$ is the remaining time offset, Λ is the set of possible offset values and $C(\Delta\theta) = \sum_{n=0}^{31} g^*_{LTF}(n)r(n+\Delta\theta)$ with $g_{LTF}(n)$ being the known first 32 samples of the LTF field.

Note that in this reference, to reduce the effect of the CFO on the performance of the FTS stage using the CCF, the CFO of the received signal after the CTS stage is compensated based on the ACF that will be described in detail in the next

section. This algorithm is considered as one of the most common algorithm using the recommendation of the IEEE 802.11a standard. We provide the simulation results illustrated in Figure 3.6 under COST207-RA channel model. It is easy to see that compared with the algorithms mentioned in [85], [22], the performance of [16] is improved significantly.

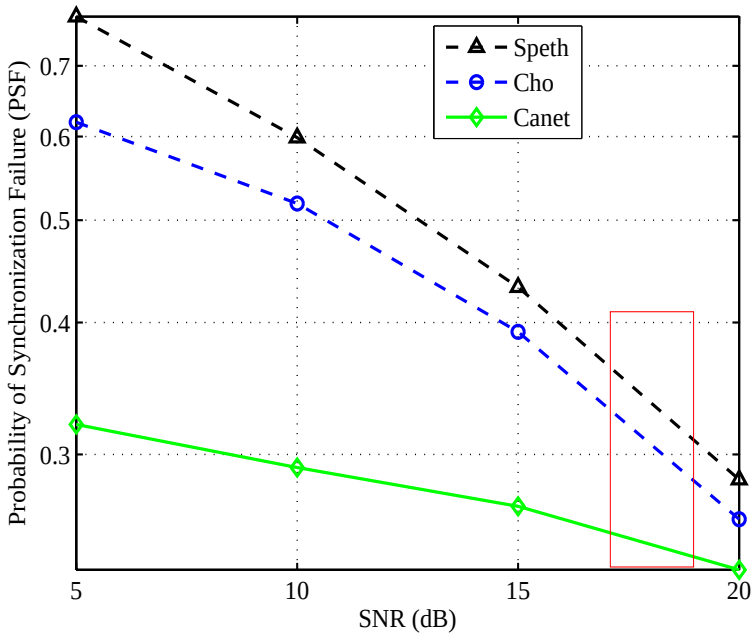

Figure 3.6. PSF of algorithms [85] (Speth), [22] (Cho), [16] (Canet) with no time deviation and $\epsilon = 0$ under COST207-RA model (the rectangular box represents the operating area of the IEEE 802.11a standard)

In the same manner, the authors of [57] proposed an approach where the symbol timing is the index maximizing

$$R(\theta) = \sum_{n=0}^{L_C-1} r^*(n+\theta)r(n+\theta+16),$$

where L_C should be $16 \times i$ with i being an integer from 0 to 9. After the CFO of the received signal is compensated using the ACF (will be described in detail in the next section), the remaining STO denoted by $\Delta\theta$, is estimated according to the maximum absolute value of the following function:

$$Z(\Delta\theta) = \sum_{n=0}^{31} r^*(n+\Delta\theta)r(n+\Delta\theta+N),$$

where $r(n)$ is the received signal with the remaining STO $\Delta\theta$ and N is the length of one LTF repetition.

A time synchronization algorithm using two stages for the IEEE 802.11a standard is also found in [17]. However, in this reference, before implementing the algorithm, the signal detection estimation, denoted as $\hat{\theta}_{SS}$, has been assumed to be performed and to belong to the STF interval. Therefore, the first stage of the algorithm defines the time offset between the position of the current repetition (i.e. signal detection position) and the beginning of the STF. The time offset estimation is given by

$$\widehat{\Delta\theta}_{SS} = \arg \max_{0 \leq \Delta\theta \leq 15} \{ | \sum_{n=0}^{15} r(n + \Delta\theta) g_{SS}^{*}(n) | \}, \tag{3.33}$$

where $g_{SS}(n)$ is the known repetition of the STF which has the length of 16. Note that the first step only allows to estimate the transition between the repetitions of the STF, to define the number of STF repetitions (in integer) from the signal detection position to the start sample of the GI2 of the LTF field, the authors use the ML-based algorithm studied in [92]. The ML function, after deployed, is a subtraction between the ACF of the received signal with itself delayed the STF repetition period and the power of the signals as follows:

$$f_{ML} = | \sum_{n=0}^{15} r^{*}(n + \Delta\theta) r(n + \Delta\theta + 16) | - \frac{\rho}{2} \sum_{n=0}^{15} \Big[|r(n + \Delta\theta)|^2 + |r(n + \Delta\theta + 16)|^2 \Big], \tag{3.34}$$

where $\rho = \frac{SNR}{SNR+1}$. Due to the uncorrelated property between the STF repetitions and the GI2 of the LTF field, the receiver counts the number of STF samples and then the number of STF repetitions from the signal detection position to the start sample of the GI2 at which the ML function is smaller than a threshold β:

$$\widehat{N}_{SS-GI2} = \lfloor \arg \min_{n} \{ f_{ML} < \beta \} / 16 \rfloor, \tag{3.35}$$

where $\widehat{N}_{SS-GI2}$ is the estimation of the number of STF repetitions from the signal detection position to the start sample of the GI2. The starting-point of the GI2 is then defined by $\widehat{\theta}_{GI2} = 16 \times \widehat{N}_{SS-GI2} + \widehat{\Delta\theta}_{SS} + \hat{\theta}_{SS}$, $\widehat{\Delta\theta}_{SS}$ is the estimation value of the offset from the current repetition of the STF to the beginning of the next repetition.

The disadvantage of this algorithm is the use of the CCF in the first stage that usually results in a large time deviation in presence of the CFO. In [97], the CCF is replaced by using the generalized ML rule given by

$$\Phi(\Delta\theta_{SS}) = \ln\{ l(\Delta\theta_{SS} | \mathbf{r}) \} - \frac{1}{2} \ln\{ \det(I(\Delta\theta_{SS})), \tag{3.36}$$

where $l(\Delta\theta_{SS}|\mathbf{r})\}$ is the likelihood function of $\Delta\theta_{SS}$ (which is the offset from the current repetition of the STF to the beginning of the next repetition) given $\mathbf{r}$ as

expressed by

$$l(\Delta\theta_{SS}|\mathbf{r})\} = \frac{1}{\pi^N \sigma_g^{2N}} e^{-||\mathbf{r}-\mathbf{G}_{\Delta\theta_{SS}}\mathbf{h}||^2/\sigma_g^2}, \tag{3.37}$$

$I(\Delta\theta_{SS})$ is the Fisher information matrix given by

$$I(\Delta\theta_{SS}) = \frac{1}{\sigma_g^2}\begin{pmatrix} 2\Re\{\mathbf{G}_{\Delta\theta_{SS}}^H \mathbf{G}_{\Delta\theta_{SS}}\} & -2\Im\{\mathbf{G}_{\Delta\theta_{SS}}^H \mathbf{G}_{\Delta\theta_{SS}}\} & 0 \\ 2\Im\{\mathbf{G}_{\Delta\theta_{SS}}^H \mathbf{G}_{\Delta\theta_{SS}}\} & 2\Re\{\mathbf{G}_{\Delta\theta_{SS}}^H \mathbf{G}_{\Delta\theta_{SS}}\} & 0 \\ 0 & 0 & \frac{1}{\sigma_g^2} \end{pmatrix}, \tag{3.38}$$

with σ_g^2 being the noise variance and $\mathbf{G}_{\Delta\theta_{SS}}$ of size $16 \times L$ containing the known STF samples from position corresponding to $\Delta\theta_{SS}$ and L being the channel length. The time offset is estimated by

$$\widehat{\Delta\theta}_{SS} = \arg \min_{\Delta\theta_{SS}\in 0,1,...,15} \{\Phi(\Delta\theta_{SS}\}, \tag{3.39}$$

where $\Phi(\Delta\theta_{SS})$ is given by (3.36).

So, the starting sample of the next repetition is $\widehat{\theta}_0 = \widehat{\theta}_{SS} + 16 - \widehat{\Delta\theta}_{SS}$. To determine the transition point between the STF and the GI2 of the LTF (i.e. the first sample of the GI2), the Neyman-Pearson (NP) detection approach in [44] is handled. Two conditional probability functions are set up. The first one is the probability of the received signal given the assumption that it belongs to the GI2 (P_{GI2}) and the other is the probability of the received signal given the assumption that it belongs to the STF field (P_{SS}). The first sample of the GI2 is determined by the smallest index q, $q = 0, 1, 2...$, which satisfies the condition $P_{GI2} > P_{SS}$ which corresponds to the following expression:

$$\mathbf{r}_{n_q}^H \mathbf{G}_0 (\mathbf{G}_0^H \mathbf{G}_0)^{-1} \mathbf{G}_0^H \mathbf{r}_{n_q} > \mathbf{r}_{n_q}^H \mathbf{B}_0 (\mathbf{B}_0^H \mathbf{B}_0)^{-1} \mathbf{G}_0^H \mathbf{r}_{n_q}, \tag{3.40}$$

where $\mathbf{r}_{n_q} = (r(0)_{n_q}, r(1)_{n_q}, ..., r(15)_{n_q})$, $n_q = \widehat{\theta}_0 + q \times 16$; $\mathbf{G}_0$ contains the GI2 samples while $\mathbf{B}_0$ contains the STF samples, both of them have the size of $16 \times L$. This algorithm has better performance compared to [92] since the noise information is included in the generalized ML rule. However, it is also more complex.

To improve the performance of time synchronization process in a frequency selective fading channel, the time synchronization algorithms are performed jointly with channel estimation as mentioned in [18], [96], [47], [94], and [103]. These techniques are classically used in the fine synchronization stage to estimate the remaining time offset (i.e. remaining STO). The general idea of the approach in these references is based on the relationship between the remaining STO and the channel estimation process (see Figure 3.7). First, a set of possible STO is given as a result of

coarse synchronization stage. Then, in the fine synchronization stage, the channel estimation (based on Least Square (LS) criterion) is implemented for a given STO. In [18], [96] and [47], the correct STO is estimated according to the first path of the channel by comparing it with a predefined threshold. However, it is usually difficult to analytically choose the threshold because it can be affected by the channel condition (i.e. SNR) (and sometimes IFFT leakage).

In [94] and [64], energies of the different Channel Impulse Responses (CIR) over a given window (depending on the length of the channel) are compared and the estimated STO is chosen as the one that corresponds to the CIR with the maximum energy. In [103], a Mean Square Error (MSE) criterion between the received symbol and estimated symbol is computed and the estimated STO is chosen as the one that minimizes the criterion. Both algorithms in [94] and [103] are described with more detail below.

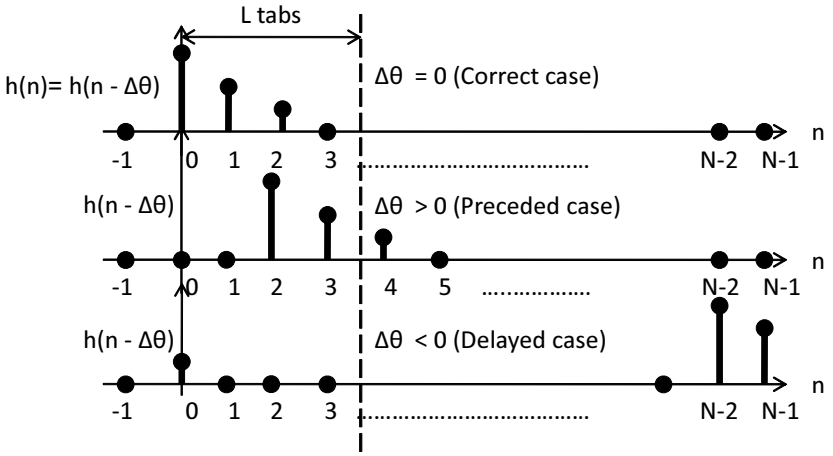

Figure 3.7. Relationship between the STO and channel estimation

Assume that the received signal $r(n)$ corresponding to the LTF (without the GI2) with the remaining time offset after the coarse time synchronization process is given (the CFO is assumed perfectly removed):

$$r(n) = \sum_{i=0}^{L-1} h(i)x(n - i - \Delta\theta) + g(n), \tag{3.41}$$

where $\Delta\theta = \theta - \hat{\theta}$, is the time offset computed between the true symbol timing and its estimate. In [94] and [103], this time offset is estimated jointly with the channel estimation using the LS criterion.

First the authors define a finite set $\mathbf{\Lambda}$ containing $2M + 1$ possible offset values as follows $\{-\Delta\theta_M, .., \Delta\theta_M\}$. For a given value $\Delta\theta_m$ in $\mathbf{\Lambda}$, the LS-based CIR is then

estimated in the frequency domain as follows [22]:

$$\widetilde{\mathbf{H}}_{\Delta\theta_m} = (\mathbf{X}^H\mathbf{X})^{-1}\mathbf{X}^H\mathbf{R}_{\Delta\theta_m}, \tag{3.42}$$

where $\widetilde{\mathbf{H}}_{\Delta\theta_m}$ is the LS channel estimate at $\Delta\theta_m$; $\mathbf{X} = \text{diag}(X(0), X(1), ..., X(N-1))$ with $X(k)$ $(0 \leq k \leq N-1)$ being the known LTF symbol and $\mathbf{R}_{\Delta\theta_m}$ being the vector of received symbols (i.e. the received signals in frequency domain) corresponding to the given time offset $\Delta\theta_m$.

For each time offset value $\Delta\theta_m$ in $\mathbf{\Lambda}$, we obtain an estimate $\widetilde{\mathbf{h}}_{\Delta\theta_m}$ of the CIR using the IFFT transform. Among M estimates, ones consider only those satisfying the following condition:

$$\omega_i = \{\Delta\theta_m : |\widetilde{h}_{\Delta\theta_m}(0)| > \beta\}, \tag{3.43}$$

where β is a given threshold which is defined depending on the noise level and type of channel model used. Therefore the set $\mathbf{\Lambda}$ becomes $\mathbf{\Gamma}$

$$\mathbf{\Gamma} = \{\omega_0, \omega_1, ..., \omega_{M'-1}; \quad M^{'} \leq M\}. \tag{3.44}$$

In [94], the time offset is estimated by

$$\Delta\hat{\theta} = \arg\max_{\omega_i}\{\sum_{n=0}^{L-1}|\widetilde{h}_{\omega_i}(n)|^2\}, \tag{3.45}$$

while in [103], the offset is defined as follows:

$$\Delta\hat{\theta} = \arg\min_{\omega_i}\{||\mathbf{R}_{\omega_m} - \mathbf{X}\widetilde{\mathbf{H}}_{\omega_m}||^2\}. \tag{3.46}$$

Figure 3.8 illustrates the PSF versus SNR of the two algorithms proposed in [94] and [103]. The simulation parameters are summarized in Tables 3.2 and 3.3. Note that the two algorithms were mentioned for only the fine time synchronization stage, the CTS is to achieve $\hat{\theta}$ can be performed by any algorithm. Here we implement the CTS stage by using the CCF between the received signal and the known STF specified by the IEEE 802.11a standard. The symbol timing estimation is given by the value of θ maximizing the absolute value of the CCF as follows:

$$\hat{\theta} = \arg\max_{\theta}|\sum_{n=0}^{L_{\text{STF}}-1} c^*(n)r(n+\theta)|, \tag{3.47}$$

where $r(n)$ is the received signal containing the symbol timing θ, the known bit-stream $c(n)$ is obtained from the first ten repetitions of the STF and L_{STF} is the number of samples of $c(n)$.

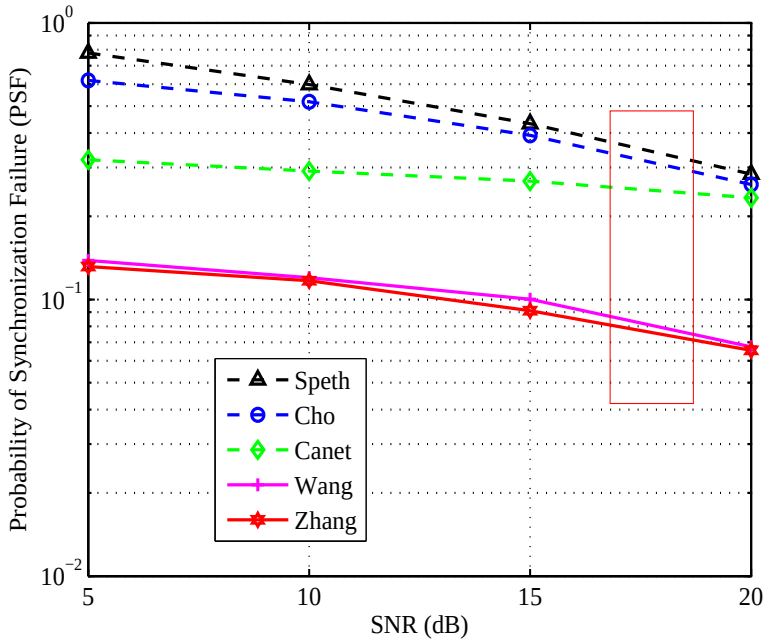

Figure 3.8. PSF of algorithms [85] (Speth) (Figure 3.2), [22] (Cho) (Figure 3.2), [16] (Canet) (Figure 3.6), [94] (Wang) and [103] (Zhang) with no time deviation and $\epsilon = 0$ under COST207-RA channel model

Table 3.3. Simulation parameters

Parameters	*Values*
L_{STF}	160
Threshold (β)	0.5
N	64
M	30

After this stage, we get the signal with the remaining STO given in equation (3.41). And after that, the algorithms of joint fine time synchronization and channel estimation of the two references [94] and [103] are implemented to obtain the performance shown in Figure 3.8. The PSF values of algorithms in [94] and [103] are almost similar. Indeed the two proposed metrics depend heavily on the channel estimation (see equations (3.45) and (3.46)) which is performed by the LS technique. The performance of the LS estimation method combined with the timing synchronization algorithm is presented in Figure 3.9 in terms of Mean Square Error (MSE) of channel estimation versus SNR. Note that in this figure, the carrier frequency offset is set to zero.

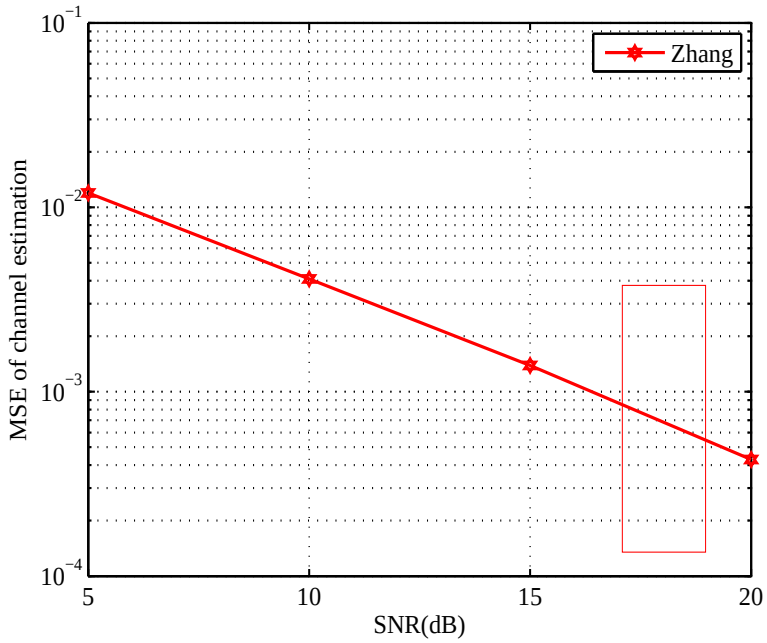

Figure 3.9. MSE of channel estimation based on LS criterion with $\epsilon = 0$

3.2.2.2 Frequency-domain time synchronization algorithms

After the symbol timing is estimated by the time synchronization stages, the received signal may still be hit by some remaining (smaller) time offset that makes phase rotation of the received symbols in the frequency domain. Frequency-domain synchronization algorithms have been developed to estimate this offset. The offset value, denoted by δ, can be estimated via the phase difference between the adjacent components of the received signal in the frequency domain. For example, assuming that $X[k]$, $X[k-1]$ are training symbols and $X[k] = X[k-1]$, then from Table 3.1, we have $R[k]R^*[k-1] = |X[k]|^2 e^{j2\pi\delta/N}$, where δ is the remaining STO that is defined by [22]

$$\hat{\delta} = \frac{N}{2\pi} \arg\Big\{ \sum_{k=1}^{N-1} R[k]R^*[k-1] \Big\}. \tag{3.48}$$

One can also find in the literature some papers that employ cross-correlation property in the frequency domain to estimate the symbol timing as proposed in [51]. First, the receiver performs an FFT in the observation sliding window as follows:

$$R(k) = \sum_{n=0}^{N-1} r(n+\theta) e^{-j2\pi(n+\theta)k/N}, \tag{3.49}$$

where $R(k)$ is the received symbol in the frequency domain at θ, k is the subcarrier index and θ is the sampling index.

The symbol timing is then estimated as follows:

$$\hat{\theta} = \arg\max_{\theta} \left| \Re\Big\{ \sum_{k=0}^{N-1} R(k)C^*(k)\}/N \Big\} \right|, \tag{3.50}$$

where $\Re(x)$ denotes the real part of x, $*$ means the conjugate operator and $C(k)$ is the known pilot. It is interesting in this reference that the training pilot is designed to get the training sequence vector in the time domain in the form $[0, ..., 0, 1, 0, ..., 0]$. It means that among elements of the time-domain sequence, there is only one of value 1 while the others are zero. This allows to save transmit power.

3.2.2.3 Conclusion

This section reviewed the main time synchronization algorithms that are proposed in the literature. They are summarized in Table. 3.4 where they are classified based on the mathematical tools and the type of data used for each algorithm.

Table 3.4. Time synchronization algorithms (ϵ is known)

Reference	**Tool**	**DA/NDA**	**Adapted to standard**	**Type of data**	**Domain**
[90], [85]	MSE	NDA	No	Cyclic Prefix	Time
[92],[91]	ML	NDA	No	Cyclic Prefix	Time
[80],[81],[58]	ACF	DA	No	Long training symbols	Time
[57]	ACF/ACF	DA	Yes	STF/LTF	Time
[16]	ACF/CCF	DA	Yes	STF/LTF	Time
[17],[97]	CCF/ML	DA	Yes	STF/LTF	Time
[94],[103], [87]	CCF/LS/MMSE Joint with CE	DA	Yes	STF/LTF	Time
[26]	CCF	DA	No	Long training symbols	Time
[70],[27],[20]	ML	DA	No	Long training symbols	Time
[43],[5],[4]	CCF	DA	No	CSP	Time
[51]	CCF	DA	No	Pilots	Frequency
[22]	ACF	DA	No	Pilots	Frequency

Based on the analysis of simulation results, we can draw the following conclusions for these algorithms:

- the spectral efficiency of NDA-based algorithms is lower than that of DA algo-

rithms;
- the DA-based algorithms have better performance than the NDA-based algorithms;
- the algorithms employing joint time synchronization and channel estimation proposed in references [94], [103] achieves good performance in terms of PSF. Moreover, these algorithms allow to estimate simultaneously the channel coefficients.

3.3 Frequency synchronization techniques in OFDM system

This section first analyzes the effect of the CFO and then reviews frequency synchronization algorithms developed in literature.

3.3.1 Effect of CFO

Before being transmitted via the channel, a baseband signal is up-converted to some high frequency carrier. Then at the receiver, it is down-converted with the same carrier frequency. The carrier frequencies are generated by the local oscillators and should take exactly the same value. However, in practical systems, they are not exactly equal, therefore some Carrier Frequency Offset -CFO- between the carrier frequencies at transmitter and receiver is found in the received signal. This CFO is generally a result of two parts [41]: (i) the tolerance of the oscillators at local stations; and (ii) the Doppler frequency, that is determined by

$$f_d = \frac{v f_c}{c}, \tag{3.51}$$

where f_c is the carrier frequency at the transmission side, v is the velocity of the terminal or the reflected objects and c is the speed of light.

As a result, the carrier frequency of the received signal is different from that at the transmitter by some value $\Delta f_c = f_c' - f_c$ where f_c' is the carrier frequency of the signal at the receiver. This offset may result in a loss of the orthogonality among subcarriers that substantially affects the performance of the system.

Usually, the quantity of interest is the CFO normalized by the subcarrier spacing Δf as follows (see equation (2.8)):

$$\epsilon = \Delta f_c T_s = \frac{\Delta f_c}{\Delta f}. \tag{3.52}$$

In order to simplify the study of the CFO influence on the system performance, the normalized CFO is usually divided into two parts: Integer CFO (IFO) and Fractional CFO (FFO) expressed as follows:

$$\epsilon = \epsilon_i + \epsilon_f. \tag{3.53}$$

Moreover, in what follows, time synchronization is assumed to be perfect, while the noise is ignored. Therefore, from equation (2.8), we can express the received signal as follows:

$$r(n) = \sum_{i=0}^{L-1} h(i)x(n-i)e^{j\frac{2\pi\epsilon n}{N}}, \tag{3.54}$$

by replacing

$$x(n-i) = \sum_{k=0}^{N-1} X(k)e^{j\frac{2\pi k(n-i)}{N}},$$

we get

$$r(n) = \frac{1}{N}\sum_{k=0}^{N-1} H(k)X(k)e^{j\frac{2\pi(\epsilon+k)n}{N}}. \tag{3.55}$$

Table 3.5 shows the impact of the CFO ofnthe received signal in time and frequency domain.

Table 3.5. The effect of Carrier Frequency Offset (CFO)

	Received signal	CFO
Time domain	$r(n)$	$x(n)e^{j2\pi n\epsilon/N}$
Frequency domain	$R(k)$	$X(k-\epsilon)$

In the next section, we investigate separately the effects of each part of the CFO (IFO and FFO) on the system performance.

3.3.1.1 Effect of IFO

Assuming that the FFO part is zero, it is seen from Table 3.5 that the received signal impacted by some IFO is expressed in the time-domain as $x(n)e^{j2\pi n\epsilon_i/N}$ and in the frequency-domain $X(k-\epsilon_i)$. Because the parameters k, ϵ_i are integers, then $(k-\epsilon_i)$ is also an integer, and the orthogonality between the subcarriers is maintained. However, because now $X(k)$ becomes $X(k-\epsilon_i)$, the system performance in terms of Symbol Error Ratio (SER) is degraded and can be very bad.

3.3.1.2 Effect of FFO

To better explain the effect of the FFO part, consider the FFT of the received signal given in equation (3.55). The received signal in the frequency-domain containing

some FFO reads

$$\begin{aligned}
R(k) &= \sum_{n=0}^{N-1} r(n) e^{-j2\pi nk/N} \\
&= \sum_{n=0}^{N-1} \frac{1}{N} \sum_{m=0}^{N-1} H(m)X(m) e^{j2\pi(m+\epsilon_f)n/N} e^{-j2\pi nk/N} \\
&= \frac{1}{N} \sum_{n=0}^{N-1} \sum_{m=0}^{N-1} H(m)X(m) e^{j2\pi(m+\epsilon_f-k)n/N} \\
&= \frac{1}{N} H(k)X(k) \sum_{n=0}^{N-1} e^{j2\pi\epsilon_f n/N} + \frac{1}{N} \sum_{m=0, m\neq k}^{N-1} H(m)X(m) \sum_{n=0}^{N-1} e^{j2\pi(m+\epsilon_f-k)n/N} \\
R(k) &= \frac{1}{N} \frac{1-e^{j2\pi\epsilon_f}}{1-e^{j2\pi\epsilon_f/N}} H(k)X(k) + \frac{1}{N} \sum_{m=0, m\neq k}^{N-1} H(m)X(m) \frac{1-e^{j2\pi(m-k+\epsilon_f)}}{1-e^{j2\pi(m-k+\epsilon_f)/N}}.
\end{aligned} \tag{3.56}$$

After some mathematical manipulations, we get (see further in [7], [8])

$$R(k) = \frac{sin(\pi\epsilon_f)}{Nsin(\pi\epsilon_f/N)} e^{j\pi\epsilon_f(N-1)/N} H(k)X(k) + I(k), \tag{3.57}$$

where

$$I(k) = e^{j\pi\epsilon_f(N-1)/N} \sum_{m=0, m\neq k}^{N-1} \frac{sin(\pi(m-k+\epsilon_f))}{Nsin(\pi(m-k+\epsilon_f)/N)} H(k)X(k) e^{j\pi(m-k)(N-1)/N}. \tag{3.58}$$

It can be observed from equation (3.57) that the received signal in the frequency domain is composed of two terms. The first term represents the attenuation and phase rotation of the kth subcarrier ($\frac{sin\pi\epsilon_f}{Nsin(\pi\epsilon_f/N)} e^{j\pi\epsilon_f(N-1)/N}$) while the latter one represents the ICI from other subcarrier components impacting the kth component. To visually illustrate the effect of the FFO, Figure 3.10 shows the frequency spectrum of one OFDM signal with three subcarriers in the frequency domain with the presence and absence of the FFO. It is obvious from the figure that in the case of absence of the FFO (presented by the solid lines), the FFT output only contains the transmitted subcarriers without any interference from the neighbour subcarriers. However, in presence of the FFO (dashed lines), the signal received at some subcarrier consists of the subcarrier corresponding to the transmitted symbol (i.e. the useful symbol) and the interferences from the two other subcarriers.

3.3.2 Frequency synchronization techniques

Just like in the case of the time synchronization algorithms, the frequency synchronization algorithms can be performed either in the time domain or in the frequency

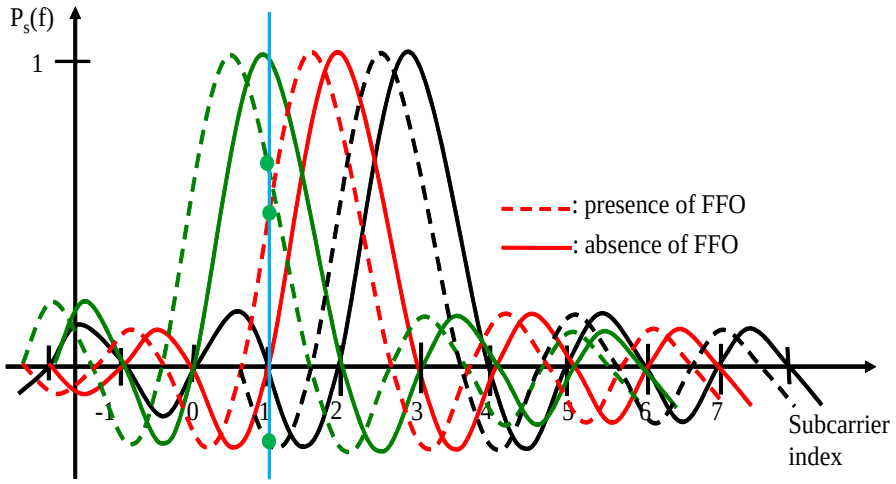

Figure 3.10. The effect of the FFO on the subcarriers orthogonality

domain. In this section, we concentrate on the CFO estimation techniques, and the STO parameter included in the received signal is thus assumed to be perfectly compensated.

3.3.2.1 Time-domain frequency synchronization algorithms

To estimate the CFO in the time domain, NDA or DA techniques can be used. For the first one, the CP of OFDM symbol is usually employed.

(a) Frequency synchronization based on Cyclic Prefix

It can be seen from Table 3.5 that due to the existence of the CFO, the received signal in the time domain at sample n is rotated by a phase of $2\pi n\epsilon/N$, N being the number of FFT/IFFT points. In the case of the IEEE 802.11a standard, N is also the distance between the CP and its copy at the end of the OFDM symbol. Therefore, the phase difference between the received signals at n and $n+N$ is $2\pi(n+N)\epsilon/N - 2\pi n\epsilon/N = 2\pi\epsilon$. Based on this observation, the CFO can be estimated by taking the phase angle of the product between the samples of the CP and its copy in the OFDM symbol as follows:

$$\hat{\epsilon} = \frac{1}{2\pi} \arg\{r^*(n)r(n+N)\}, \tag{3.59}$$

where arg() is the argument operator performed by taking arctan(.) function. It is easy to see that because the period of arctan(.) function is π, the range of CFO estimation, $\hat{\epsilon}$, in (3.59) is limited within $[-\pi, +\pi]/2\pi = [-0.5, +0.5]$.

To reduce the effect of the noise, one usually averages (3.59) over the CP interval

as follows [22], [14]:

$$\hat{\epsilon} = \frac{1}{2\pi} \arg \Big\{ \sum_{n=0}^{N_g-1} r^*(n) r(n+N) \Big\}, \tag{3.60}$$

where N_g is the CP length.

To evaluate the performance of the algorithm relying on the CP, Figure 3.11 shows the MSE of CFO estimation versus SNR. The simulation parameters are chosen according to the IEEE 802.11a standard (see Section 3.2.2). In this section, the time offset is assumed to be perfectly compensated (i.e. $\Delta\theta = 0$) while the tolerance of internal oscillator at each station belongs to the range $[-20, 20]$ ppm and thus the total tolerance of two stations falls in $[-40, 40]$ ppm. For the carrier frequency $f_c = 5.2$ GHz and the OFDM symbol duration $T = 3.2\mu s$, the normalized frequency offset ϵ is taken randomly according to a uniform distribution in the range $[-0.6, 0.6]$.

In order to evaluate the quality of the estimation, we simulated two cases: (i) ϵ is taken randomly in $[-0.5, 0.5]$ and (ii) $\epsilon = 0.6$. It can be observed from Figure 3.11 that in the case $\epsilon = 0.6$, the system performance in terms of MSE is significantly degraded compared to the case $|\epsilon| \leq 0.5$. In fact, this means that the algorithms based on the CP can not be efficient when $\epsilon > 0.5$.

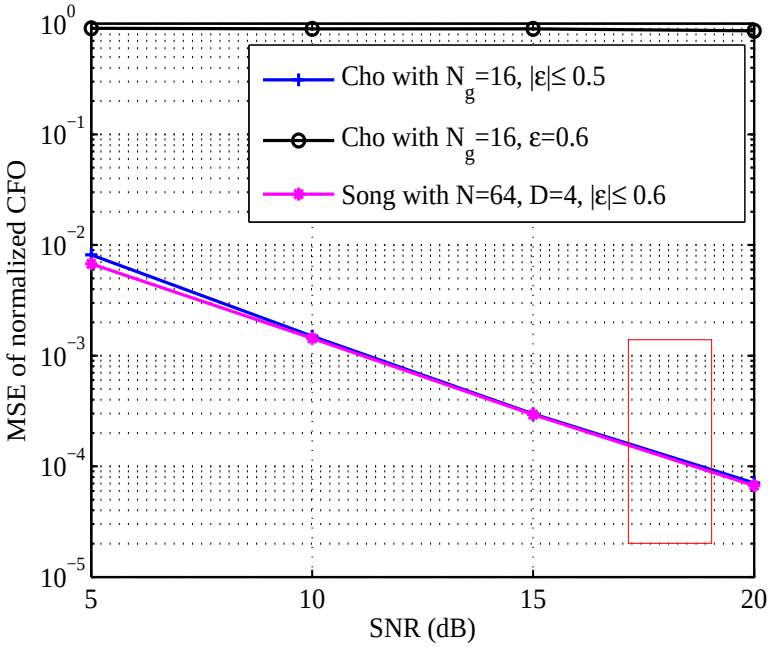

Figure 3.11. MSE of CFO estimation algorithms [22] (Cho), [84] (Song) (the rectangular box is considered as the operating area)

(b) Frequency synchronization using DA based on training sequence

In general, for the frequency synchronization algorithms based on CP, despite their low computational complexity, the estimation accuracy is affected by multi-path distortion [99]. Moreover, as mentioned above, the range of the CFO estimation is limited within the range $[-0.5, +0.5]$ which does not correspond to practical situations. Training sequence, as described below, allows to improve the range as well as the accuracy of the CFO estimation. The general idea for increasing the estimation range is to reduce the distance between the two repetitions as mentioned in [84].

Assume that $x(n)$ is one sample of the training sequence of N samples containing D repetitive patterns (i.e. each repetition contains N/D samples). At the receiver, the CFO estimation is implemented as follows:

$$\hat{\epsilon} = \frac{D}{2\pi} \arg\Big\{ \sum_{n=0}^{N/D-1} r^*(n) r(n + N/D) \Big\}. \tag{3.61}$$

It is obvious that the CFO estimation range depends on the parameter D with $|\epsilon| \leq D/2$. This means that the range, depending on the parameter D, is wider if D increases. Nevertheless, the window length (i.e. the number of samples to compute the correlation) is reduced, thus the accuracy is degraded. This obviously corresponds to some trade-off between the accuracy and estimation range of CFO.

The simulation results for $D = 4$ and $N = 64$ are shown on Figure 3.11 (denoted as "Song"). Even if for the case of $\epsilon = 0.6$ (> 0.5), the MSE curve is the same as that of the case based on CP with $|\epsilon| \leq 0.5$. Meaning that the estimation range has been increased.

The CFO estimation can be refined by taking the average of the estimates over all repetitive sequences as follows [84]:

$$\hat{\epsilon} = \frac{D}{2\pi} \arg\Big\{ \sum_{m=0}^{D-2} \sum_{n=0}^{N/D-1} r^*(n + mN/D) r(n + (m+1)N/D) \Big\}. \tag{3.62}$$

(c) Frequency synchronization using DA based on the IEEE 802.11a preamble structure

Recommended by the IEEE 802.11a standard, the frequency synchronization process studied in [16], [57] is performed in two steps: a CFS step followed by a FFS step. In the CFS, the authors compute the auto-correlation function based on

the repetitions of the STF as follows:

$$Z(L_S) = \sum_{n=0}^{L_{CFS}-1} r^*(n)r(n+L_S), \tag{3.63}$$

where L_S is the period of the STF and L_{CFS} is the window length corresponding to the two repetitions of STF (i.e. 2×16 samples) in the standard. The coarse estimation of the CFO is given by

$$\epsilon_c = \hat{\epsilon} = \frac{N}{2\pi L_S} \arg(Z(L_S)), \tag{3.64}$$

where N denotes the number of the FFT points.

Let $r_f(n)$ be the received signal containing the residual CFO, $\Delta\epsilon = \epsilon - \epsilon_c$. To estimate $\Delta\epsilon$, the ACF is computed between the received signal corresponding to the LTF and itself delayed by L_L samples as follows:

$$Z(L_L) = \sum_{n=0}^{L_{FFS}-1} r_f^*(n)r_f(n+L_L), \tag{3.65}$$

where L_L is the period of LTF sequence that is equal to 64 samples, L_{FFS} is the window length corresponding to one repetition of LTF (i.e. 1×64 samples). The estimation of $\Delta\epsilon$ is thus given by

$$\epsilon_f = \Delta\hat{\epsilon} = \frac{N}{2\pi L_L} \arg(Z(L_L)). \tag{3.66}$$

Therefore the normalized frequency offset estimation is

$$\hat{\epsilon}_{total} = \epsilon_c + \epsilon_f. \tag{3.67}$$

The same scheme is found in [42], however in the first step, a nonlinear square cost function between the received signal and the known STF multiplexing with the frequency offset is used. The coarse frequency offset is obtained by minimizing this function as follows:

$$\hat{\epsilon}_c = \arg\min_{\epsilon} \sum_{n=0}^{L_S-1} |r(n) - x(n)e^{j2\pi\epsilon n/N}|^2. \tag{3.68}$$

By exploiting the repetitive symbols with the short period of 16, these algorithms allow a larger range of estimation compared to the algorithms using the CP. Moreover, the use of two long symbols helps to improve the accuracy of the CFO estimation. Figure 3.12 shows the improved performance in terms of MSE versus SNR that is denoted by "Manusani, Canet" [57], [16].

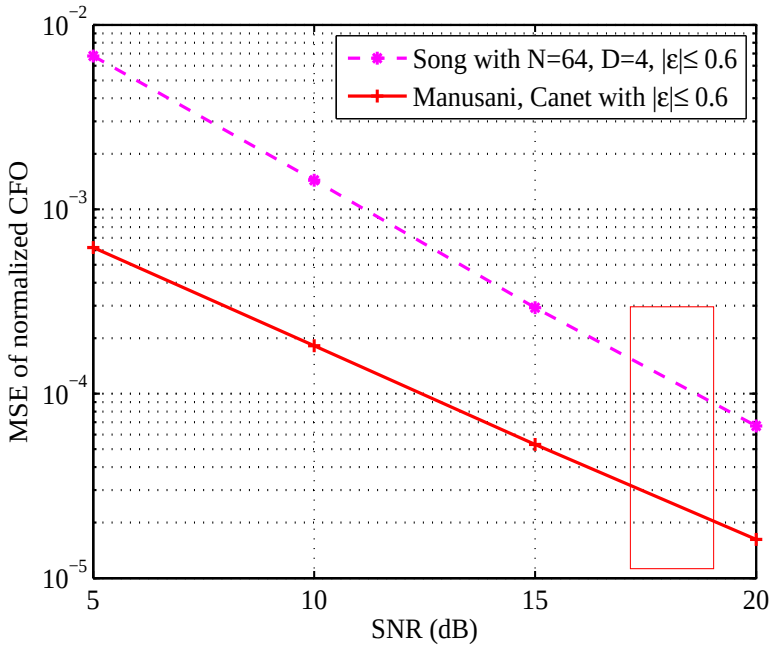

Figure 3.12. MSE of CFO estimation algorithms [84] (Song), [57] (Manusani) and [16] (Canet) with $|\epsilon| \leq 0.6$

Apart from the above algorithms, the MAP criterion is also used to improve the accuracy of the CFO estimation. In [52], the authors propose a joint CFO and channel estimation using the MAP criterion based on a burst of training symbols. Specifically, an *a posteriori* probability function of the CFO and channel coefficient parameters is investigated. The unknown parameters are then estimated by finding the values maximizing this function. This algorithm will be adapted to the IEEE 802.11a standard and further described in Chapter 5.

3.3.2.2 Frequency-domain frequency synchronization algorithms

Frequency domain techniques exploit the FFT output to construct CFO estimators. We first introduce a technique reported in references [98], [99] and [102]. This technique relies on the subcarriers included in all OFDM symbols and it is called the Power Difference Estimator-Frequency (PDE-F). Consider two consecutive OFDM symbols and assume that the channel coefficients does not change during this time. Let $X_1(k)$ and $X_2(k)$ be the subcarriers at frequency k, $0 \leq k \leq N-1$, of the OFDM symbols 1 and 2, respectively. Assuming that the symbol timing is perfectly known, then the kth FFT output of the first OFDM symbol for the noise-free is expressed by

$$R_1(k)|_{\hat{\epsilon}=\epsilon} = H_1(k)X_1(k). \tag{3.69}$$

We can deduce the following expression:

$$|R_1(k)|_{\hat{\epsilon}=\epsilon}|^2 = |H_1(k)|^2|X_1(k)|^2. \tag{3.70}$$

If all subcarriers (included in the OFDM symbols) have equal power, then we have $|X_1(k)|^2 = |X_2(k)|^2$ and under the assumption that the channel changes slowly, we get

$$|R_1(k)|_{\hat{\epsilon}=\epsilon}|^2 \approx |R_2(k)|_{\hat{\epsilon}=\epsilon}|^2, \tag{3.71}$$

The approximation given by equation (3.71) is true if $\hat{\epsilon} = \epsilon$. If it is not the case, the ICI corresponding to the term $I(k)$ given in (3.57) will be introduced at the FFT outputs $R_1(k)$ and $R_2(k)$, and equation (3.71) is no longer valid. In other words $|R_1(k)|_{\hat{\epsilon}=\epsilon}|^2 - |R_2(k)|_{\hat{\epsilon}=\epsilon}|^2 \neq 0$. From this observation, the CFO value ϵ can be estimated by minimizing the following cost function:

$$J(\epsilon) = \sum_{k=0}^{N-1}(|R_1(k)|^2 - |R_2(k)|^2)^2. \tag{3.72}$$

A more classical technique is based on the phase relationship of the received signals in the time domain as proposed in [60]. In this reference, two repetitive training symbols with distance N are exploited. Based on Table 3.5, the relationship between the two signals is $r_2(n) = r_1(n)e^{j2\pi\epsilon}$, where $r_1(n)$ and $r_2(n)$ are the received signals corresponding to the first and second training symbol, correspondingly in the frequency domain, the relationship is expressed by $R_2(k) = R_1(k)e^{j2\pi\epsilon}$. Therefore, the CFO estimation is defined by

$$\hat{\epsilon} = \frac{1}{2\pi}\arg\Big\{\sum_{k=0}^{N-1}\Im[R_1^*(k)R_2(k)]. \tag{3.73}$$

Another technique that allows the estimation of the CFO is to employ the pilots inserted into the data OFDM symbols. In the OFDM modulation, the transmitter inserts the pilots into the OFDM subcarriers in the frequency domain. At the receiver, after the received signals are transformed into frequency domain, the pilot tones are extracted. Based on these pilots, a frequency synchronization algorithm is implemented in two steps as proposed in [23]. First, in the CFS stage, the integer part of the CFO is estimated according to correlation property between the received symbols and known pilots as follows:

$$\hat{\epsilon}_C = \arg\max_{\epsilon}\Big\{\Big|\sum_{j=0}^{L-1} R_{(l+1)}[p(j)]R_l^*[p(j)]X_{(l+1)}^*[p(j)]X_l[p(j)]\Big|\Big\}, \tag{3.74}$$

where L is the number of pilots in one OFDM symbol, $p(j)$ is the position of the jth pilot in the symbol, $X_l[p(j)]$ is the known pilot value at the position $p(j)$ of the lth OFDM symbol.

The value $\hat{\epsilon}_C$ is then used to compensate the received signal in the time domain as $r(n) \times e^{-j2\pi\hat{\epsilon}_C n/N}$. And the fine CFO is estimated as follows:

$$\hat{\epsilon}_F = \frac{1}{2\pi T_{sub} N} \arg\{\Big| \sum_{j=0}^{L-1} R_{(l+1)}[p(j)] R_l^*[p(j)] X_{(l+1)}^*[p(j)] X_l[p(j)] \Big|\}, \tag{3.75}$$

where $R_l[p(j)]$ is the received signal that has been compensated by the coarse CFO estimation, $\hat{\epsilon}_C$.

At the end of this section, we introduce an approach relying on the periodogram as reported in [6], [13], [48], [53], [75] and [83]. We here describe the approach developed in [75] where the values of the periodogram are fully exploited. This scheme is organized in three steps. The first step concerns the IFO estimate which is deduced from the index of the periodogram of the received training symbol as follows:

$$\hat{\epsilon}_I = \arg \max_{-N/2 \le k \le N/2} \{R(k)\}, \tag{3.76}$$

where $R(k)$ is the FFT transform of the received signal.

The second step refers to the FFO estimate deduced from the IFO estimation. Specifically, the fractional part of the frequency offset is estimated via the values of the periodogram at the estimation value as follows:

$$\hat{\epsilon}_F = \frac{\sqrt{R(\hat{\epsilon}_I + 1)}}{\sqrt{R(\hat{\epsilon}_I)} + \sqrt{R(\hat{\epsilon}_I + 1)}} \tag{3.77}$$

In order to further improve the accuracy of the CFO estimation, the author employs the proposal in literature [6] to estimate the residual frequency error between $\hat{\epsilon}_I + \hat{\epsilon}_F$ and the true value ϵ. The remaining frequency offset is estimated by

$$\hat{\epsilon}_{res} = \frac{\sqrt{R(\hat{\epsilon}_I + \hat{\epsilon}_F + 0.5)} - \sqrt{R(\hat{\epsilon}_I + \hat{\epsilon}_F - 0.5)}}{2(\sqrt{R(\hat{\epsilon}_I + \hat{\epsilon}_F + 0.5)} + \sqrt{R(\hat{\epsilon}_I + \hat{\epsilon}_F - 0.5)})}. \tag{3.78}$$

The estimation of the frequency offset is then deduced as follows:

$$\hat{\epsilon} = \hat{\epsilon}_F + \hat{\epsilon}_I + \hat{\epsilon}_{res}. \tag{3.79}$$

3.3.2.3 Conclusion

In this section, algorithms for frequency synchronization and their main properties were presented. The performance of these algorithms was also illustrated. In conclusion, the mathematical tools and type of data used for each algorithm are summarized in Table. 3.6.

Table 3.6. Frequency synchronization algorithms (with $\theta = 0$)

Reference	Tool	DA/NDA	Adapted to standard	Type of data	Domain
[22],[14]	ACF	NDA	No	Cyclic Prefix	Time
[84]	ACF	DA	No	Short training symbols	Time
[57],[16]	ACF	DA	Yes	STF/LTF	Time
[42]	CCF/ACF	DA	Yes	STF/LTF	Time
[52],[93]	MAP	DA	No	Long training symbols	Time
[60]	ACF	DA	No	Long training symbols	Frequency
[83],[13],[6] [75],[48],[53]	Periodogram	DA	No	Long training symbols	Frequency
[23],[101]	CCF	DA	No	Pilots	Frequency
[98],[102],[99]	PDE-F	NDA	No	data OFDM symbols	Frequency

3.4 Time and frequency synchronization techniques in OFDM system

In the above sections, we introduced separately the algorithms concerning time and frequency synchronization. While time synchronization algorithms are considered, frequency synchronization is assumed as perfectly performed and vice versa. However, in practice, both CFO and STO exist and thus the algorithms for time and frequency synchronization must be implemented simultaneously. In this section, we describe the most common time and frequency synchronization schemes developed in literature.

3.4.1 Time and frequency synchronization algorithms using the CP

We begin this section by the time and frequency synchronization algorithm using the Maximum Likelihood (ML) relying on the CP (or GI) of the OFDM symbols as proposed in [78] and [92]. First, a window of $(2N + N_g)$ received samples $r(n)$ is observed. This size ensures that there is always a full OFDM symbol of $(N + N_g)$ samples included in the window. Let L and L' be the index sets that are defined by $L = \{\theta, ..., \theta + N_g - 1\}$ and $L' = \{\theta + N, ..., \theta + N + N_g - 1\}$ (see Figure 3.13). It is known that if L falls in the CP (or GI) area, the two parts are correlated each other.

The log-likelihood function based on the probability density function ($p()$) of the

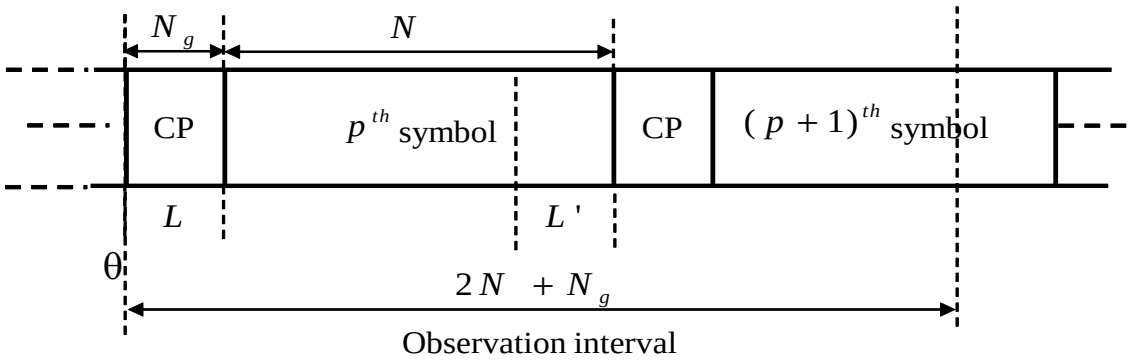

Figure 3.13. Structure of OFDM signal with CP (GI)

$(2N + N_g)$ observed samples $r(n)$ given the parameters θ and ϵ is expressed by

$$\begin{aligned}\Lambda(\theta,\epsilon) &= \log p(\mathbf{r}|\theta,\epsilon) \\ &= \log \prod_{n\subset L} p(r(n), r(n+N)|\theta,\epsilon) \prod_{n\subsetneq L\cup L'} p(r(n)|\theta,\epsilon) \\ \Lambda(\theta,\epsilon) &= \log \prod_{n\subset L} \frac{p(r(n), r(n+N)|\theta,\epsilon)}{p(r(n)|\theta,\epsilon)p(r(n+N)|\theta,\epsilon)} \prod_{n} p(r(n)|\theta,\epsilon). \end{aligned} \tag{3.80}$$

After some mathematical derivations, [95], $\Lambda(\theta,\epsilon)$ is given by

$$\Lambda(\theta,\epsilon) = |\gamma(\theta)|\cos(2\pi\epsilon + \arg\{\gamma(\theta)\}) - \rho\Phi(\theta), \tag{3.81}$$

where $\arg\{\}$ is the argument of a complex number, and

$$\gamma(\theta) = \sum_{n=0}^{N_g-1} r^*(n+\theta)r(n+\theta+N),$$

$$\Phi(\theta) = \frac{1}{2}\sum_{n=0}^{N_g-1}(|r(n+\theta)|^2 + |r(n+\theta+N)|^2),$$

$\rho = \frac{\sigma_s^2}{\sigma_s^2+\sigma_n^2}$ with σ_s^2 and σ_n^2 being the variances of the signal and noise, respectively. The ML estimations of θ and ϵ are defined by

$$\hat{\theta}_{ML} = \arg\max_{\theta}\{|\gamma(\theta)| - \rho\Phi(\theta)\} \tag{3.82}$$

and

$$\hat{\epsilon}_{ML} = -\frac{1}{2\pi}\arg\{\gamma(\hat{\theta}_{ML})\}. \tag{3.83}$$

It can be seen from equation (3.83) that the range of CFO estimation is also limited in the interval $[-0.5, 0.5]$ (as was the case for the algorithm mentioned in [22]). For simulations, we select the same parameters as in the IEEE 802.11a standard (see Section 3.2.2.1, (a)). The CFO is a uniformly distributed random

variable that falls in the range $[-0.5, 0.5]$ and θ is also taken randomly according to a uniform distribution. Simulation results are provided in Figures 3.14 and 3.15 where the performance is measured in terms of PSF versus SNR.

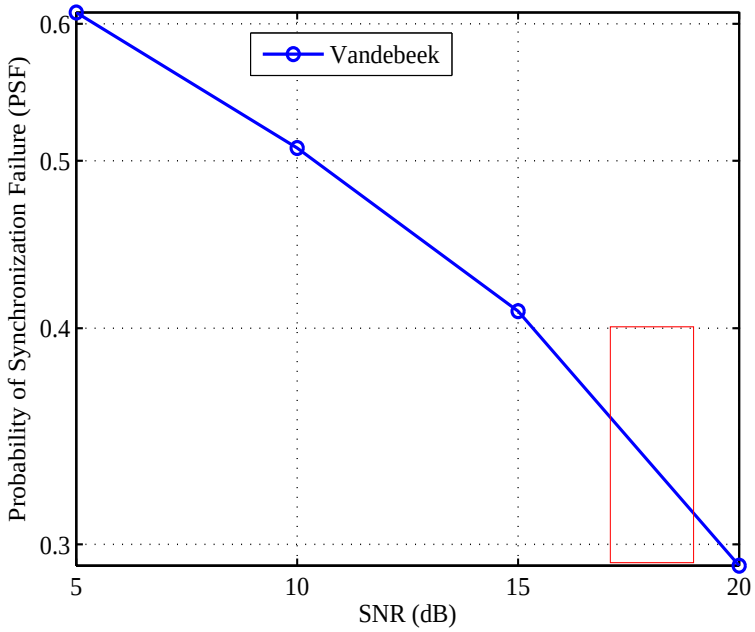

Figure 3.14. PSF of algorithm [92] (Vandebeek) with no time deviation (i.e. $\theta - \hat{\theta} = 0$) and $|\epsilon| \leq 0.5$ under COST207-RA model (the rectangular box is considered as the operating area)

3.4.2 Proposed training sequence in the literature

In order to improve the performance of synchronization process, the training sequence is usually included in the packet transmission. Training sequences have been proposed by authors in literature or recommended by the standards. This is discussed in the next section.

3.4.2.1 Time and frequency synchronization based on DA using training sequence

An example of time and frequency synchronization algorithm using a proposed training sequence can be found in [81]. In this reference, the transmission frame is preceded by a training sequence of two OFDM symbols. The first symbol has two identical halves. Based on the two halves, the time synchronization stage is performed by the following metric:

$$M(\theta) = \frac{P(\theta)}{R(\theta)}, \tag{3.84}$$

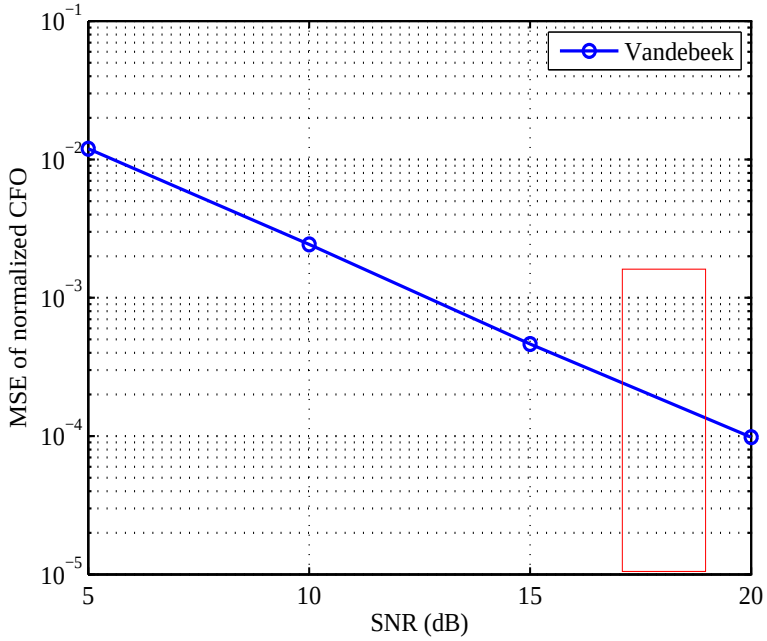

Figure 3.15. MSE of normalized CFO of algorithm [92] (Vandebeek) with $|\epsilon| \leq 0.5$ under COST207-RA model

with

$$P(\theta) = \sum_{n=0}^{N/2-1} r^*(n+\theta) r(n+\theta+N/2) \tag{3.85}$$

and

$$R(\theta) = \sum_{n=0}^{N/2-1} |r(n+\theta)|^2, \tag{3.86}$$

where N is the length of one training symbol, $r(n)$ is the received signal. The timing symbol estimation is defined by

$$\hat{\theta} = \arg\max_{\theta} M(\theta). \tag{3.87}$$

Based on this estimated position, a frequency synchronization algorithm is performed. In a first step, one estimates the fractional part of the CFO (i.e. $\hat{\epsilon}_f$) that is deduced from the argument of $P(\theta)$ at $\hat{\theta}$ as follows:

$$\hat{\epsilon}_f = \frac{1}{\pi} \arg\{P(\hat{\theta})\}. \tag{3.88}$$

The received signal is then compensated in the time domain by multiplying itself with $e^{-j2\pi\hat{\epsilon}_f n/N}$.

The integer part of the CFO ϵ_i is the index l that maximizes $B(l)$ given by

$$B(l) = \frac{|\sum_{k\in F} R^*_{1,k+2l} X^*(k) R_{1,k+2l}|^2}{2|\sum_{k,F} R^*_{2,k}|^2}, \tag{3.89}$$

where $R_{1,k+2l}$, $R_{2,k+2l}$ are the received symbols in the frequency domain (the signal has been compensated by the fractional part of the CFO) corresponding to the first and second training symbols, respectively. $X(k)$ is the known pilot of the second training symbol while F is the set of indices for even frequency components of the second training symbol.

For this algorithm, if the CP is placed at the beginning of the first training symbol as mentioned in [74], the metric given by (3.84) may result in a large deviation (equal to the CP length) due to the repetitions of the CP in the first and second halves of the training symbol (i.e. the CP is repeated two times). In [10], $M(\theta)$ is replaced by $M'(\theta)$ given by

$$M'(\theta) = \frac{1}{N_g + 1} \sum_{n=0}^{N_g} |M(\theta - n)|^2, \tag{3.90}$$

where N_g is the length of CP, $M(\theta)$ is given in equation (3.84). The term $M(\theta - n)$ determines the beginning of the packet with the CP given up, if using $M(\theta + n)$, i.e. we will determine the beginning of the packet with the CP included.

To implement the time and frequency synchronization jointly with channel estimation, a multistage algorithm was proposed in [59]. A training symbol containing L_{minn} identical parts with K samples for each.

First, the symbol timing θ is estimated by

$$\hat{\theta} = \arg\max_{\theta} M_{minn}(\theta), \tag{3.91}$$

where $M_{minn}(\theta)$ is given in equation (3.21) (see Section 3.2.2.1).

To determine the CFO, the authors follow the frequency synchronization strategy mentioned in [61] and [44] given by

$$\hat{\epsilon} = \frac{L}{2\pi} \sum_{m=1}^{H} \omega(m)\varphi(m), \tag{3.92}$$

where

$$\omega(m) = 3\frac{(L-m)(L-m+1) - H(L-H)}{H(4H^2 - 6LH + 3L^2 - 1)}, \tag{3.93}$$

$$\varphi(m) = \arg\{R_r(m)\} - \arg\{R_r(m-1)\}, \tag{3.94}$$

with

$$R_r(n) = \frac{1}{N - mK} \sum_{n=mK}^{N-1} r^*(n - mK)r(n), \tag{3.95}$$

H is a design parameter satisfying $1 \leq H \leq L - 1$ ($H = L/2$ in this reference), $0 \leq m \leq H$ and $r(n)$ is the received signal after the coarse time synchronization.

The remaining STO and channel estimation are then implemented according to a joint time and channel estimation algorithm based on LS criterion as proposed in reference [94] (see Section 3.2.2.1).

To finish this section, we introduce a low complex scheme for the joint timing and integer frequency detection by using a cross-correlation function as mentioned in [54] [11]. First the symbol timing estimation $\hat{\theta}$ is the index maximizing the absolute value of the following CCF:

$$Z(\theta) = \sum_{n=0}^{N-1} r(n+\theta)s^*(n), \tag{3.96}$$

where $s(n)$ is the training sequence of N samples.

The integer part of the CFO is defined as follows:

$$\hat{\epsilon}_I = \arg \max_{-N/2 \leq k \leq N/2} I(\hat{\theta}, k), \tag{3.97}$$

where

$$I(\hat{\theta}, k) = \Big| \sum_{n=0}^{N-1} r(n+\hat{\theta})s^*(n)e^{-j2n\pi k/N} \Big|. \tag{3.98}$$

Note that (3.97) is actually the form of the periodogram function given in equation (3.76).

3.4.2.2 Training sequence recommended by the IEEE 802.11a standard

In [57], adapted to the IEEE 802.11a standard, an algorithm for time and frequency synchronization is proposed. First, the coarse estimation of the arrival time of the received signal is given by

$$\hat{\theta} = \arg \max_{\theta} \Big| \sum_{n=0}^{L_{CTS}-1} r^*(n+\theta)r(n+\theta+L_S) \Big|, \tag{3.99}$$

where L_S is the period duration of the STF, L_{CTS} is the length of the computation window and $r(n)$ is the received signal containing the symbol timing and the CFO parameters.

The received signal after this stage is expressed by

$$r_c(n) = \sum_{i=0}^{L-1} x(n-i-\Delta\theta)e^{\frac{j2\pi\epsilon(n-\Delta\theta)}{N}} + g(n), \tag{3.100}$$

where $\Delta\theta$ is the remaining time offset.

Next, a frequency synchronization algorithm based on CFS and FFS stages is performed to estimate ϵ_c. The estimation of the CFO is defined as $\hat{\epsilon} = \hat{\epsilon}_c + \hat{\epsilon}_f$ with

$$\hat{\epsilon}_c = \frac{N}{2\pi L_S} \arg\Big\{ \sum_{n=0}^{L_{CFS}-1} r_c^*(n) r_c(n + L_S) \Big\} \tag{3.101}$$

and

$$\hat{\epsilon}_f = \frac{N}{2\pi L_L} \arg\Big\{ \sum_{n=0}^{L_{FFS}-1} r_f^*(n) r_f(n + L_L) \Big\}, \tag{3.102}$$

where $r_f(n) = r_c(n) e^{-j2\pi\hat{\epsilon}_c n/N}$, L_L is the period duration of one LTF repetition, L_{CFS} and L_{FFS} are the lengths of the computation window.

Subsequently, the remaining time offset (i.e. $\Delta\theta$) of the received signal is estimated by the index at which the value of

$$S(\Delta\theta) = \frac{|a(\Delta\theta)|^2}{(b(\Delta\theta)^2)} \tag{3.103}$$

exceeds a threshold, with $a(\Delta\theta) = \sum_{n=0}^{N/2-1} r(n + \Delta\theta) r^*(n + \Delta\theta + N)$ and $b(\Delta\theta) = \sum_{n=0}^{N/2-1} |r(n + \Delta\theta)|^2$, where $r(n)$ is received signal, the frequency offset of which has been compensated by $\hat{\epsilon}_c + \hat{\epsilon}_f$. Here $N = 64$ and this means that the algorithm employs only one half of one LTF repetition of the standard.

In reference [16], similar to [57], but after the CFO of the received signal is compensated with $\hat{\epsilon} = \widehat{\epsilon}_c + \widehat{\epsilon}_f$, the fine time synchronization stage is carried out using the cross-correlation function between the received signal and a part of LTF (32 of 128 samples) of the standard as follows:

$$\Delta\widehat{\theta} = \arg \max_{\Delta\theta \in \mathbf{\Lambda}} \{|C(\Delta\theta)|^2\}, \tag{3.104}$$

where $\mathbf{\Lambda}$ is the set of possible positions and

$$C(\Delta\theta) = \sum_{n=0}^{N/2-1} g_{LTF}^*(n) r(n + \Delta\theta),$$

where $g_{LTF}(n)$ is the known LTF samples.

The algorithms based on training sequence developed in [16] not only have low computational complexity but also are adapted to the IEEE 802.11a standard. We simulate this algorithm which will be used as a reference to compare with our algorithms in the rest of this thesis. Simulation results are shown in Figures 3.16 and 3.17. The simulation parameters are taken from Table. 3.2 with the COST207-RA channel model. In addition, the normalized CFO ϵ is taken randomly according to a uniform distribution from the range $[-0.6, 0.6]$ (according to the tolerance of the

oscillator in the IEEE 802.11a standard) and the symbol timing θ is also randomly introduced according to a uniform distribution.

Figure 3.16 measures the PSF of the transmitted physical packet versus the SNR for the case of time deviation (between the true symbol timing and its estimation) equal to 0 and time deviation belonging to $[0, 4]$. The reason for accepting the deviation up to 4 samples is related to the channel model and the cyclic prefix length and will be further explained in the next chapter.

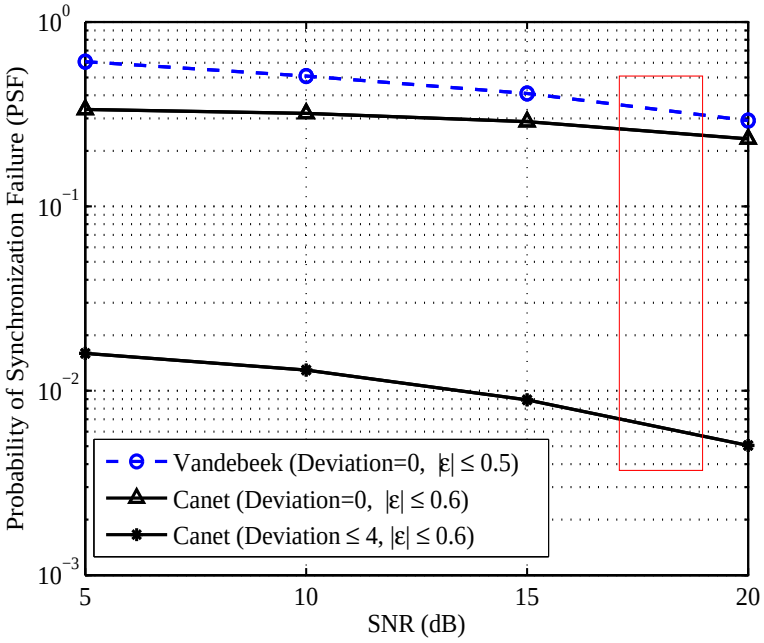

Figure 3.16. PSF of algorithms [92] (Vandebeek) and [16] (Canet) (the rectangular box represents the operating area of the 802.11a)

The curves of Figure 3.17 illustrate the MSE between the true CFO and its estimate ($E\{|\epsilon - \hat{\epsilon}|^2\}$) versus SNR. The results show that even if the symbol timing (i.e. θ) has been estimated according to time synchronization algorithm, the MSE is very close to a perfect time synchronization (i.e. that we set $\theta = 0$).

Table 3.7 summarizes the algorithms reviewed in Section 3.4.

3.5 Conclusion

In this chapter, we presented the impact of STO and CFO on the performance of the OFDM system. To estimate parameters of STO and CFO, many time and frequency synchronization schemes have been developed in the literature. The most common algorithms have been described in this chapter. Moreover, some of them have been

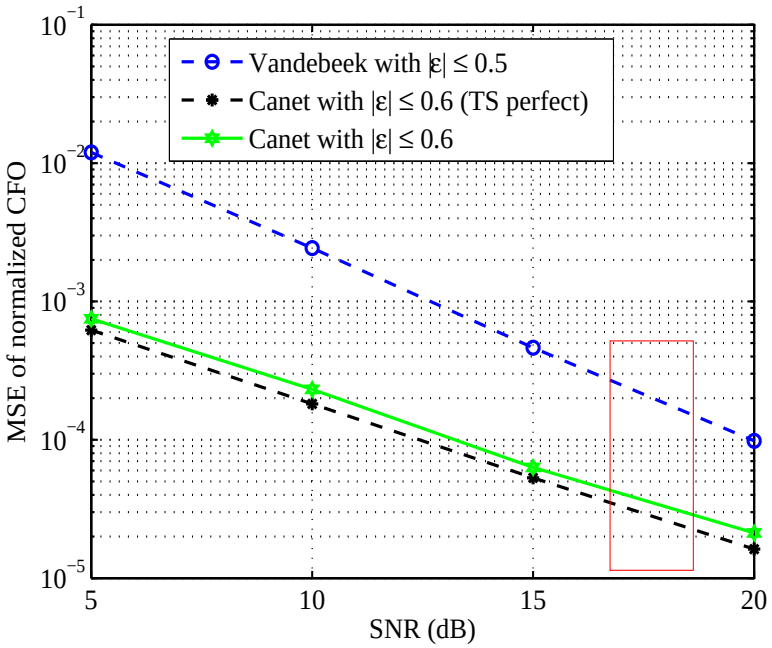

Figure 3.17. MSE of normalized CFO of algorithms [92], [16]

Table 3.7. Time and frequency synchronization algorithms

Reference	**Tool**	**DA/NDA**	**Adapted to standard**	**Type of data**	**Domain**
[92],[78]	ML	NDA	No	Cyclic Prefix	Time
[81], [74], [10]	ACF/CC	DA	No	Long training symbols	Time/ Frequency
[57]	ACF	DA	Yes	STF/LTF	Time
[16]	ACF/CCF	DA	Yes	STF/LTF	Time
[11]	CCF/ Periodgram	DA	No	Long training symbols	Time/ Frequency
[59]	ACF/ Joint with CE	DA	No	Long training symbols	Time

simulated to evaluate their performance in terms of probability of synchronization failure (PSF) or mean square errors (MSE).

CHAPTER 4

Time synchronization algorithms

Contents

4.1 Introduction

Let us review the requirement of time synchronization in OFDM system. An OFDM physical packet consists of multiple OFDM symbols concatenated in the time domain. At the receiver, before transformed to the frequency domain using the FFT function, the boundaries between the OFDM symbols need to be determined. In practical wireless communication environments, locating the exact boundaries between the OFDM symbols is often difficult due to the multipath channel as well as the noise effect. Otherwise, incorrect identification of boundaries between OFDM symbols results in the the appearance of ISI and ICI which seriously degrade the system performance (see Chapter 3). To deal with the problem, accurate time synchronization algorithms are required at the receiver.

As described in Chapter 3, a time synchronization process can be performed by relying either on some redundancy in the available information (i.e. Non-Data-Aided (NDA) techniques) or on the training sequence (i.e. Data-Aided (DA) techniques). The NDA algorithms employ the Cyclic Prefix (CP) that is the copy of a part of each OFDM symbol. These algorithms have low accuracy because there is usually an ISI area included in the CP interval. However, they achieve a high spectral efficiency since the transmission of training symbol is not required. This is in contrast to the DA algorithms that obtain higher performance but at the cost of a lower spectral efficiency. Due to the better performance, the trend is to use the DA techniques. The existing DA-based algorithms rely purely on training sequences proposed by authors or on the preamble specified by the standards (as in IEEE 802.11a/b/g/n...) while the exploitation of any additional redundancy which may be available (as for the NDA algorithms) has not been considered.

To combine the advantages from the NDA and DA-based algorithms, we propose time synchronization algorithms which make use of both the IEEE 802.11a preamble and also of the redundant information introduced by this standard. Specifically, in addition to the 802.11a preamble composed of the STF and LTF commonly used, the proposed algorithms exploit the SIGNAL field of the IEEE 802.11a standard at physical layer since its unknown parts are predictable via the Request to Send (RtS) control frame when the Carrier Sense Multiple Access with Collision Avoidance (CSMA/CA) mechanism is activated. Next, we take full advantage of the mechanism by employing the channel information obtained via the RtS control frame reception as additional information for time synchronization of DATA frame ("DATA frame or packet" is used to distinguish the data frames from the

control ones). To further improve the time synchronization performance, we finally develop a timing metric in presence of all Channel Estimation Errors (CEE). For each algorithm, simulation results are provided. Simulations are performed under two channel models that are COST207-RA and BRAN A and confirm the improved performance of the proposed algorithms.

For more convenience, for the rest of this thesis, the discrete received signal in time domain is denoted by $r_\Delta(n)$ instead of $r(n)$ given in (2.8).

4.2 Time synchronization algorithm using the SIGNAL field

To improve the performance of the time synchronization algorithms summarized in Table 3.4 (see Chapter 3), this section presents a time algorithm compliant with the IEEE 802.11a standard. This algorithm is performed in two stages: coarse and fine time synchronization, as shown in Figure 4.1. In the coarse time synchronization stage we propose to incorporate an additional synchronization step using the SIGNAL field, presented by the block as "SIGNAL-based CCF" in Figure 4.1. In other words, the traditional 802.11a preamble is replaced by a new preamble (see Figure 4.2). In addition, the fine synchronization stage "LTF-based MMSE' is then carried out jointly with the channel estimation based on Minimum-Mean-Squared Error (MMSE) criterion where the true channel is approximated according to a Least Square (LS) technique rather than using the PDP function as proposed in [87].

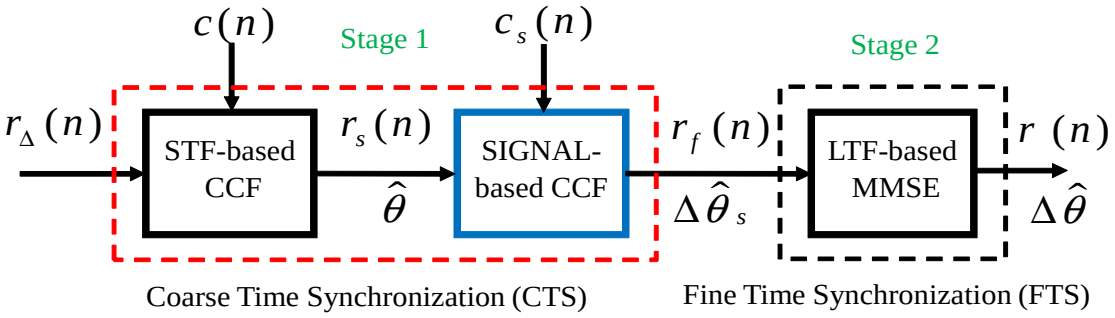

Figure 4.1. Time synchronization algorithm using SIGNAL field (SIGNAL-MMSE)

The underlying idea of our algorithm is based on specific properties of the headers of the frames, and requires a precise characterization of the various parts of the SIGNAL field of the 802.11a physical frame as described below.

4.2.1 A new preamble conform to the IEEE 802.11a standard

The objective of this section is to determine the two main parts of the SIGNAL field (i.e. "RATE" and "LENGTH") as shown in Figure 4.2 in order to be used as

additional known information by the receiver.

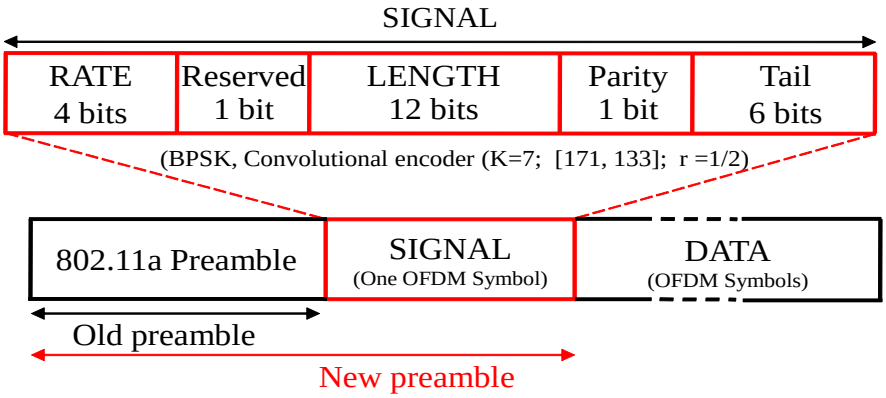

Figure 4.2. SIGNAL field specified by the IEEE 802.11a standard

These subfields are mainly used to inform the receiver about the transmission rate and the length of the physical packet, respectively. They have also been exploited for robust transmission issues. The RATE and the LENGTH bitstreams are predictable at the reception side as explained below.

Assume that the CSMA/CA medium reservation procedure is triggered. If any transmitter in a wireless network wishes to send a physical packet without collisions with other stations, it initiates the process by sending a RtS control frame (structure of which is shown in Figure 4.4) to ask the receiver if it is available [29] (see Figure 4.3). If it is the case, the receiver performs a rate adaptation (link adaptation or autorate) algorithm by measuring the SNR level of the received RtS frame to estimate the channel conditions [55], [37], [77], [77], [66]. Then it replies with a Clear to Send (CtS) control frame (see Figure 4.4): (i) to allow other stations to update their Network Allocation Vector (NAV) with the information contained in the duration field of the CtS frame; (ii) to inform other stations of its unavailability to receive information coming from other stations during a NAV period; and (iii) to suggest to the transmitter a transmission rate that the sender should use to transmit its physical data packet. Therefore the receiver has the knowledge of the transmission rate corresponding to the value of the RATE subfield of the SIGNAL field. From the RATE value, the unknown LENGTH subfield of the SIGNAL is deduced according to the relationship given in (4.2) [2].

Under assumption that the RATE field is known, to predict the LENGTH field (in octets), the knowledge of the required time to transmit the physical frame,

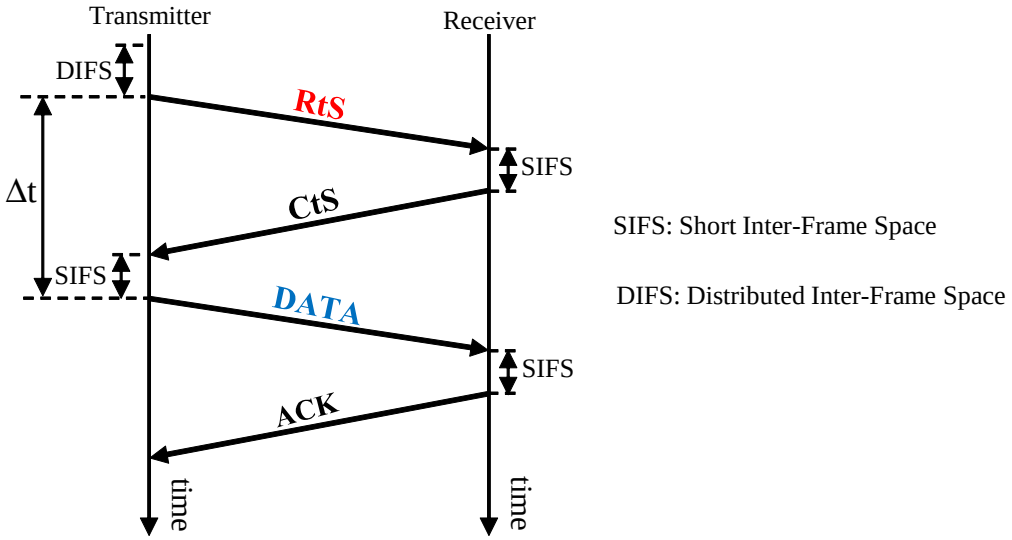

Figure 4.3. RtS/CtS handshake with active CSMA/CA mechanism

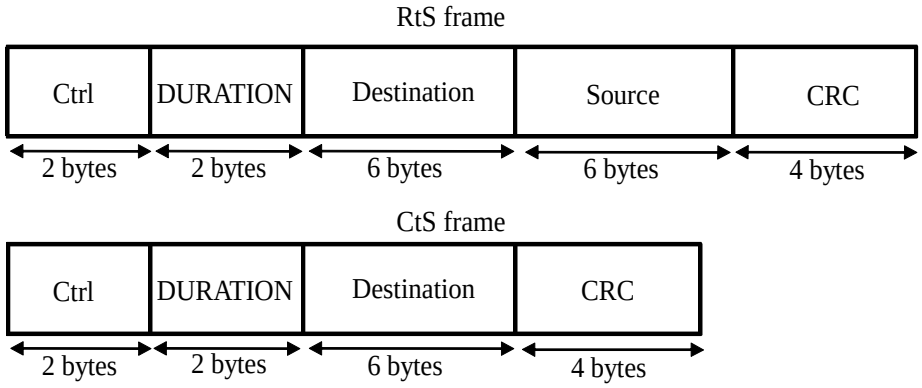

Figure 4.4. Control frame formats

T_{packet}, is necessary since it is given by the following relationship:

$$\text{LENGTH} = \text{RATE} \times \frac{(T_{\text{packet}} - T_{\text{pre}} - T_{\text{SIGNAL}} - (T_{\text{symb}}/2)) - 22}{8}, \tag{4.1}$$

where T_{pre}, T_{SIGNAL} and T_{symb} are the durations of the preamble, the SIGNAL field and the OFDM symbol, respectively. These durations are known at the receiver and given by Table 4.1. The T_{packet} is deduced from the information provided by the RtS control frame namely the DURATION field (in micro-seconds) [32]:

$$\text{DURATION} = 3T_{\text{SIFS}} + T_{\text{CtS}} + T_{\text{ACK}} + T_{\text{packet}}, \tag{4.2}$$

where T_{SIFS} is the duration (in micro-seconds) of a Short Inter-Frame Space, T_{CtS} and T_{ACK} are the durations of the required time to transmit the frame CtS and

frame ACK respectively. They are also known parameters (see Table 4.1). This strategy allows the receiver to deduce the SIGNAL field bitstream.

Table 4.1. Time-related parameters according to IEEE 802.11a standard at a code rate 6 Mbps

Parameter	Definition	Value
T_{pre}	Physical packet preamble duration	$16\mu s$
T_{SIGNAL}	SIGNAL field duration	$4.0\mu s$
T_{symb}	OFDM symbol interval	$4.0\mu s$
T_{SIFS}	SIFS duration	$16\mu s$
T_{RtS}	RtS physical frame duration	$52\mu s$
T_{CtS}	CtS physical frame duration	$44\mu s$

The remaining subfields of the SIGNAL field consist of the Reserved, Parity and Tail fields. The Reserved subfield is reserved for the future and can be considered as known while the Parity is an even parity computed from the previous subfields (RATE, Reserved and LENGTH). 6 zero tail bits are appended to close the frame. The SIGNAL field composed of 24 bits is now fully predicted.

According to the IEEE 802.11a standard, the SIGNAL field bitstream undergoes a modulation process before being transmitted over the channel. The modulation is characterized by parameters in Figure 4.2 and was described in Section 2.1.1 of Chapter 2 (a convolutional encoder with a constraint length $K = 7$, a polynomial generator $[171, 133]$, a code rate $R = 1/2$; and BPSK modulation). The resulting SIGNAL stream, denoted as $c_s(n)$, is thus composed of 80 samples (16 for the cyclic prefix and 64 for the useful part).

4.2.2 First stage: Coarse time synchronization

This first stage (see Figure 4.1) is performed in two steps as described below.

4.2.2.1 Coarse synchronization using STF

This step concerns the block "STF-based CCF". Symbol timing is estimated using the cross-correlation between the received signal $r_\Delta(n)$ and the known bitstream $c(n)$ corresponding to the first ten repetitions of the preamble STF. The CCF is given by:

$$Z(\theta) = \sum_{n=0}^{L_{\mathrm{STF}}-1} c^*(n) r_\Delta(n+\theta), \tag{4.3}$$

where L_{STF} is the number of samples of $c(n)$. Then, the symbol timing is coarsely estimated by

$$\hat{\theta} = \arg\max_{\theta} |Z(\theta)|. \tag{4.4}$$

4.2.2.2 Coarse synchronization using SIGNAL field

This step concerns the block "SIGNAL-based CCF". Assume that the received signal after the step of "Coarse synchronization using STF" is

$$r_s(n) = \sum_{i=0}^{L-1} h(i)x(n-i-\Delta\theta_s)^{j\frac{2\pi\epsilon(n-\Delta\theta_s)}{N}}, \tag{4.5}$$

where L is the number of channel taps, and $\Delta\theta_s = \theta - \hat{\theta}$.

As described in Section 4.2.1, when the CSMA/CA mechanism is activated, the SIGNAL field specified in the 802.11a physical frame can be used at the receiver as a reference sequence. Therefore, in this section we exploit the SIGNAL field to compensate for the remaining time offset in coarse synchronization $\Delta\theta_s$, as shown in Figure 4.1.

Define a set $\Theta = \{\Delta\theta_s^{(k)} | k = -K, \ldots, K\}$, where K is a predefined number. Then, for a given $\Delta\theta_s^{(k)}$, we compute the cross-correlation between $r_s(n)$ and the known SIGNAL field stream $c_s(n)$ as follows:

$$Z(\Delta\theta_s^{(k)}) = \sum_{n=0}^{L_{\mathrm{SIG}}-1} c_s^*(n) r_s(n+\Delta\theta_s^{(k)}), \tag{4.6}$$

where L_{SIG} is the combined length of the SIGNAL field. The remaining time offset is then estimated by

$$\widehat{\Delta\theta_s} = \arg\max_{\Delta\theta_s^{(k)}} |Z(\Delta\theta_s^{(k)})|. \tag{4.7}$$

Therefore the received signal with the remaining time offset is given by

$$r_s'(n) = \sum_{i=0}^{L-1} h(i)x(n-i-\Delta\theta)e^{j\frac{2\pi\epsilon(n-\Delta\theta)}{N}} + g(n), \tag{4.8}$$

where $\Delta\theta = \Delta\theta_s - \widehat{\Delta\theta_s}$ is the remaining time offset computed between the true symbol timing and its estimate.

This section focuses only on time synchronization and assumes a perfect knowledge of the frequency offset (i.e. ϵ is known). The frequency offset compensation is thus performed as follows: $r_s'(n)e^{-j\frac{2\pi\epsilon n}{N}}$. The received signal becomes

$$\begin{aligned} r_s''(n) &= \sum_{i=0}^{L-1} h(i)x(n-i-\Delta\theta)e^{j\frac{-2\pi\epsilon\Delta\theta}{N}} + g(n)e^{-j\frac{2\pi\epsilon n}{N}} \\ &= \sum_{i=0}^{L-1} h'(i)x(n-i-\Delta\theta) + g'(n), \end{aligned} \tag{4.9}$$

where $h'(i) = h(i)e^{j\frac{-2\pi\epsilon\Delta\theta}{N}}$ (with $0 \leq i \leq L-1$) and $g'(n) = g(n)e^{-j\frac{2\pi\epsilon n}{N}}$. Note that characteristic of mean and variance of $g'(n)$ does not change compared to $g(n)$. For simplicity, these terms are renamed as follows:

$$r_f(n) = \sum_{i=0}^{L-1} h(i)x(n-i-\Delta\theta) + g(n). \tag{4.10}$$

where $r_f(n)$, $h(i)$ and $g(n)$ are denoted as $r''_s(n)$, $h'(i)$ and $g'(n)$, respectively.

4.2.3 Second stage: Joint fine time synchronization and channel estimation based on MMSE algorithm

The second stage of the proposed algorithm, i.e. fine time synchronization (Figure 4.1), represented by the block "LTF-based MMSE" makes use of the LTF specified by the IEEE 802.11a standard to estimate the remaining time offset $\Delta\theta$ in equation (4.10). For convenience, $r_f(n)$ is expressed in the frequency-domain in matrix form as follows:

$$\mathbf{R}_f = \mathbf{XH} + \mathbf{G}, \tag{4.11}$$

where $\mathbf{R}_f$ is the received frequency-domain vector of size $N \times 1$ (FFT transform applied to $r_f(n)$). $\mathbf{G}$ is the noise vector of size $N \times 1$. $\mathbf{H}$ of size $N \times 1$ is the FFT transform of $\mathbf{h}$ and thus it contains parameter $\Delta\theta$.

First, a finite set $\mathbf{\Lambda}$ containing $2M+1$ time offsets is defined as follows $\mathbf{\Lambda} = \{\Delta\theta_m | m = -M, \ldots, M\}$. For a given value $\Delta\theta_m$, the CIR is then estimated in the frequency domain, based on MMSE, as follows [22]:

$$\hat{\mathbf{H}}_{\Delta\theta_m} = \mathbf{R_H}(\mathbf{R_H} + \frac{\sigma_g^2}{\sigma_x^2}\mathbf{I})^{-1}\widetilde{\mathbf{H}}_{\Delta\theta_m}, \tag{4.12}$$

where the $N \times 1$ vector $\widetilde{\mathbf{H}}_{\Delta\theta_m}$ is the LS channel estimate, σ_x^2 and σ_g^2 are, respectively, variances of the transmitted signal and the noise, $\mathbf{R_H}$ is the frequency-domain correlation matrix of the true channel, and $\mathbf{I}$ is the identity matrix. The LS channel estimate is given by

$$\widetilde{\mathbf{H}}_{\Delta\theta_m} = \mathbf{X}^{-1}\mathbf{R}_f, \tag{4.13}$$

where $\mathbf{R}_f$ is the received symbol vector in frequency domain and $\mathbf{X}$ is a diagonal matrix whose diagonal elements are the known LTF symbols.

To compute (4.12), the frequency-domain channel correlation matrix $\mathbf{R_H}$ is required. This matrix is defined as

$$\mathbf{R_H} = \mathbf{F}\mathbf{R_h}\mathbf{F}^H, \tag{4.14}$$

where $\mathbf{F}$ is the $N \times N$ FFT matrix, $\mathbf{F}^H$ is the conjugate transpose operator of matrix $\mathbf{F}$, $\mathbf{R_h} = E\{\mathbf{h}\mathbf{h}^H\}$ is correlation matrix of time domain true channel vector $\mathbf{h}$ (with $\mathbf{h} = (h(0), h(1), \ldots, h(N-1))$ and E is the expectation operator. $\mathbf{R_h}$ is expressed by

$$E\{\mathbf{h}\mathbf{h}^H\} = E\begin{pmatrix} h(0)h^*(0) & h(0)h^*(1) & \cdots & h(0)h^*(N-1) \\ h(1)h^*(0) & h(1)h^*(1) & \cdots & h(1)h^*(N-1) \\ \vdots & \vdots & \vdots & \vdots \\ h(N-1)h^*(0) & h(N-1)h^*(1) & \cdots & h(N-1)h^*(N-1) \end{pmatrix}. \tag{4.15}$$

To compute the elements of $E\{\mathbf{h}\mathbf{h}^H\}$, two cases are possible:

- If Doppler frequency is introduced (i.e. there is a relative speed between the transmitter and the receiver) and the Doppler spectrum is modeled as Jakes, then according to theory of the Rayleigh fading [22]:

$$E\{h(i)h^*(i+m)\} = J_0(2\pi f_d m T_s)\}, \tag{4.16}$$

  where $J_0(x)$ is the zero-order Bessel function of first kind, T_s is the sampling time and f_d is the Doppler frequency.

- If there is no Doppler frequency (or the relative speed between the transmitter and the receiver is very small) and the channel coefficients are statistically independent each other [49] then $E\{h(i)h^*(i+m)\} = 0$ with $\forall m \neq 0$ and $E\{\mathbf{h}\mathbf{h}^H\}$ becomes:

$$E\{\mathbf{h}\mathbf{h}^H\} = E\begin{pmatrix} h(0)h^*(0) & 0 & \cdots & 0 \\ 0 & h(1)h^*(1) & \cdots & 0 \\ \vdots & \vdots & \vdots & \vdots \\ 0 & 0 & \cdots & h(N-1)h^*(N-1) \end{pmatrix} \tag{4.17}$$

  or

$$E\{\mathbf{h}\mathbf{h}^H\} = E\begin{pmatrix} |h(0)|^2 & 0 & \cdots & 0 \\ 0 & |h(1)|^2 & \cdots & 0 \\ \vdots & \vdots & \vdots & \vdots \\ 0 & 0 & \cdots & |h(N-1)|^2 \end{pmatrix}. \tag{4.18}$$

In our work, the (complex valued) channel model is considered as being slowly-varying with time and the channel coefficients are independent of each other in pairs, therefore, the latter case is retained.

To calculate (4.18), rather than using the PDP function, where the true value is difficult to obtain exactly, we propose to estimate $\mathbf{h}$ using LS approximation as follows:

$$\mathbf{R_h} = E\{\mathbf{h}\mathbf{h}^H\} \approx E\{\tilde{\mathbf{h}}_{\Delta\theta_m}\tilde{\mathbf{h}}^H_{\Delta\theta_m}\}, \tag{4.19}$$

where $\tilde{\mathbf{h}}_{\Delta\theta_m}$ is the inverse Fourier transform of $\tilde{\mathbf{H}}_{\Delta\theta_m}$. $\mathbf{R_h}$ is then written as follows:

$$\mathbf{R_h} \approx \begin{pmatrix} E\{|\widetilde{h}_{\Delta\theta_m}(0)|^2\} & 0 & \cdots & 0 \\ 0 & E\{|\widetilde{h}_{\Delta\theta_m}(1)|^2\} & \cdots & 0 \\ \vdots & \vdots & \vdots & \vdots \\ 0 & 0 & \cdots & E\{|\widetilde{h}_{\Delta\theta_m}(N-1)|^2\} \end{pmatrix}. \tag{4.20}$$

Next, for each time offset $\Delta\theta_m$ in $\mathbf{\Lambda}$, we obtain a time-domain estimate $\hat{\mathbf{h}}_{\Delta\theta_m}$ of the CIR. Among the M estimates, we consider the $\Delta\theta_m$ that satisfies the following condition:

$$|\hat{h}_{\Delta\theta_m}(0)| > \beta \max_{\Delta\theta_m} |\hat{h}_{\Delta\theta_m}(0)|, \tag{4.21}$$

where β is a given threshold defined depending on the noise level and type of channel model. Therefore, the set $\mathbf{\Lambda}$ becomes $\mathbf{\Gamma}$

$$\mathbf{\Gamma} = \{\omega_0, \ldots, \omega_{M'}; \quad M^{'} \leq 2M\}. \tag{4.22}$$

Finally, the remaining time offset is estimated as

$$\widehat{\Delta\theta} = \arg\max_{\omega_{m'}}\{Z(\omega_{m'})\}, \tag{4.23}$$

where $Z(\omega_{m'})$ is the energy associated to the estimated CIR $\hat{\mathbf{h}}_{\omega_{m'}}$ and is given by

$$Z(\omega_{m'}) = \sum_{n=0}^{L-1} |\hat{h}_{\omega_{m'}}(n)|^2. \tag{4.24}$$

with L the length of channel.

4.2.4 Numerical results

This section provides the performance of time synchronization algorithms described above. In particular, we compare to the following five algorithms:

i) **Algorithm 1 (Canet)** [16] (see Table 3.7): This algorithm uses the auto-correlation function based on STF for the coarse time synchronization stage and the cross-correlation function based on the LTF in the fine time synchronization.

ii) **Algorithm 2 (LS)** [94] (see Table 3.4): This algorithm uses STF for coarse time synchronization and LS for channel estimation in fine time synchronization.

iii) **Algorithm 3 (MMSE)** [87] (see Table 3.4): This algorithm is the same as Algorithm 2, but MMSE is used instead of LS for channel estimation.

iv) **Algorithm 4 (SIGNAL-LS)**: This algorithm additionally uses the SIGNAL field for coarse time synchronization while the fine time synchronization is the same as in Algorithm 2.

v) **Algorithm 5 (SIGNAL-MMSE)**: This algorithm is similar to Algorithm 4, but MMSE criterion is used for channel estimation instead of LS.

The simulation parameters of the communication system (see Figure 2.3) are specified in Table. 3.2 (see Section 3.2.2.1, Chapter 3) in accordance with the IEEE 802.11a standard [2]. Simulations are performed under two channel models COST207-RA and BRAN A (i.e. CH-A). The normalized CFO ϵ is randomly taken from the range $[-0.6, 0.6]$ (specified by the standard). Note that the CFO is compensated after the CTS stage (before the FTS stage for each algorithm where the CFO value is assumed to be perfectly known at the receiver.

First we discuss the performance of the algorithms in the channel COST207-RA corresponding to figures 4.5, 4.6 and 4.7. The PFS versus SNR is shown in Figure 4.5 with no deviation between the true symbol timing and its estimation (i.e. $\theta - \hat{\theta} = 0$). It is also possible to accept physical packets when the arrival time is estimated after the true position with a deviation (different from zero) due to the use of CP [63]. Here we accept the packets with a delay time no more than 4 samples [16], if we consider the $\widehat{\theta}_{new} = \widehat{\theta} - 4$. This timing delay is tolerated at least for the COST207-RA channel since the CP of the OFDM symbol and the maximum delay of this channel response are respectively equal to 16 and 13 samples and the average power of tap 0 is one hundred times larger than the one of tap 12 (i.e. $P(0) = 0$ dB while $P(12) = -20$ dB, see Table 2.1). In this case, although there exists a phase offset, the orthogonality of subcarrier frequency components is completely preserved by using a single-tap frequency-domain equalizer [67]. Fig 4.6 illustrates the PSF of algorithms for a deviation no more than 4.

It is clear that in both figures, the proposed Algorithm 5 (SIGNAL-MMSE) is the best in terms of PSF. Indeed, with no deviation case, for a given $SNR = 17.5$ dB (the operating mode of the IEEE 802.11a standard), the PSF for Algorithms 1, 2, 3, 4 and 5 are respectively 0.26; 0.11; 0.086; 0.084 and 0.055.

We can also see that when the MMSE (Algorithm 3) is performed, the performance in terms of PSF is better than that of LS (Algorithm 2). Indeed the algorithm based on joint time synchronization and channel estimation depends heavily on the channel estimation. However when the channel estimation technique is based on

the MMSE, the performance in terms of MSE of channel estimate is better than the LS as illustrated in Figure 4.7. For instance, the MSE of channel estimation related to LS (Algorithm 2) at $SNR = 17.5$ dB is 1.5×10^{-3} while the MSE based on MMSE (Algorithm 3) is 7×10^{-4}.

The proposed Algorithms 4 (SIGNAL-LS) and 5 (SIGNAL-MMSE) significantly reduces the MSE as compared, respectively, with the conventional Algorithms 2 (LS) and 3 (MMSE). For example, for a given $SNR = 17.5$ dB, the MSE of channel estimate for Algorithm 3 (MMSE) and Algorithm 5 (SIGNAL-MMSE) are respectively 7×10^{-4} and 1.8×10^{-4}. These promising results are achieved by exploiting the SIGNAL field in the proposed algorithm. Indeed it helps to increase the accuracy of the signal detection performed by the CTS stage. Since the CTS stage is before the joint fine time synchronization and channel estimation, this results also in an improvement of the channel estimation.

Our algorithm also achieves the best performance when simulated in the BRAN A channel model as shown in Figure 4.8. However, compared with the case using the COST207-RA, the PSF with no deviation of algorithms under the BRAN A is higher. For example, at $SNR = 17.5$ dB with no deviation, the PSF of Algorithm 5, when the channel is considered as COST207-RA or BRAN A model, is respectively 0.084 or 0.11. This is explained by the fact that the COST207-RA contains a line of sight component, the power of which is much larger than the others paths, while there is no such component in the BRAN A model (see Chapter 2).

4.3 Joint time synchronization and channel estimation based on the MAP criterion

In the previous section, we presented the time synchronization algorithm exploiting the SIGNAL field of the physical frame of the IEEE 802.11a standard as an additional reference sequence to improve the coarse time synchronization. In order to increase the accuracy of the fine time synchronization, this section proposes to refine the time synchronization jointly with the channel estimation based on the MAP criterion based on the 802.11a preamble LTF. The idea has been inspired by the joint time synchronization and channel estimation algorithm proposed in [94]. The proposed algorithm is depicted on Figure 4.9 where the first CTS stage is based on the SIGNAL field as proposed in Section 4.2. Similar to Section 4.2, the CFO of the received signal after the CTS stage is compensated with a known CFO value by the receiver. The residual time offset $\Delta\theta$ from the CTS stage is estimated jointly with the MAP-based channel estimation in the following section.

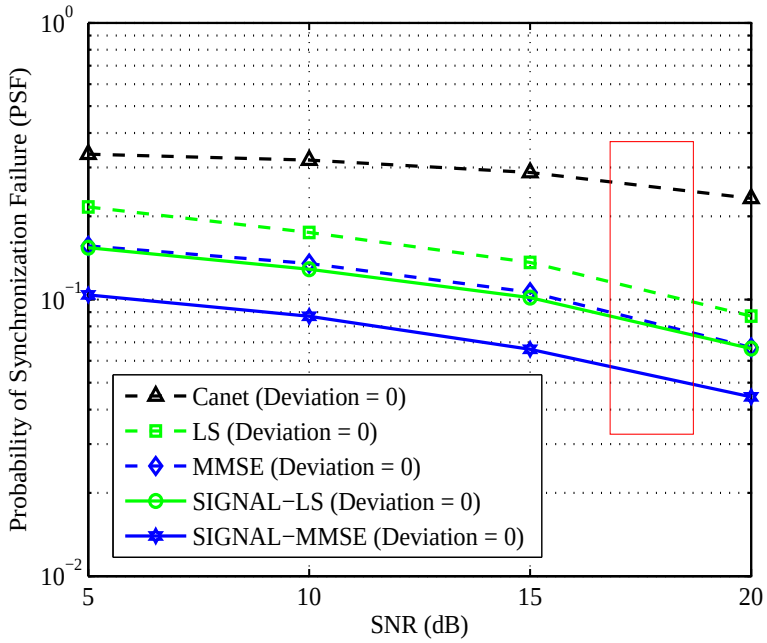

Figure 4.5. PSF of algorithms [16] (Canet), [94] (LS), [87] (MMSE) and the proposed algorithms exploiting the SIGNAL field with no deviation under COST207-RA channel model (the rectangular box represents the operating mode of the 802.11a)

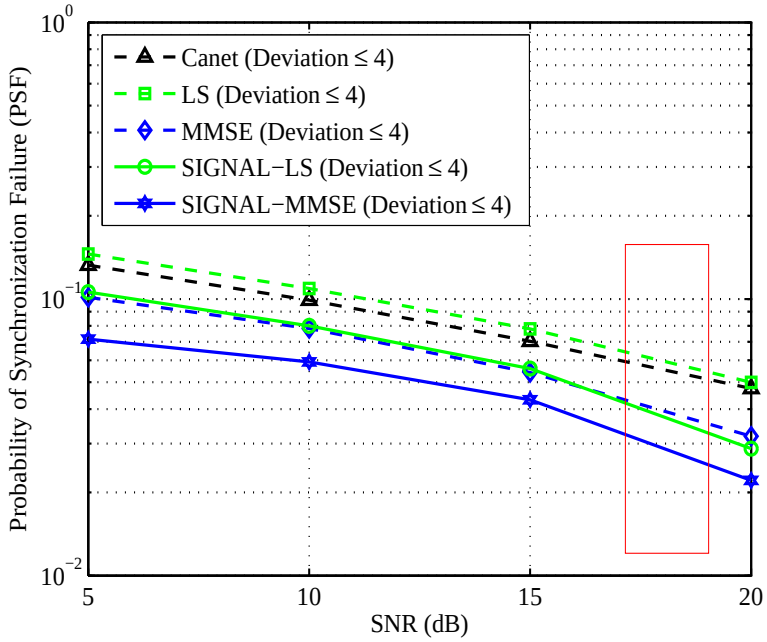

Figure 4.6. PSF of algorithms [16] (Canet), [94] (LS), [87] (MMSE) and the proposed algorithms exploiting the SIGNAL field with deviation less than 4 under COST207-RA channel model

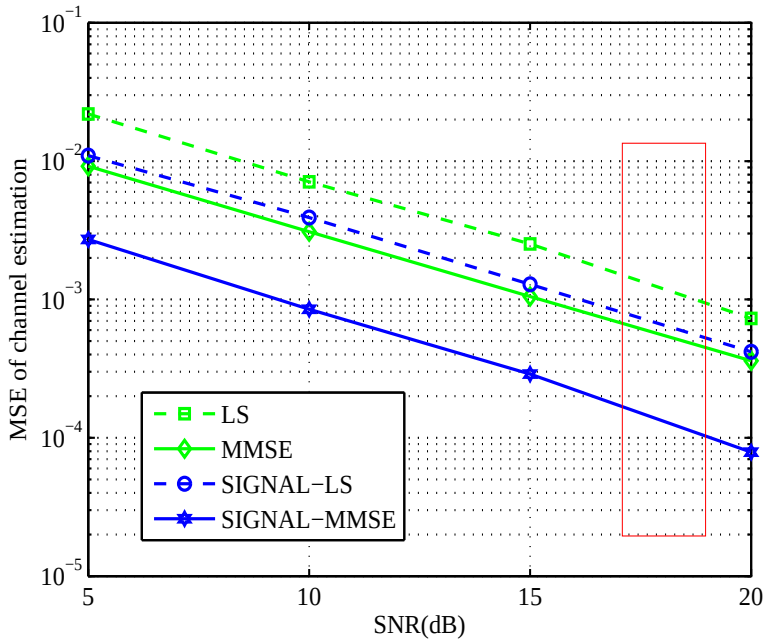

Figure 4.7. MSE of channel estimation of algorithms [94] (LS), [87] (MMSE) and the proposed methods exploiting the SIGNAL field with no deviation under COST207-RA channel model

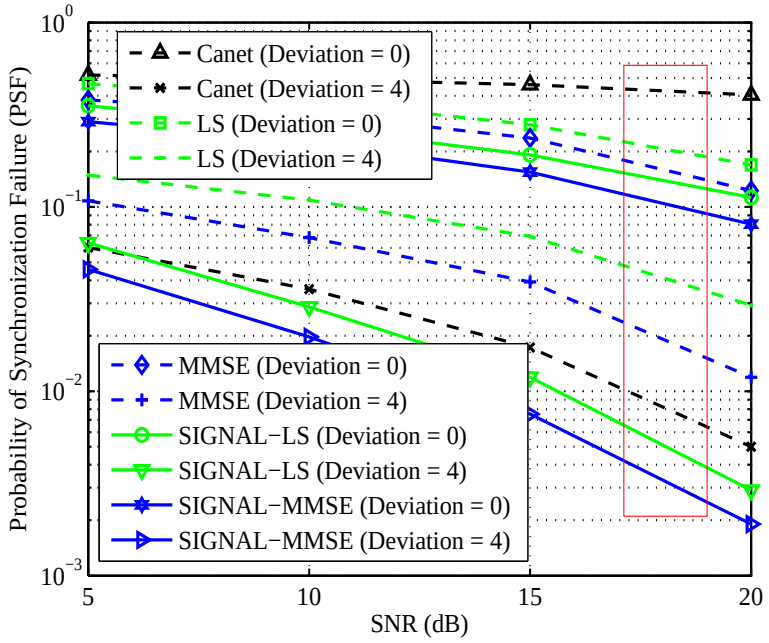

Figure 4.8. PSF of algorithms [16] (Canet), [94] (LS), [87] (MMSE) and the proposed algorithms exploiting the SIGNAL field under BRAN A (CH-A) channel model

4.3.1 The algorithm

The proposed time synchronization algorithm is summarized in Figure 4.9. The second stage of the algorithm is organized as follows. The received signal corresponding

to the LTF samples reads

$$r_f(n) = \sum_{i=0}^{L-1} h(i)x(n-i-\Delta\theta) + g(n), \tag{4.25}$$

where $\Delta\theta = \Delta\theta_s - \Delta\widehat{\theta_s}$ is the remaining time offset between the true symbol timing and its coarse estimate (using (4.7)).

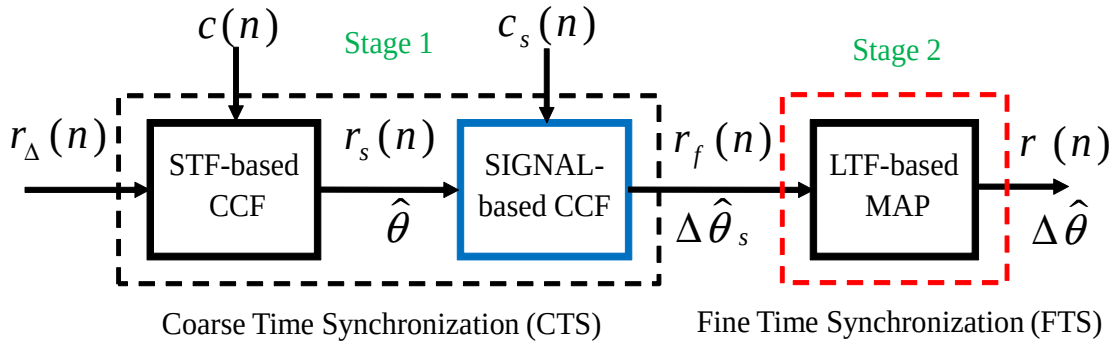

Figure 4.9. Time synchronization algorithm based on MAP criterion (SIGNAL-MAP)

For convenience, equation (4.25) is rewritten in a matrix form as follows:

$$\mathbf{r}_f = \mathbf{G}\mathbf{h}_{\Delta\theta} + \mathbf{g}, \tag{4.26}$$

with $\mathbf{r}_f$ is the $N \times 1$ received signal vector, $\mathbf{h}_{\Delta\theta}$ is the CIR $N \times 1$ vector ($N - L$ complex elements are added) following the Gaussian distribution, $\mathbf{g}$ is the Gaussian noise vector and $\mathbf{G} = \mathbf{F}^H\mathbf{X}\mathbf{F}$ with $\mathbf{F}$ the $N \times N$ FFT matrix and $\mathbf{X}$ the $N \times N$ diagonal matrix where the diagonal elements correspond to the known LTF symbols. $(\cdot)^H$ denotes the conjugate transpose operator.

Define a set $\mathbf{\Lambda}$ containing $2M + 1$ possible time offset values as follows $\mathbf{\Lambda} = \{-\Delta\theta_M, .., \Delta\theta_M\}$. For a given value $\Delta\theta_m \in \mathbf{\Lambda}$, the MAP estimator developed in [52] is used to estimate the corresponding $\mathbf{h}_{\Delta\theta_m}$ as follows:

$$\widehat{\mathbf{h}}_{\Delta\theta_m} = (\mathbf{G}^H\mathbf{G} + \sigma_g^2\mathbf{R}_\mathbf{h}^{-\mathbf{1}})^{-1}(\mathbf{G}^H\mathbf{r}_f + \sigma_g^2\mathbf{R}_\mathbf{h}^{-\mathbf{1}}\mu_h), \tag{4.27}$$

where $\mathbf{R}_\mathbf{h} = E\{\mathbf{h}\mathbf{h}^H\}$ is the autocorrelation matrix of $\mathbf{h}$, the true CIR vector. The channel is assumed to be complex, slowly time-varying. Therefore $\mathbf{R}_\mathbf{h}$ is a diagonal matrix requiring some knowledge of the true CIR coefficients. Just like in the previous section, rather than using the PDP function, (the true values are difficult to obtain exactly), $\mathbf{R}_\mathbf{h}$ is estimated by the following Least Squares process:

$$\mathbf{R}_\mathbf{h} = E\{\mathbf{h}\mathbf{h}^H\} \approx E\{\tilde{\mathbf{h}}_{\Delta\theta_m}\tilde{\mathbf{h}}_{\Delta\theta_m}^H\}, \tag{4.28}$$

We select among the $2M+1$ values in $\widehat{\mathbf{h}}_{\Delta\theta_m}$ obtained from (4.27), the subset that satisfies the following condition:

$$|\hat{h}_{\Delta\theta_m}(0)| > \beta \max_{\Delta\theta_i} |\hat{h}_{\Delta\theta_i}(0)|, \tag{4.29}$$

where β is a given threshold depending on the noise level and type of channel model. Therefore we get the new set $\mathbf{\Gamma}$ as

$$\mathbf{\Gamma} = \{\omega_0, \ldots, \omega_{M'}; \quad M^{'} \leq 2M\}. \tag{4.30}$$

The best time offset is deduced as

$$\Delta\widehat{\theta} = \arg\max_{\omega_{m'}} \{\sum_{n=0}^{L-1} |\hat{h}_{\omega_{m'}}(n)|^2\}. \tag{4.31}$$

4.3.2 Numerical results

To evaluate the performance of the proposed time synchronization algorithm, simulations are run on the COST207-RA (shown in Figures 4.10, 4.11, 4.12) and BRAN A (Figure 4.13) channel models and the results allow to compare the following time synchronization algorithms:

i) **Algorithm 1 (Canet)** [16]: In this algorithm the coarse time synchronization uses the auto-correlation function based on STF while the cross-correlation function based on the LTF is realized in fine time synchronization stage.

ii) **Algorithm 2 (MMSE)** [87]: This algorithm uses coarse time synchronization based on ten repetitions of the STF and then joint fine synchronization and channel estimation based on MMSE.

iii) **Algorithm 3 (MAP)**: This algorithm is the same as Algorithm 2, but MAP estimation is used instead of MMSE for channel estimation.

iv) **Algorithm 4 (SIGNAL-MMSE)** (mentioned in Section 4.2): This algorithm additionally uses the SIGNAL field for coarse time synchronization (apart from the use of ten STF repetitions) while fine time synchronization is the same as described in Algorithm 2.

v) **Algorithm 5 (SIGNAL-MAP)** (proposed in this section): This algorithm is similar to Algorithm 4, but MAP is used for channel estimation instead of MMSE criterion.

Simulation parameters identical to those used in Section 4.2 are used in this section. Figure 4.12 compares the MSE of the CIR estimation under the COST207-RA channel model. Clearly, using MAP for channel estimation provides better performance than using MMSE. For example, at SNR = 17.5 dB: MSE(MMSE) = 7×10^{-4},

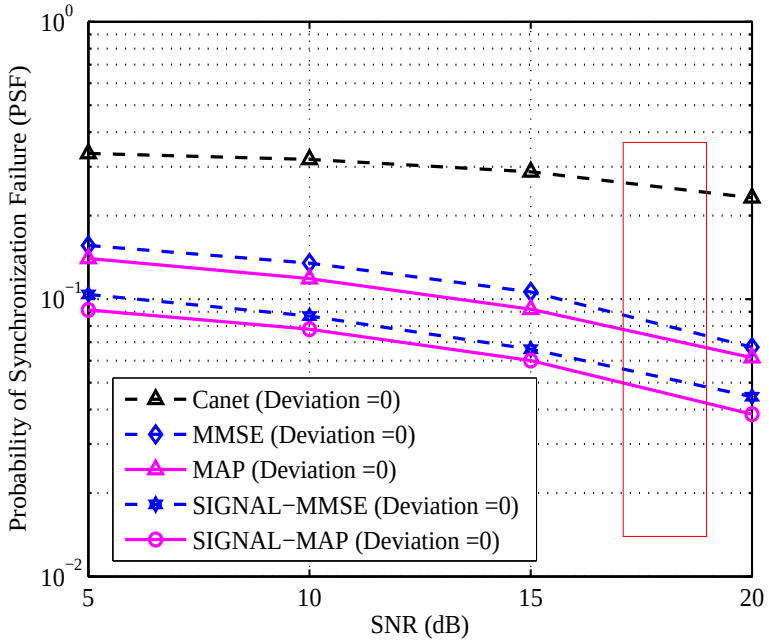

Figure 4.10. PSF of algorithms [16] (Canet), [87] (MMSE) and the proposed algorithms with no deviation under COST207-RA channel model (the rectangular box represents the operating area of the 802.11a)

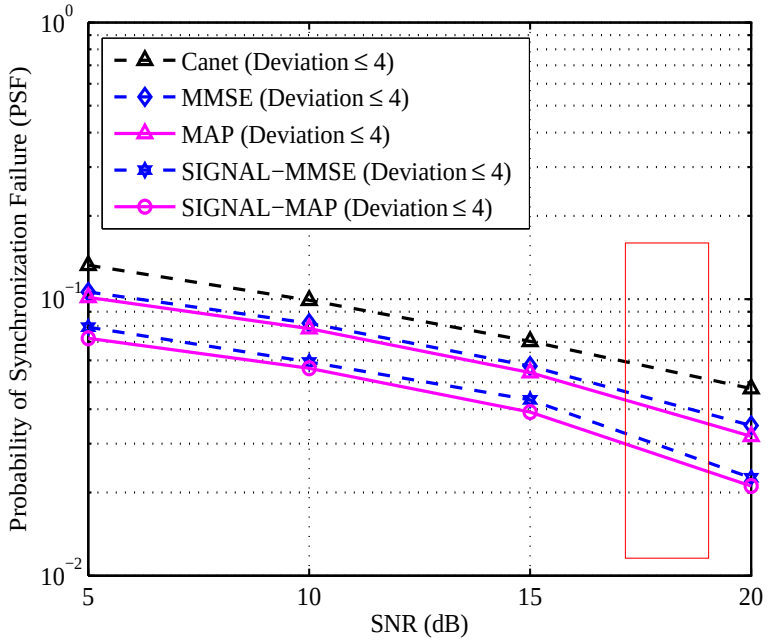

Figure 4.11. PSF of algorithms [16] (Canet), [87] (MMSE) and the proposed algorithms with deviation less than 4 under COST207-RA channel model

MSE(MAP) $= 6 \times 10^{-4}$, MSE(SIGNAL-MMSE) $= 1.8 \times 10^{-4}$ and MSE(SIGNAL-MAP) $= 1.5 \times 10^{-4}$.

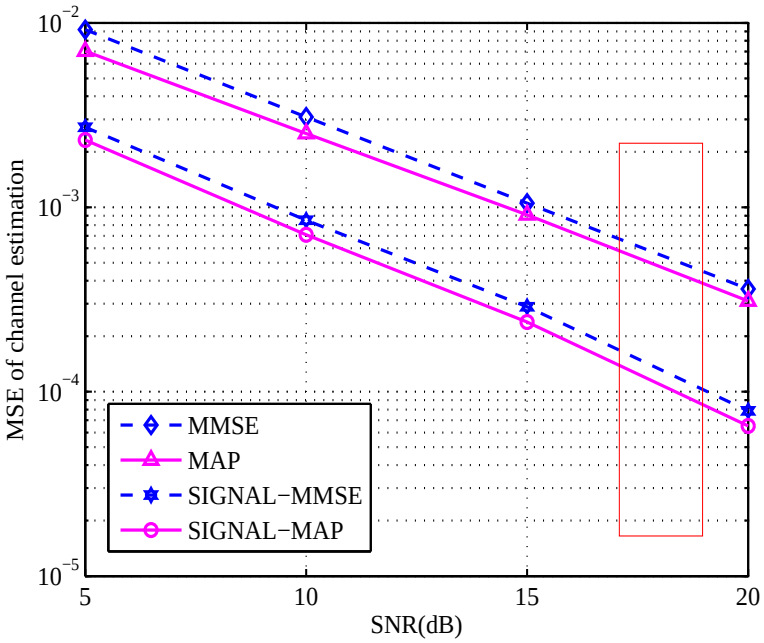

Figure 4.12. MSE of channel estimation of algorithms [16] (Canet), [87] (MMSE) and the proposed algorithms under COST207-RA channel model

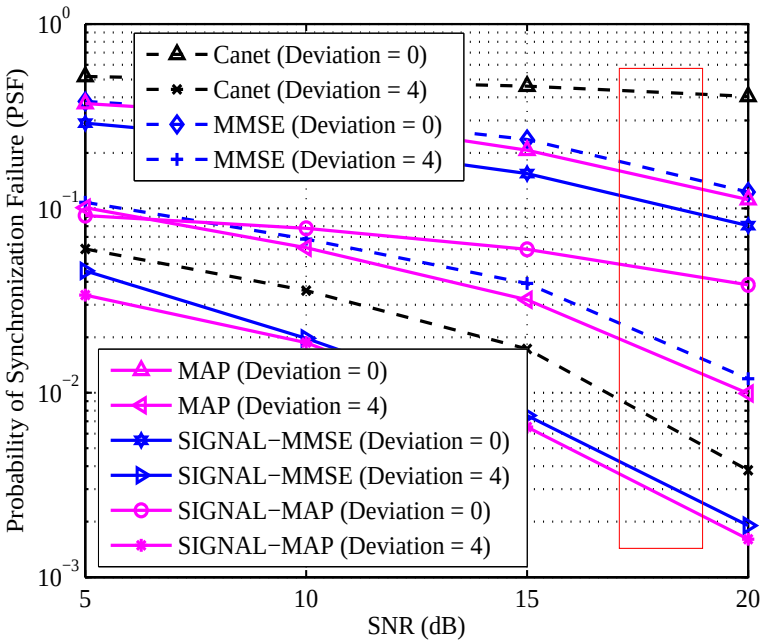

Figure 4.13. PSF of algorithms [16] (Canet), [87] (MMSE) and the proposed algorithms with no deviation under BRAN A channel model

Under the COST207-RA with the two cases of (1) time deviation equal to 0 (Figure 4.10) and (2) time deviation with respect to the true arrival time of packet

smaller than 4 (Figure 4.11), the PSF of Algorithm 3 (respectively, Algorithm 5) is smaller than the PSF of Algorithm 2 (respectively, Algorithm 4). Indeed, with no deviation, at SNR = 17.5 dB we obtain: PSF(MMSE) = 8×10^{-2}; PSF(MAP) = 7.3×10^{-2}; PSF(SIGNAL-MMSE) = 5.5×10^{-2} and PSF(SIGNAL-MAP) = 4.8×10^{-2}.

When the channel follows the BRAN A model, the PSF of the proposed algorithm as illustrated in Figure 4.13 also shows the high performance of our algorithm. For instance, with no deviation, at SNR = 17.5 dB: PSF(MMSE) = 1.7×10^{-1}, PSF(MAP) = 1.5×10^{-1}, PSF(SIGNAL-MMSE) = 1×10^{-1} and PSF(SIGNAL-MAP) = 5×10^{-2}.

4.4 Time synchronization using Channel Estimation (CE) based on CSMA/CA mechanism

This section introduces a time synchronization algorithm for data physical packet by taking advantage of the channel estimate performed from the RtS control frame reception when the CSMA/CA mechanism is triggered to avoid collisions with stations. The proposed algorithm is summarized in Figure 4.14 and consists in two main stages as described below.

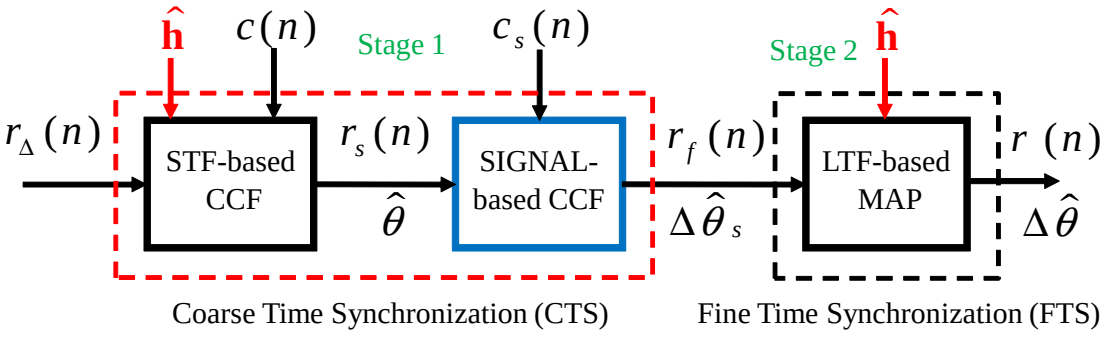

Figure 4.14. Time synchronization algorithm using the CE from RtS control frame reception (CE-SIGNAL-MAP)

4.4.1 First stage: Coarse time synchronization

First consider equation (4.3) in Section 4.2.2. This equation estimates the symbol timing θ of the received signal via some cross-correlation between the known sequence corresponding to the STF and received signal.

The symbol timing estimation in equation (4.4) provides more accurate results when the received signal $r_\Delta(n)$ is strongly correlated to the training sequence $c(n)$. However, in most cases, the received signal is severely distorted by noise and multi-

path channel making it quite different of the true signal $c(n)$, a fact which degrades the estimation performance. Therefore instead of calculating the cross-correlation between the training sequence $c(n)$ and the received signal $r_{\Delta}(n)$, as explained in Section 4.2.2 (see equation (4.3)), we propose to replace the received signal by the transmitted signal $x(n)$ which is however considered as an unknown information at the receiver. Faced with this problem we developed an estimation strategy of the true signal (i.e. $x(n)$) using the channel estimate related to the RtS control frame when the CSMA/CA medium reservation procedure is triggered. This process will be presented by next subsections but first let us recall briefly the CSMA/CA mechanism mentioned in the previous section.

4.4.1.1 CSMA/CA medium reservation procedure

If any transmitting station in the same wireless network wishes to send data, it initiates the process by sending a RtS control frame to ask the receiving station if it is available. When it is the case, the receiver replies to the transmitter with a CtS frame, which also informs other stations in the same network of its unavailability to receive information during a specified period of time. The transmitting station then sends the DATA frame to the receiver (see Section 4.2, Figure 4.3).

Assume that the CSMA/CA mechanism is active. To ensure that all nodes in the wireless network receive the RtS control frame, the transmitter has to send this frame with a power level higher than the nominal transmission power level at which the DATA frame is sent [33] meaning that a robust physical frame synchronization is necessary to reduce the number of retransmission. In this particular context we assume that the transmitter and receiver stations have been correctly synchronized during the medium reservation negotiation (i.e. RtS/CtS) for preparing the transmission of the physical packet. Note that the same PREAMBLE field is used both for control (e.g. RtS, CtS) and DATA frames (see Figure 2.2). We then take advantage of this situation to estimate the channel according to the LTF field of the RtS PREAMBLE field in order to approximate the true transmitted signal (i.e. $x(n)$).

4.4.1.2 MAP channel estimation based on RtS control frame

The channel state is assumed to remain either constant between the transmission duration of RtS and DATA frames or slowly time-varying. Indeed since under good transmission/reception conditions of the CtS control frame the interval time between the transmitted DATA physical packet and RtS control frame ($T_{RtS}+T_{CtS}+2T_{SIFS}$)

is small (e.g. 124 μs with the lowest rate equal to 6 Mb/s) meaning that the Doppler frequency can be considered as small. Therefore, a MAP channel estimation is given by

$$\widehat{\mathbf{h}} = (\mathbf{G}^H\mathbf{G} + \sigma_g^2\mathbf{R}_\mathbf{h}^{-\mathbf{1}})^{-1}(\mathbf{G}^H\mathbf{r} + \sigma_g^2\mathbf{R}_\mathbf{h}^{-\mathbf{1}}\mu_h), \tag{4.32}$$

where $\mathbf{r}$ is the received RtS frame signal corresponding to the LTF sequence. Matrix $\mathbf{G}$ contains the LTF training samples with σ_g^2 the noise variance. $\mathbf{R_h}$ (respectively μ_h) is the covariance matrix (respectively mean vector) of the true channel. Instead of using a PDP to calculate $\mathbf{R_h} = E\{\mathbf{h}\mathbf{h}^H\}$, we propose to replace the true channel $\mathbf{h}$ by its LS estimation $\tilde{\mathbf{h}}$ given by the IFFT of $\tilde{\mathbf{H}} = \mathbf{X}^{-1}\mathbf{R}$ where $\mathbf{X}$ is the diagonal matrix formed by the known LTF symbols and $\mathbf{R}$ is the received symbol vector corresponding to the LTF symbols (refer to Section 4.3). The MSE of the MAP channel estimation is provided in Figure 4.15.

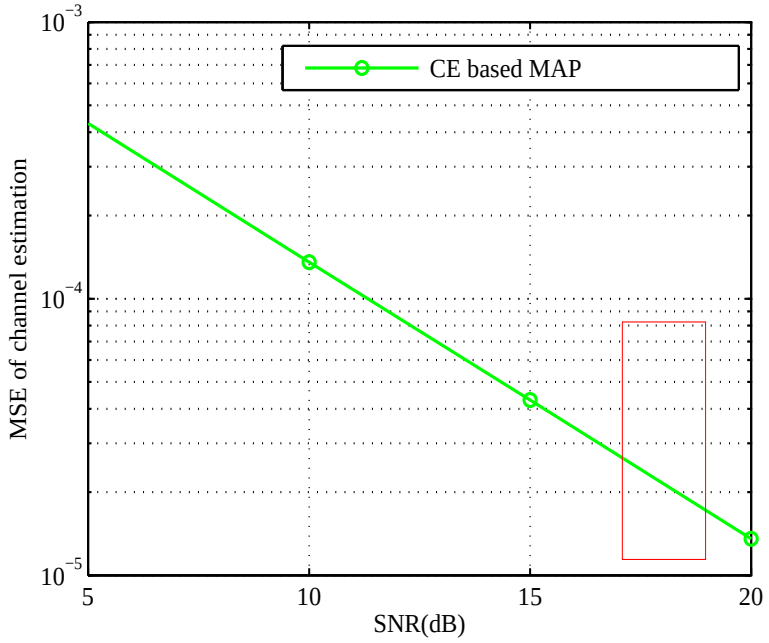

Figure 4.15. MSE of MAP channel estimation with no frequency and time offset

4.4.1.3 Transmitted signal estimate

Denote $\hat{H}(k)$ (with $0 \leq k \leq N-1$) as the channel frequency response deduced from (4.32) and $R_\Delta(k)$ as the received symbols in frequency domain corresponding to the DATA frame (see equation (2.8)). The transmitted symbol estimate $\hat{X}(k)$ based on a Zero-Forcing (ZF) equalizer is given by

$$\hat{X}(k) = R_\Delta(k)/\hat{H}(k). \tag{4.33}$$

Thefore the estimate of the transmitted DATA signal in the time domain is deduced as follows:

$$\hat{x}(n) = \frac{1}{N} \sum_{i=0}^{N-1} \hat{X}(k) e^{j2\pi k \frac{n}{N}}. \tag{4.34}$$

4.4.1.4 Symbol timing estimate

The symbol timing estimate is based on the cross-correlation (see equation (4.3)) which is here performed between the known stream $c(n)$ of length L_{STF} and the transmitted signal $\hat{x}(n)$ given by equation (4.34) as follows:

$$\hat{\theta} = \arg\max_{\theta} \{ | \sum_{n=0}^{L_{\mathrm{STF}}-1} c^*(n) \hat{x}(n+\theta) | \}. \tag{4.35}$$

where L_{STF} is the number of $c(n)$ samples.

To estimate the remaining time offset $\Delta\theta_s = \theta - \hat{\theta}$, the receiver exploits the 802.11a SIGNAL field as an additional known training sequence according to equation (4.7) (see Section 4.2).

4.4.2 Second stage: Joint time synchronization and MAP channel estimation

The received signal after the coarse time synchronization step performed on the LTF samples is expressed as follows (the CFO is assumed as perfectly compensated):

$$r_f(n) = \sum_{i=0}^{L-1} h(i) x(n - i - \Delta\theta) + g(n), \tag{4.36}$$

where $\Delta\theta = \Delta\theta_s - \Delta\widehat{\theta_s}$ is the remaining time offset.

To estimate the residual time offset $\Delta\theta$, the proposed algorithm exploits the strategy of the joint time synchronization and MAP channel estimate algorithm based on the LTF sequences of the PREAMBLE as described in Section 4.3.

Specifically a set of possible time offset values $\mathbf{\Lambda} = \{-\Delta\theta_M, .., \Delta\theta_M\}$ is defined. For each value a MAP channel estimation $\hat{\mathbf{h}}_{\Delta\theta_m}$ is obtained. The best time offset is chosen as the one that maximizes the total energy of channel coefficients as follows:

$$\Delta\widehat{\theta} = \arg\max_{\Delta\theta_m} \{ \sum_{n=0}^{L-1} |\hat{h}_{\Delta\theta_m}(n)|^2 \}, \tag{4.37}$$

where L is the channel length.

4.4.3 Numerical results

Simulation parameters provided in Section 4.3 are also used in this section. The performance of the following algorithms is compared:

i) **Algorithm 1 (MAP)** is joint fine time synchronization and channel estimation algorithm, developed in Section 4.3.
ii) **Algorithm 2 (SIGNAL-MAP)** has been described in Section 4.3 where the CTS exploits the SIGNAL field as an additional training sequence and the FTS is based on the MAP channel estimation.
iii) **Algorithm 3 (CE-SIGNAL-MAP)** is the proposed algorithm presented in this section where the CTS exploits the channel estimation from the RtS frame reception.

We first discuss the case using the channel model COST207-RA. Figure 4.16 measures the probability of estimating the arrival time of a physical packet for a given deviation with respect to its true time position (i.e. $\widehat{\theta} - \theta$) at SNR=15 dB for Algorithm 1, 2 and 3 using 7.10^4 test physical packets. It can be seen from the figure that the proposed algorithm (Algo. 3) provides the highest estimation accuracy (equal to 99%) at zero deviation. At deviations different from zero, the probability of estimating the arrival time approximates zero.

The curves of Figure 4.17 also illustrate that the PSF of the proposed algorithm (in solid lines) is much smaller than that of algorithms 1 and 2 (dashed lines) more particularly in the operating area of the 802.11a represented by the rectangular box. For a given SNR=17.5 dB and with no time deviation respect to the true arrival time of packet (i.e. deviation equal to zero), the PSF of algorithms 1, 2 and 3 are PSF(Algo.1)=2.5×10^{-1}; PSF(Algo.2)=5.1×10^{-2} and PSF(Algo.3)=7.2×10^{-3} respectively. The performance is improved when accepting packets with time deviation no more than 4 samples. Indeed for a given SNR=17.5 dB, we respectively obtain PSF(Algo.1)=7×10^{-2}; PSF(Algo. 2)=3.5×10^{-2} and PSF(Algo.3)=1.3×10^{-3}.

One might ask how the performance of our algorithm is affected when the estimated channel $\widehat{\mathbf{h}}$ during the negotiation of the transmission medium (see equation (4.32)) has been slightly modified according to the walking speed of the receiving station just when the physical data packet (denoted by "DATA", see Figure 4.3) is transmitted. In fact, if the CtS control frame has been correctly received, the interval time Δt (see Figure 4.3) given by the difference between the starting time of the transmitted DATA and the RtS control frame is equal to 124 μs (i.e. $T_{RtS} + T_{CtS} + 2T_{SIFS}$) when the rate is set to 6 Mb/s (the worst case) [29]. If we assume that the walking speed is equal to 1.5 m/s with a carrier frequency of 5.2 GHz, the maximum Doppler frequency f_D is a small value equal to 26 Hz. Indeed each jth channel tap is multiplied by $e^{j2\pi f_D \Delta t} \approx e^{j0.02}$ which has very little impact

on the estimated channel $\widehat{\mathbf{h}}$. This is confirmed by the simulation results provided by Figures 4.16 and 4.17.

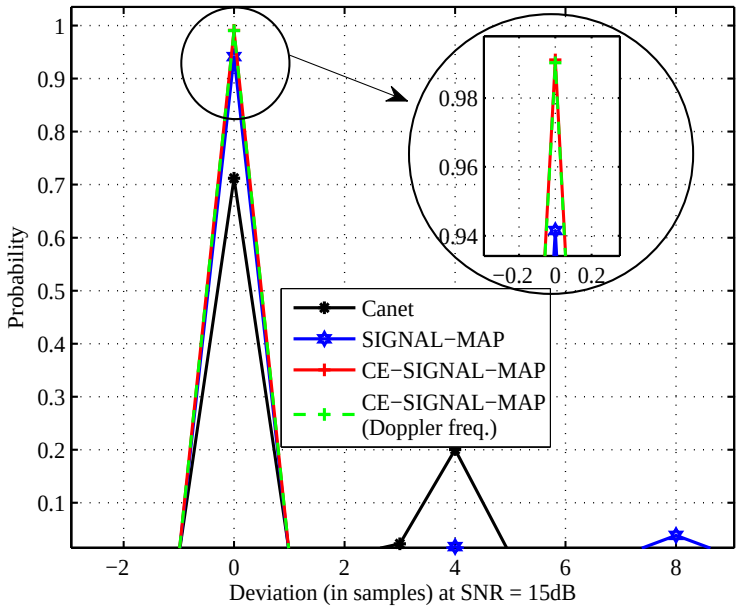

Figure 4.16. Deviation with respect to the true time position of a physical packet of algorithm [16] and the proposed algorithms under COST207-RA channel model

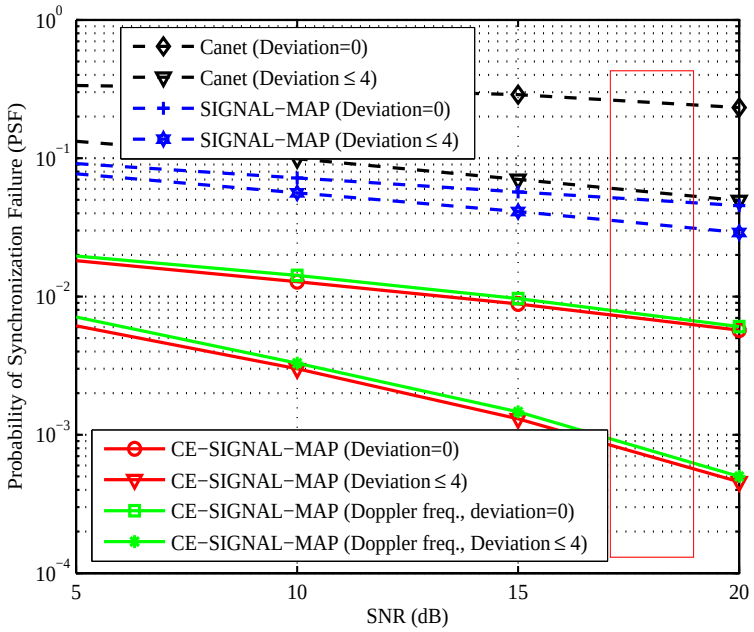

Figure 4.17. PSF of algorithm [16] (Canet) and the proposed algorithms under COST207-RA channel model

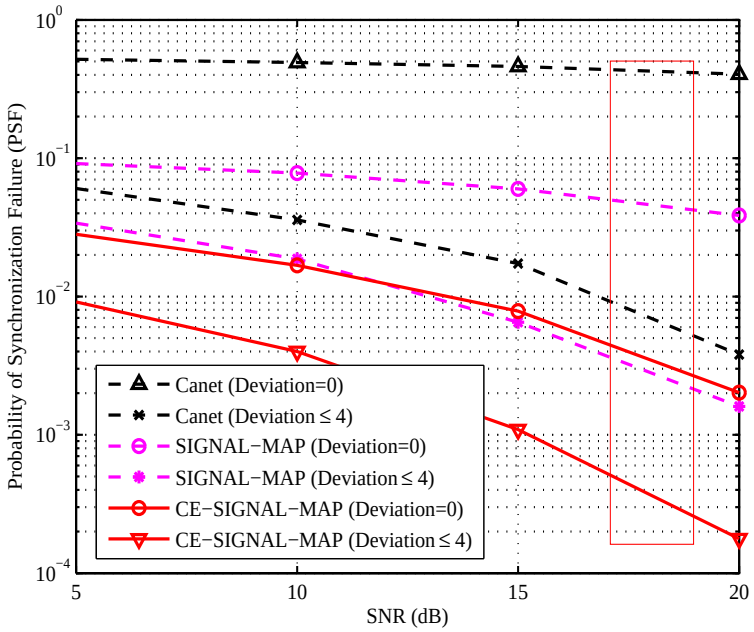

Figure 4.18. PSF of algorithm [16] (Canet) and the proposed algorithms under BRAN A channel model

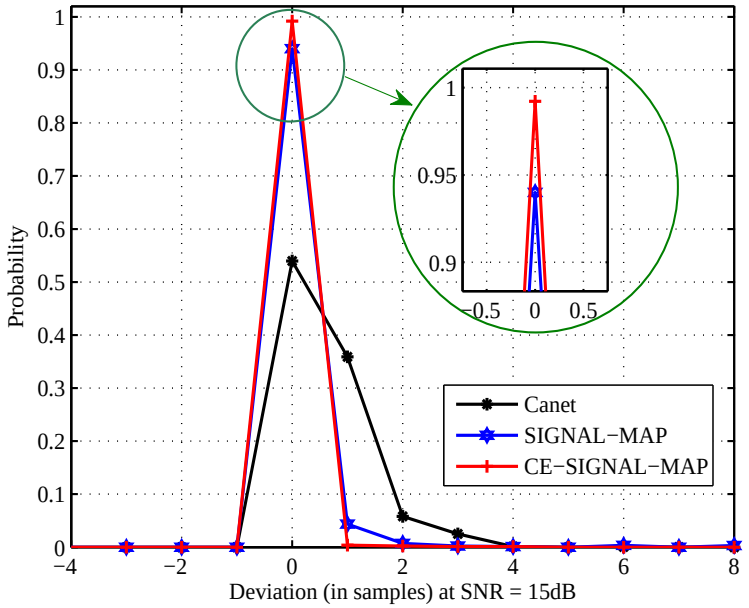

Figure 4.19. Deviation with respect to the true time position of a physical packet of algorithm [16] (Canet) and the proposed algorithms under BRAN A channel model

The proposed time synchronization algorithm also gives good performance under the channel BRAN A as shown in Figures 4.18 and 4.19.

4.5 Time synchronization in presence of imperfect channel state information

In the previous sections, the proposed synchronization algorithm exploited not only traditional training sequences as specified by the IEEE 802.11a standard but also additional knowledge available when the CSMA/CA is triggered. Indeed, additional information which should be known by the receiver has been used. To enhance the performance of this algorithm, we proposed to modify the FTS stage (see Figure 4.14) based on a joint fine time synchronization and channel estimation which results in the smallest Channel Estimate Errors (CEE) according to the selected criterion (e.g. LS, MAP) (see the analysis of the proposed solutions in Sections 4.2 and 4.3). This idea is related to the fact that the PSF heavily depends on the channel estimate accuracy. Indeed when the channel estimation error is smaller, the performance of the time synchronization is improved. Based on this observation, rather than trying to find the best channel estimate algorithm, we now propose an optimal time synchronization metric that minimizes the average of transmission error over all possible Channel Estimation Errors (CEE). The proposed algorithm is summarized in Figure 4.20 and described below.

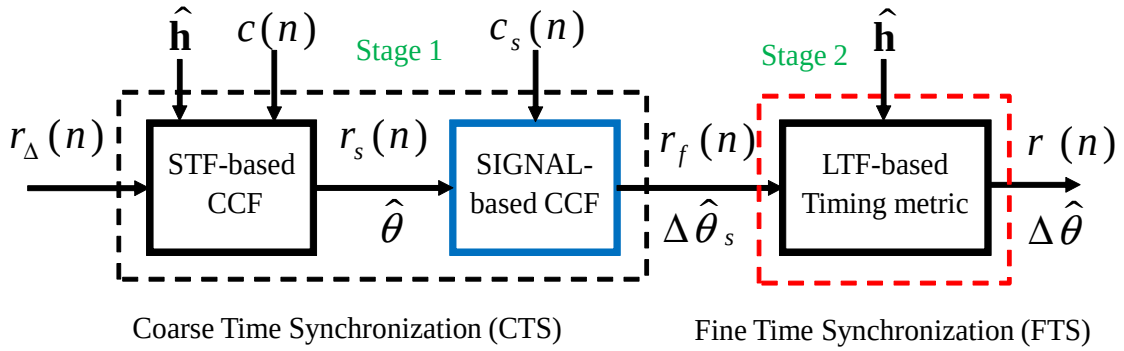

Figure 4.20. Time synchronization algorithm in presence of imperfect channel state information (CE-SIGNAL-CEE)

4.5.1 First stage: Coarse time synchronization

The first stage concerns coarse time synchronization process as described in Section 4.4 where equation (4.35) is used for the symbol timing estimation. The remaining time offset is then estimated as described in Section 4.2 (equation (4.6)) where the SIGNAL field is exploited.

4.5.2 Second stage: Fine time synchronization

The purpose of this section is to estimate the residual time offset $\Delta\theta$ from the coarse time synchronization stage, as given in equation (4.36). For convenience, the signal can be expressed in the frequency-domain in a matrix form as follows:

$$\mathbf{R}_f = \mathbf{XH} + \mathbf{G}, \tag{4.38}$$

where $\mathbf{R}_f$ is the received frequency-domain vector of size $N \times 1$ (FFT transform applied to $r_f(n)$). $\mathbf{G}$ is the noise vector of size $N \times 1$. $\mathbf{H}$ of size $N \times 1$ is the FFT transform of $\mathbf{h}_{\mathbf{\Delta\theta_m}}$ and thus it contains parameter $\Delta\theta$. The PDF of $\mathbf{H}$, denoted $\Psi(\mathbf{H})$, is assumed to follow a circular Gaussian distribution with zero mean; that is, $\mathbf{H} \sim C\aleph(0, \mathbf{R_H})$, where $\mathbf{R_H}$ is the covariance matrix of size $N \times N$ (note that it is different from $\mathbf{R}_f$ denoted as received symbol vector). This PDF is thus given by

$$\Psi(\mathbf{H}) = \frac{1}{\pi^N det(\mathbf{R_H})} \exp\left(\mathbf{H}^H {\mathbf{R_H}}^{-1} \mathbf{H}\right). \tag{4.39}$$

The remaining time offset $\Delta\theta$ to be estimated is considered as the one which minimizes the following new metric:

$$\Delta\hat{\theta} = \arg \min_{\Delta\theta \in \mathbf{\Lambda}} \{\widetilde{D}(\Delta\theta)\}, \tag{4.40}$$

where $\mathbf{\Lambda}$ is given in Section 4.4.2, $\widetilde{D}(\Delta\theta)$ is the average of the transmission error $D(\mathbf{H}) = \|\mathbf{R}_f - \mathbf{XH}\|^2$ over all Channel Estimation Errors (CEE) and is given by

$$\widetilde{D}(\Delta\theta) = E_{\mathbf{H}|\hat{\mathbf{H}}}[D(\mathbf{H})] = \int_{\mathbf{H}} D(\mathbf{H}) \Psi(\mathbf{H}|\hat{\mathbf{H}}) d(\mathbf{H}), \tag{4.41}$$

where $\Psi(\mathbf{H}|\hat{\mathbf{H}})$ is the PDF of $\mathbf{H}$ (true unknown channel) given $\hat{\mathbf{H}}$; and $\hat{\mathbf{H}}$ is considered in this section as the LS channel estimate provided by $\hat{\mathbf{H}} = \mathbf{X}^{-1}\mathbf{R}_f$. Note that the form of equation (4.41) has been inspired from [68]. To solve this equation, it requires the knowledge of the PDF $\Psi(\mathbf{H}|\hat{\mathbf{H}})$ that can be determined as follows:

$$\Psi(\mathbf{H}|\hat{\mathbf{H}}) = \frac{\Psi(\hat{\mathbf{H}}|\mathbf{H})\Psi(\mathbf{H})}{\Psi(\hat{\mathbf{H}})}, \tag{4.42}$$

where $\Psi(\mathbf{H})$ is given by equation (4.39). $\Psi(\hat{\mathbf{H}}|\mathbf{H}) \sim C\aleph(\mu_{\hat{\mathbf{H}}|\mathbf{H}}, \mathbf{\Sigma}_{\hat{\mathbf{H}}|\mathbf{H}})$ and $\Psi(\hat{\mathbf{H}}) \sim C\aleph(\mu_{\hat{\mathbf{H}}}, \mathbf{\Sigma}_{\hat{\mathbf{H}}})$.

To calculate the parameters $\mu_{\hat{\mathbf{H}}|\mathbf{H}}$, $\mathbf{\Sigma}_{\hat{\mathbf{H}}|\mathbf{H}}$, $\mu_{\hat{\mathbf{H}}}$ and $\mathbf{\Sigma}_{\hat{\mathbf{H}}}$, we use the definitions of mean and covariance as follows: $\mu_{\hat{\mathbf{H}}|\mathbf{H}} = E\{\hat{\mathbf{H}}|_{\mathbf{H}}\} = E\{(\mathbf{H} + \mathbf{X^{-1}G})|_{\mathbf{H}}\} = E\{\mathbf{H}|_{\mathbf{H}}\} = \mu_{\mathbf{H}} = 0$, $\mathbf{\Sigma}_{\hat{\mathbf{H}}|\mathbf{H}} = E\{\hat{\mathbf{H}}\hat{\mathbf{H}}^H|_{\mathbf{H}}\} = E\{(\mathbf{H} + \mathbf{X^{-1}G})(\mathbf{H} + \mathbf{X^{-1}G})^H|_{\mathbf{H}}\} - \mu_{\hat{\mathbf{H}}|\mathbf{H}}\mu^{\mathbf{H}}_{\hat{\mathbf{H}}|\mathbf{H}} = E((\mathbf{X^{-1}G})^H(\mathbf{X^{-1}G}))\mathbf{I} = \mathbf{\Sigma}_\epsilon$ with $\mathbf{I}$ the $N \times N$ identity matrix.

In the same way, we compute $\Psi(\hat{\mathbf{H}}) \sim C\aleph(\mu_{\hat{\mathbf{H}}}, \mathbf{\Sigma}_{\hat{\mathbf{H}}}) = C\aleph(0, \mathbf{R_H} + \mathbf{\Sigma}_\epsilon)$ where $\mathbf{R_H} = E\{\mathbf{H}\mathbf{H}^H\}$. The calculation of $\mathbf{R_H}$ is based on the MAP channel estimate (see equation (4.32)) as given by $\mathbf{R_H} \approx E\{\hat{\mathbf{H}}_{MAP}\hat{\mathbf{H}}_{MAP}^H\}$.

Substituting $\Psi(\mathbf{H})$, $\Psi(\hat{\mathbf{H}}|\mathbf{H})$ and $\Psi(\hat{\mathbf{H}})$ into (4.42) yields $\Psi(\mathbf{H}|\hat{\mathbf{H}}) \sim C\aleph(\mu_{\mathbf{H}|\hat{\mathbf{H}}}, \mathbf{\Sigma}_{\mathbf{H}|\hat{\mathbf{H}}})$ with $\mu_{\mathbf{H}|\hat{\mathbf{H}}} = \mathbf{\Sigma}_\Delta\hat{\mathbf{H}}$ and $\mathbf{\Sigma}_{\mathbf{H}|\hat{\mathbf{H}}} = \mathbf{\Sigma}_\Delta\mathbf{\Sigma}_\epsilon$ where $\mathbf{\Sigma}_\Delta = \mathbf{R_H}(\mathbf{R_H}+\mathbf{\Sigma}_\epsilon)^{-1}$. For simplicity, equation (4.41) is reduced to the following calculation:

$$\widetilde{D}(\Delta\theta) = E_{\mathbf{W}}[D(\mathbf{W})] = \int_{\mathbf{W}} D(\mathbf{W})\Psi(\mathbf{W})d(\mathbf{W}), \tag{4.43}$$

where $\mathbf{W} \sim \Psi(\mathbf{W}) = C\aleph(\mu_{\mathbf{H}|\hat{\mathbf{H}}}, \mathbf{\Sigma}_{\mathbf{H}|\hat{\mathbf{H}}})$ and $D(\mathbf{W}) = \|\mathbf{R}_f - \mathbf{X}\mathbf{W}\|^2$.

After some mathematical manipulations, we obtain

$$\begin{aligned}\widetilde{D}(\Delta\theta) = E[\mathbf{R}_f^H\mathbf{R}_f] - E[\mathbf{R}_f^H\mathbf{X}]\mu_{\mathbf{H}|\hat{\mathbf{H}}} - \mu_{\mathbf{H}|\hat{\mathbf{H}}}^H E[\mathbf{X}^H\mathbf{R}_f] + tr(\mathbf{\Sigma}_{\mathbf{H}|\hat{\mathbf{H}}}\mathbf{X}\mathbf{X}^H) + \\ + \mu_{\mathbf{H}|\hat{\mathbf{H}}}^H\mathbf{X}^H\mathbf{X}\mu_{\mathbf{H}|\hat{\mathbf{H}}},\end{aligned} \tag{4.44}$$

where $tr(.)$ indicates the trace operator. The remaining time offset $\Delta\hat{\theta}$ is then deduced from equation (4.40).

4.5.3 Numerical Results

This section discusses the performance of the proposed time synchronization algorithm. The simulation parameters in Section 4.4 are used again in this section for the channel models COST207-RA and BRAN A. The frequency offset is assumed to be known at the receiver and compensated after coarse time synchronization stage. Figures 4.21 and 4.23 compare respectively the PSF of the following time synchronization algorithms:

i) **Algorithm 1 (SIGNAL-MAP)**: This algorithm is described in Section 4.3. The CTS stage based on equation (4.4) for the symbol timing estimation and the SIGNAL field as an additional training sequence. The fine time synchronization is then performed according to the joint time synchronization and MAP channel estimation (see Figure 4.9).

ii) **Algorithm 2 (CE-SIGNAL-MAP)**: This algorithm is similar to Algorithm 1 but in the symbol timing estimation stage, the channel is first estimated according to the RtS reception and then the symbol timing is determined via equation (4.35) (see Figure 4.14).

iii) **Algorithm 3 (CE-SIGNAL-CEE)**: This is the proposed time synchronization algorithm described in Section 4.5.

Under both channel models, the PSF of the proposed time synchronization algorithm (shown by solid lines in Figures 4.21 and 4.23) is much lower than those

of the previous time synchronization algorithms (shown by dash lines). Indeed for COST207-RA channel model as shown in Figure 4.21, at SNR=17.5 dB and with no time deviation with respect to the true arrival time of packet (i.e. deviation equal to zero), the PSF of algorithms 1, 2 and 3 respectively is: PSF(SIGNAL-MAP)= 5.1×10^{-2}; PSF(CE-SIGNAL-MAP)=7.2×10^{-3} and PSF(CE-SIGNAL-CEE)= 1.3×10^{-3}. When the time deviation no more than 4 is considered, the PSF of these is: PSF(SIGNAL-MAP)= 4×10^{-2}; PSF(CE-SIGNAL-MAP)=7×10^{-4} and PSF(CE-SIGNAL-CEE)= 2.4×10^{-4}. This confirms that the proposed algorithm improves significantly the performance in terms of PSF.

Moreover, Figures 4.22 and 4.24 that measure the probability of estimating the arrival time of a physical packet for a given deviation with respect to its true time position (i.e. $\widehat{\theta} - \theta$) also indicates the good result of the proposed algorithm in both channel models.

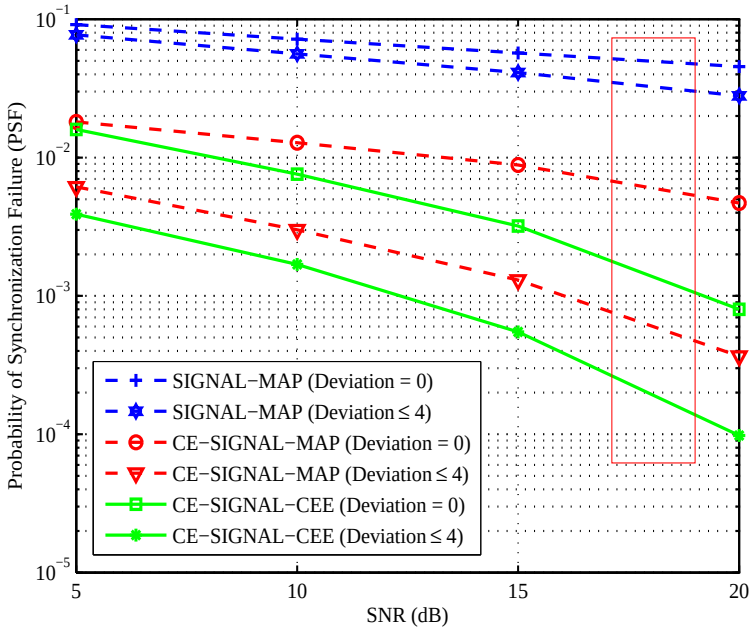

Figure 4.21. PSF of the proposed algorithms under COST207-RA channel model (the rectangular box represents the operating mode of the 802.11a)

4.6 Conclusion

This chapter proposed time synchronization algorithms adapted to the wireless OFDM IEEE 802.11a communication system.

First, in addition to using conventional STF sequence as reference sequence (as specified by the standard), we exploited the SIGNAL field of the 802.11a physi-

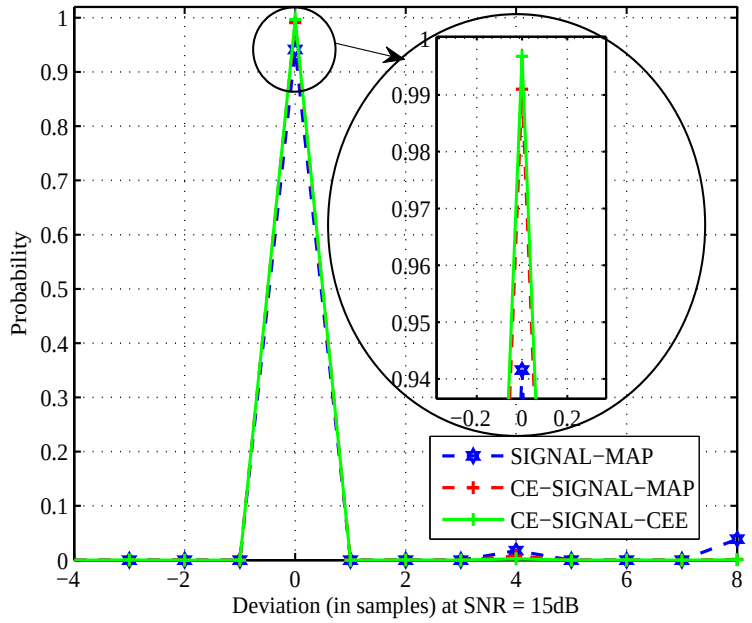

Figure 4.22. Deviation with respect to the true time position of a physical packet of the proposed algorithms under COST207-RA channel model

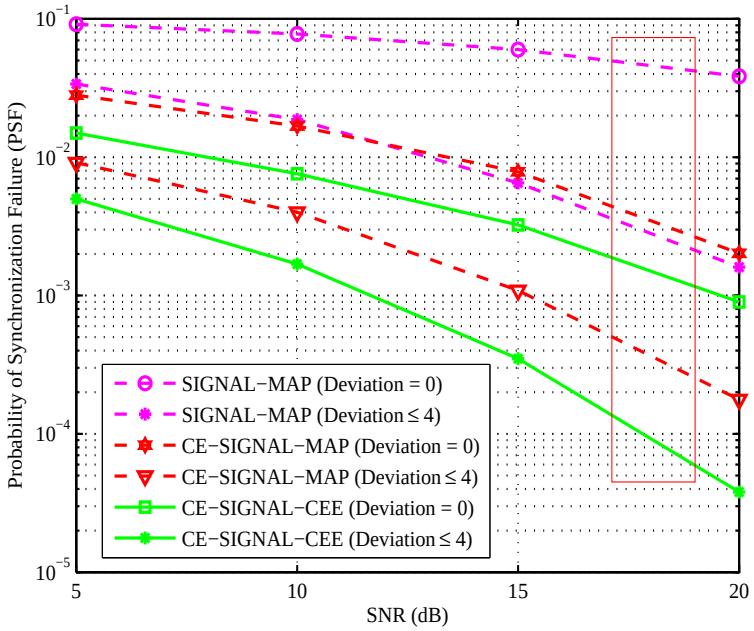

Figure 4.23. PSF of algorithm [16] (Canet) and the proposed algorithms under BRAN A channel model

cal packet as a supplementary training known sequence by the receiver to enhance the coarse time synchronization. Indeed the unknown parts of the SIGNAL field

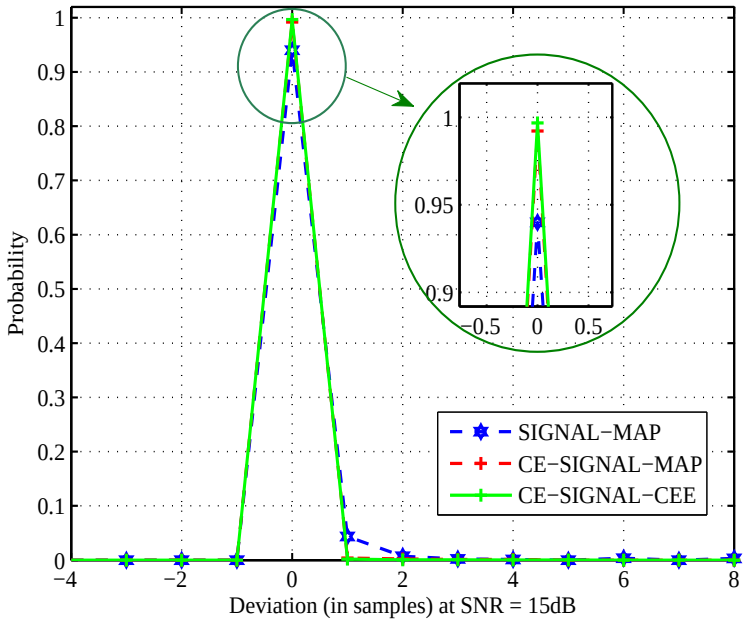

Figure 4.24. Deviation with respect to the true time position of a physical packet of the proposed algorithms under BRAN A channel model

are predicted by the receiver when the CSMA/CA medium reservation mechanism is triggered using the control frames RtS and CtS. To take full advantage of the CSMA/CA mechanism, the CIR is estimated according to the RtS control frame reception and is also used as additional information for the DATA physical packet synchronization. Moreover, from the observation that there is a relationship between time synchronization performance and channel estimation quality, a timing metric that minimizes the average of transmission error over all channel estimate errors has been proposed to enhance the performance of time synchronization process. Simulation results confirmed the performance of the developed algorithms in the various channel conditions.

This chapter concentrated only on time synchronization problem, the carrier frequency offset was assumed as known at receiver. Next chapter will focus on carrier frequency offset problems.

CHAPTER 5

Frequency synchronization algorithms

Contents

5.1 Introduction

As part of OFDM reception, two key parameters need to be estimated before demodulating the physical packet. In Chapter 4, we have proposed algorithms for determining one of the two key parameters, which is the beginning of a symbol. In this chapter, we investigate the estimation of the other key parameter, which is the Carrier Frequency Offset (CFO). The CFO is the difference between the carrier frequencies at the transmitter and receiver. It is caused by local oscillators and Doppler effect [41]. Without being correctly compensated, the CFO introduces Inter-Carrier Interference (ICI) to the frequency domain signal and dramatically degrades the system performance. In Chapter 3, we have described the most common and newest CFO estimators, among them the algorithm in reference [52] that investigates the MAP criterion for estimating the CFO and channel coefficient parameters. This algorithm, proposed in a very general setting, is now adapted to the IEEE 802.11a standard.

On the other hand, as described in Chapter 4, the time synchronization algorithms which take advantage of the information made available by the CSMA/CA mechanism have achieved impressive results. Inspired by the developed strategy in previous chapter, we propose frequency synchronization schemes adapted to the IEEE 802.11a exploiting the SIGNAL field of physical packet when the CSMA/CA mechanism is activated. Indeed the SIGNAL field can be used since its parts are either known or predictable at the receiver (see Section 4.2). Next, the channel information obtained from the RtS control frame reception of the mechanism is also exploited in a new metric. Simulations are carried out under various channel environments (COST207-RA corresponding to outdoor and BRAN A for typical indoor conditions).

In what follows, we only consider frequency synchronization algorithms, hence the symbol timing θ is assumed to be known at the receiver and then perfectly compensated.

5.2 Adaptation of the MAP frequency synchronization to the IEEE 802.11a standard

This section describes the MAP frequency synchronization algorithm developed in reference [52] with its adaptation to the IEEE 802.11a standard. The training sequences mentioned in the reference are here replaced by the two LTF repetitions specified by the standard.

From equation (3.55), for convenience, the received signal corresponding to the

two LTF repetitions is expressed in a matrix form as follows:

$$\mathbf{r} = \mathbf{\Phi}_\epsilon \mathbf{S}\mathbf{h} + \mathbf{g}, \tag{5.1}$$

where $\mathbf{r} = [r(n), r(n+1), ..., r(n+2N-1)]^T$ (N is the number of samples of one LTF repetition); $\mathbf{g} = [g(n), g(n+1), ..., g(n+2N-1)]^T$; $\mathbf{h} = [h(0), h(1), ..., h(L-1)]^T$; $\mathbf{\Phi}_\epsilon$ =diag$[e^{j\frac{2\pi\epsilon n}{N}}, e^{j\frac{2\pi\epsilon(n+1)}{N}}, ..., e^{j\frac{2\pi\epsilon(n+2N-1)}{N}}]$; $\mathbf{S} = [\mathbf{S}_0, \mathbf{S}_1, .., \mathbf{S}_{L-1}]$ with $\mathbf{S}_l = [x(n-l), x(n+1-l), .., x(n+2N-1-l)]^T$ where $x(n)$ is the known LTF sample in the time domain and $l = 0 : L-1$.

The MAP estimations of the normalized frequency offset and channel are given by

$$\{\hat{\mathbf{h}}, \hat{\epsilon}\} = \arg\max_{\mathbf{h},\epsilon} \ln\{P(\mathbf{h}, \epsilon|\mathbf{r})\}, \tag{5.2}$$

where P is the *a posteriori* probability density function of $\mathbf{h}$ and ϵ given $\mathbf{r}$.

Calculating $P(\mathbf{h}, \epsilon|\mathbf{r})$ under the assumption that ϵ is uniformly distributed in the range $[-\epsilon_0, \epsilon_0]$ provides the MAP estimations of CFO and channel coefficients as follows:

$$\{\hat{\mathbf{h}}, \hat{\epsilon}\} = \arg\min_{\mathbf{h},\epsilon} f_{MAP}(\mathbf{h}, \epsilon), \tag{5.3}$$

where $f_{MAP}(\mathbf{h}, \epsilon) = (1/\sigma_g^2)||\mathbf{r} - \mathbf{\Phi}_\epsilon \mathbf{S}\mathbf{h}||^2 + \mathbf{h}^{\mathbf{H}}\mathbf{R}_{\mathbf{h}}^{-\mathbf{1}}\mathbf{h}$ with σ_g^2 being the variance of noise and $\mathbf{R}_\mathbf{h}$ being the channel covariance matrix.

Estimating the gradient vector of $f_{MAP}(\mathbf{h}, \epsilon)$ with respect to $\mathbf{h}^H$ and setting it to zero provides the channel MAP estimation:

$$\widehat{\mathbf{h}} = (\mathbf{S}^H\mathbf{S} + \sigma_g^2\mathbf{R}_\mathbf{h}^{-\mathbf{1}})^{-1}\mathbf{S}^H\mathbf{\Phi}_\epsilon^{\mathbf{H}}\mathbf{r}. \tag{5.4}$$

Replacing $\widehat{\mathbf{h}}$ given by equation (5.4) into $f_{MAP}(\widehat{\mathbf{h}}, \epsilon)$ given in equation (5.3), the CFO estimation is provided by

$$\hat{\epsilon} = \arg\min_{\epsilon} g_{MAP}(\epsilon), \tag{5.5}$$

where $g_{MAP}(\epsilon) = \mathbf{r}^H\mathbf{\Phi}_\epsilon\mathbf{S}^+{\mathbf{\Phi}_\epsilon}^H\mathbf{r}$ with $\mathbf{S}^+ = \mathbf{S}(\mathbf{S}^H\mathbf{S} + \mathbf{R}_\mathbf{h}^{-\mathbf{1}}\sigma_g^2)^{-1}\mathbf{S}^H$.

To determine the CFO estimation, the Newton-Raphson approximation is calculated as follows:

$$\hat{\epsilon}_{i+1} = \hat{\epsilon}_i - (\frac{\partial^2 g(\epsilon)}{\partial\epsilon^2})^{-1}\frac{\partial g(\epsilon)}{\partial\epsilon}|_{\hat{\epsilon}=\epsilon_i}, \tag{5.6}$$

where $\hat{\epsilon}_i$ indicates the CFO estimation at the i^{th} iteration, $\partial g(\epsilon)/\partial\epsilon = 2\text{Re}(\mathbf{r}^H\mathbf{G}\mathbf{\Phi}_\epsilon\mathbf{S}^+\mathbf{\Phi}_\epsilon^H r)$ and $\partial g^2(\epsilon)/\partial\epsilon^2 = 2\text{Re}(\mathbf{r}^H\mathbf{G}^\mathbf{2}\mathbf{\Phi}_\epsilon\mathbf{S}^+\mathbf{\Phi}_\epsilon^H\mathbf{r} + \mathbf{r}^H\mathbf{G}\mathbf{\Phi}_\epsilon\mathbf{S}^+\mathbf{G}^H\mathbf{\Phi}_\epsilon^H\mathbf{r})$ with $\mathbf{G} = j\frac{2\pi}{N}$diag $[n, n+1, ..., n+2N-1]$.

5.3 Frequency synchronization algorithm exploiting the SIGNAL field

Some modifications are made to the MAP frequency synchronization algorithm described in the above section [52].

The proposed frequency synchronization algorithm based on the MAP criterion is performed in two stages: (i) Coarse frequency synchronization to only generate the starting frequency offset value for the Newton-Raphson approximation; and (ii) Fine frequency synchronization using the SIGNAL field. The proposed algorithm is summarized in Figure 5.1 and is described below.

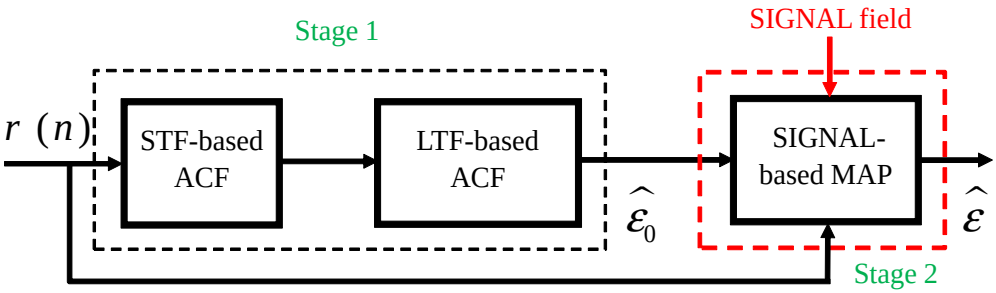

Figure 5.1. Proposed frequency synchronization algorithm exploiting the SIGNAL field (Le-based SIGNAL)

5.3.1 Starting frequency offset value

The first stage (i.e. "STF-based ACF"; "LTF-based ACF") concerns the computation of the starting frequency offset of the Newton-Raphson algorithm (see equation (5.6)). When the starting frequency offset point is initialized with a random value, the performance of the synchronization algorithm can be strongly affected since the function can have several local minima and the initial value may be far from the true frequency offset value. Therefore we propose to initialize the Newton-Raphson algorithm taking a value close to the true frequency offset given by the ACF as mentioned in reference [57]. Specifically, based on the STF, the coarse CFO estimation ϵ_c is performed by equation (3.64) and the fine CFO estimation ϵ_f is determined by equation (3.66) relying on the LTF. We then consider the CFO estimation $\hat{\epsilon}_{total} = \epsilon_c + \epsilon_f$ given by equation (3.67) as the starting frequency offset value $\hat{\epsilon}_0$.

5.3.2 Frequency synchronization based on the SIGNAL field

It is easily recognized that a better performance can be obtained if the length of the training sequence is longer than recommended. Therefore in addition to the conventional training sequence (i.e. STF and LTF), we exploit the SIGNAL field

of the IEEE 802.11a physical frame at the receiver as a reference training sequence when the CSMA/CA mechanism is triggered. The process by which the receiver has the knowledge of the SIGNAL field has been explained in Section 4.2 of Chapter 4. Therefore, rather than using only the two LTF repetitions in equation (5.1) (i.e. $2N$ samples), we extend these repetitions with the SIGNAL field and its Guard Interval (GI). Therefore, sequence $\mathbf{r}$ contains $2N + N_S + N_g$ samples where N_S and N_g are the lengths of the SIGNAL field and the GI respectively. The size of the matrices in equation (5.1) are thus updated as follows: $\mathbf{r^S} = [r(n), r(n+1), ..., r(n+2N+N_S+N_g-1)]^T$; $\mathbf{g^S} = [g(n), g(n+1), ..., g(n+2N+N_S+N_g-1)]^T$; $\mathbf{h} = [h(0), h(1), ..., h(L-1)]^T$; $\mathbf{\Phi}_\epsilon$ =diag$[e^{j\frac{2\pi\epsilon n}{N}}, e^{j\frac{2\pi\epsilon(n+1)}{N}}, ..., e^{j\frac{2\pi\epsilon(n+2N+N_S+N_g-1)}{N}}]$; $\mathbf{S^S} = [\mathbf{S}_0, \mathbf{S}_1, .., \mathbf{S}_{L-1}]$, $\mathbf{S}_l = [x(n-l), x(n+1-l), .., x(n+2N+N_S+N_g-1-l)]^T$ (with $l = 0 : L-1$) and $\mathbf{G^S} = j\frac{2\pi}{N}$diag$[n, n+1, ..., n+2N+N_S+N_g-1]$.

The channel is then estimated according to equation (5.4) and the Newton-Raphson approximation estimates the normalized frequency offset ϵ using equation (5.6) where the starting value $\hat{\epsilon}_0 = \hat{\epsilon}_{total}$.

5.3.3 Numerical Results

The performance of the proposed frequency synchronization algorithm is evaluated in terms of MSE computed between the true normalized carrier frequency offset and its estimation by averaging over 1000 independent channel realizations. The communication system shown in Figure 2.3 is implemented according to the IEEE 802.11a standard (see Section 3.2.2.1, Chapter 3) in the presence of COST207-RA and BRAN A channel models (see Tables 2.1 and 2.2). The tolerance of the internal oscillators at each station is assumed to belong to the range $[-20, 20]$ ppm, therefore the normalized frequency offset ϵ takes a random value in the range $[-0.6, 0.6]$. Note that the symbol timing θ is assumed to be known by the receiver and perfectly compensated. The additional parameters are provided in Table 5.1.

Table 5.1. Simulation parameters

Parameters	*Values*
L_{CFS}	32
L_{FFS}	64
N_S	64
N_g	16

We evaluate and compare the performance of the following algorithms:

i) **Algorithm 1 (Manusani)** [57]: The coarse frequency synchronization (the first step) uses the ACF based on the last three repetitions of the STF. The residual

frequency offset is then estimated by the fine frequency offset estimator according to the ACF based on the two LTF repetitions.

ii) **Algorithm 2 (Le-based MAP)** [52]: This algorithm is described in Section 5.2 and we adapted to the IEEE 802.11a standard. This algorithm is based on the MAP principle using one LTF repetition (Le-based MAP -1LTF) and two repetitions of the LTF (Le-based MAP -2LTF).

iii) **Algorithm 3 (Le-based SIGNAL)**: This is the proposed algorithm described in this section where the SIGNAL field of the physical packet is exploited by the frequency synchronization algorithm.

Figure 5.2 shows the MSE versus SNR of the adapted MAP frequency synchronization to the IEEE 802.11a standard when using one or two LTF repetitions (denoted "Le-based MAP-1LTF" and "Le-based MAP-2LTF", respectively). A comparison with the algorithms described in the state of the art (Chapter 3) shows that the performance of this algorithm in terms of MSE is better than that of its competitors. For instance for a given SNR=15 dB: MSE(Song)= 2.8×10^{-4}; MSE(Manusani,Canet)= 5.3×10^{-5}; MSE(Le-based MAP-1LTF)=2×10^{-5} and MSE(Le-based MAP-2LTF)=
8.7×10^{-6}.

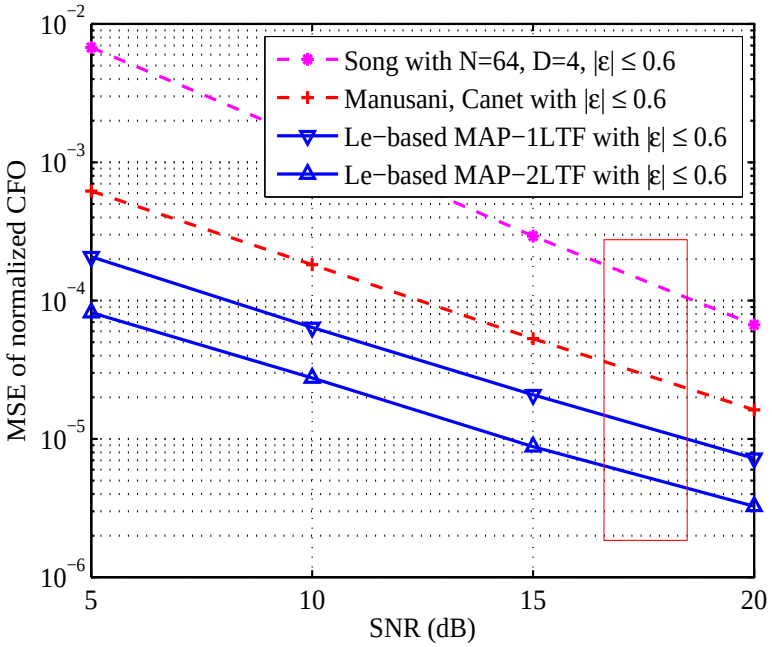

Figure 5.2. MSE of CFO estimation algorithms [84] (Song) (Figure 3.11), [57] (Manusani), [16] (Canet) (Figure 3.12), [52] (Le-based MAP-1LTF and Le-based MAP-2LTF) with $|\epsilon| \leq 0.6$ under COST207-RA model

Figure 5.3 compares the MSE of the proposed synchronization algorithm (presented by solid line) to the synchronization algorithms developed in [57], [52] (presented by dash lines) versus SNR in the channel models COST207-RA and BRAN A. It can be seen from the figure that the curves are almost similar when the COST207-RA or BRAN A model are considered. For this reason, we only discuss the algorithms under the COST207-RA channel model.

It is also observed that when we extend the training sequence by adding the SIGNAL field as proposed in Algorithm 3 (illustrated by solid line in the figure), the MSE value is much lower than for the other algorithms. For instance for a given SNR=17.5 dB, the MSE of algorithms 1, 2 and 3 is respectively: MSE(Manusani)= 3×10^{-5}; MSE(Le-based MAP-1LTF)=1×10^{-5}; MSE(Le-based MAP-2LTF)=5×10^{-6} and MSE(Le-based SIGNAL)=1.1×10^{-6}. This confirms that the performance of our algorithm is better than the algorithm of the state of the art.

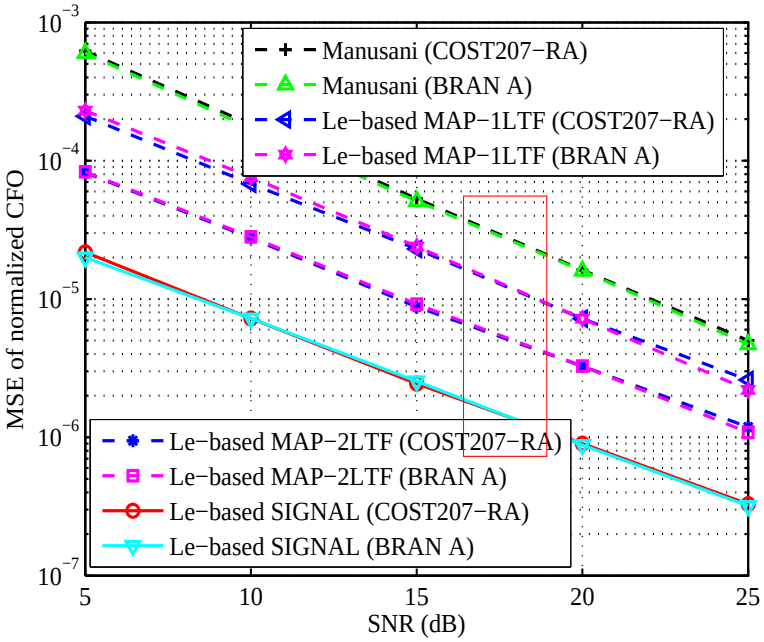

Figure 5.3. MSE of normalized CFO of the proposed algorithm compared to [57] (Manusani), [52] (Le-based MAP-1LTF and Le-based MAP-2LTF) with $|\epsilon| \leq 0.6$

5.4 Frequency synchronization algorithm exploiting channel estimation based on CSMA/CA mechanism

A new metric for frequency synchronization by exploiting the channel information from the RtS control frame reception is developed in this section. The proposed algorithm is performed in two stages (see Figure 5.4): (i) the first stage ("STF-

based ACF"; "LTF-based ACF") is used to only generate a good initial points for a proper convergence of the Newton-Raphson approximation; (ii) the second stage ("CE-based metric") is proposed to use a new metric exploiting the channel estimation.

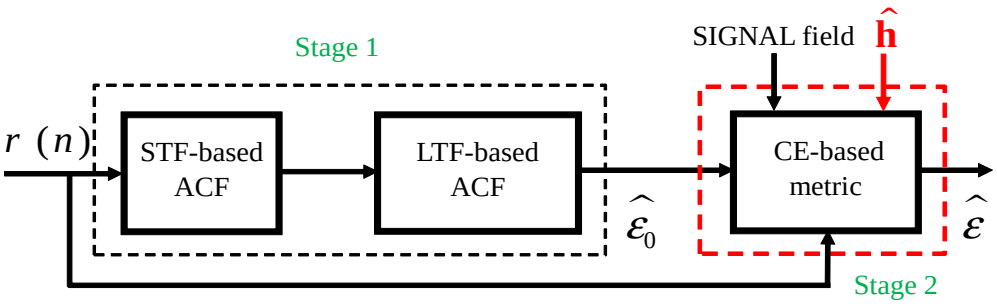

Figure 5.4. Frequency synchronization algorithm using channel information (FS-based CE)

5.4.1 Channel estimation based on RtS control frame

Before the first stage, the proposed algorithm requires the estimation of the channel when the CSMA/CA mechanism is activated. This estimation will be used in the second stage. Indeed in the CSMA/CA mechanism, the RtS frame is transmitted before DATA frame. From this observation, the channel estimation from the RtS reception was previously employed as additional information for the DATA frame time synchronization (see Section 4.4, Chapter 4). Because the PREAMBLE field of RtS and CtS frames is built similarly to DATA frame, the receiver estimates the channel denoted $\widehat{\mathbf{h}}$ according to the known LTF of the RtS frame using the MAP criterion as given by equation (4.32).

5.4.2 Frequency synchronization algorithm using channel estimation

The first stage is carried out similarly to the first stage of the algorithm proposed in Section 5.3 for the initialization of the Newton-Raphson approximation in the next step (see Section 5.3.1).

The second stage is performed according to the following metric:

$$\hat{\epsilon} = \arg\min_{\epsilon}\{g_{CE}(\epsilon)\}, \tag{5.7}$$

with

$$\begin{aligned} g_{CE}(\epsilon) =& ||\mathbf{r}_{L1} - \mathbf{\Phi}_{\epsilon,L1}\mathbf{S}_{L1}\widehat{\mathbf{h}}||^2 + ||\mathbf{r}_{L2} - \mathbf{\Phi}_{\epsilon,L2}\mathbf{S}_{L2}\widehat{\mathbf{h}}||^2 + \\ & ||\mathbf{r}_S - \mathbf{\Phi}_{\epsilon,S}\mathbf{S}_S\widehat{\mathbf{h}}||^2, \end{aligned} \tag{5.8}$$

where $\widehat{\mathbf{h}}$ is given by (4.32). Note that the indexes $L1$, $L2$ refer to the first and second repetitions of LTF while the index S concerns the SIGNAL field. $\mathbf{r}_{L1}$ and $\mathbf{r}_{L2}$ are two received signal vectors corresponding to the two LTF repetitions. It is easily seen that $\mathbf{S}_{L1} = \mathbf{S}_{L2}$ with $\mathbf{S}_{L1} = [\mathbf{S}_{0,L1}, \mathbf{S}_{1,L1}, .., \mathbf{S}_{L-1,L1}]$; $\mathbf{S}_{l,L1} = [x(n-l), x(n+1-l), .., x(n+N-1-l)]^T$ where $x(n)$ is the start sample of the LTF in the time domain (with $l = 0 : L-1$).

Let $\mathbf{\Phi}_{\epsilon,L1}$ =diag$[e^{j\frac{2\pi\epsilon n}{N}}, e^{j\frac{2\pi\epsilon(n+1)}{N}}, ..., e^{j\frac{2\pi\epsilon(n+N-1)}{N}}]$ then $\mathbf{\Phi}_{\epsilon,L2} = e^{j2\pi\epsilon}\mathbf{\Phi}_{\epsilon,L1}$. $\mathbf{r}_S$ of size $(N_S + N_g) \times 1$ is the received signal vector corresponding to the SIGNAL field and its guard interval. $\mathbf{\Phi}_{\epsilon,S} = \text{diag}[e^{j\frac{2\pi\epsilon(n+2N)}{N}}, e^{j\frac{2\pi\epsilon(n+1+2N)}{N}}, ..., e^{j\frac{2\pi\epsilon(n+N_S+N_g-1+2N)}{N}}]$. $\mathbf{S}_S = [\mathbf{S}_{0,S}, \mathbf{S}_{1,S}, .., \mathbf{S}_{L-1,S}]$, $\mathbf{S}_{l,S} = [x(n-l+2N), x(n+1-l+2N), .., x(n+N_S+N_g-1-l+2N)]^T$ where $x(n+2N)$ is the start sample of the guard interval of the SIGNAL field.

To estimate ϵ satisfying the condition given by equation (5.7), the Newton-Raphson approximation is employed as follows:

$$\hat{\epsilon}_{i+1} = \hat{\epsilon}_i - \Big(\frac{\partial^2 g_{CE}(\epsilon)}{\partial \epsilon^2}\Big)^{-1} \frac{\partial g_{CE}(\epsilon)}{\partial \epsilon}|_{\epsilon=\hat{\epsilon}_i}, \tag{5.9}$$

where the initialization value $\hat{\epsilon}_0 = \hat{\epsilon}_{total}$ provided by the first stage and

$$\begin{aligned}\partial g_{CE}(\epsilon)/\partial\epsilon = &-2\text{Re}(\mathbf{r}_{L1}^H \mathbf{G}_{L1}\mathbf{\Phi}_{\epsilon,L1}\mathbf{S}_{L1}\widehat{\mathbf{h}}) - 2\text{Re}(j2\pi e^{j2\pi\epsilon}\mathbf{r}_{L2}^H\mathbf{G}_{L1}\mathbf{\Phi}_{\epsilon,L1}\mathbf{S}_{L1}\widehat{\mathbf{h}}+\\ &+ e^{j2\pi\epsilon}\mathbf{r}_{L2}^H\mathbf{G}_{L1}\Phi_{\epsilon,L1}\mathbf{S}_{L1}\widehat{\mathbf{h}}) - 2\text{Re}(\mathbf{r}_S^H\mathbf{G}_S\mathbf{\Phi}_{\epsilon,S}\mathbf{S}_S\widehat{\mathbf{h}}),\end{aligned} \tag{5.10}$$

$$\begin{aligned}\partial^2 g_{CE}(\epsilon)/\partial\epsilon^2 = &-2\text{Re}(\mathbf{r}^H\mathbf{G}_{L1}^2\mathbf{\Phi}_{\epsilon,L1}\mathbf{S}_{L1}\widehat{\mathbf{h}}) - 2\text{Re}((2\pi)^2 e^{j2\pi\epsilon}\mathbf{r}_{L2}^H\mathbf{\Phi}_{\epsilon,L1}\mathbf{S}_{L1}\widehat{\mathbf{h}}+\\ &+ j4\pi e^{j2\pi\epsilon}\mathbf{r}_{L2}^H\mathbf{G}_{L1}\mathbf{\Phi}_{\epsilon,L1}\mathbf{S}_{L1}\widehat{\mathbf{h}} + e^{j2\pi\epsilon}\mathbf{r}_{L2}^H\mathbf{G}_{L1}^2\mathbf{\Phi}_{\epsilon,L1}\mathbf{S}_{L1}\widehat{\mathbf{h}})-\\ &- 2\text{Re}(\mathbf{r}_S^H\mathbf{G}_S^2\mathbf{\Phi}_{\epsilon,S}\mathbf{S}_S\widehat{\mathbf{h}}),\end{aligned} \tag{5.11}$$

with $\mathbf{G}_{L1} = j\frac{2\pi}{N}\text{diag}[n, n+1, ..., (n+N-1)]$, $\mathbf{G}_S = j\frac{2\pi}{N}\text{diag}[n+2N, n+1+2N, ..., (n+N+N_g-1+2N)]$.

5.4.3 Numerical Results

Similar to the previous section (i.e. Section 5.3), this section shows the performance of the proposed frequency synchronization algorithm in terms of MSE versus SNR under the two channel models.

We compare the MSE of the proposed algorithm denoted **Algorithm 4 (FS-based CE)** with the algorithms defined in Section 5.3.3: **Algorithm 1 (Manusani)** [57], **Algorithm 2 (Le-based MAP-2LTF)** [52] and **Algorithm 3 (Le-based SIGNAL)**. The communication system and parameters used for simulating these algorithms are completely similar to the ones in Section 5.3.

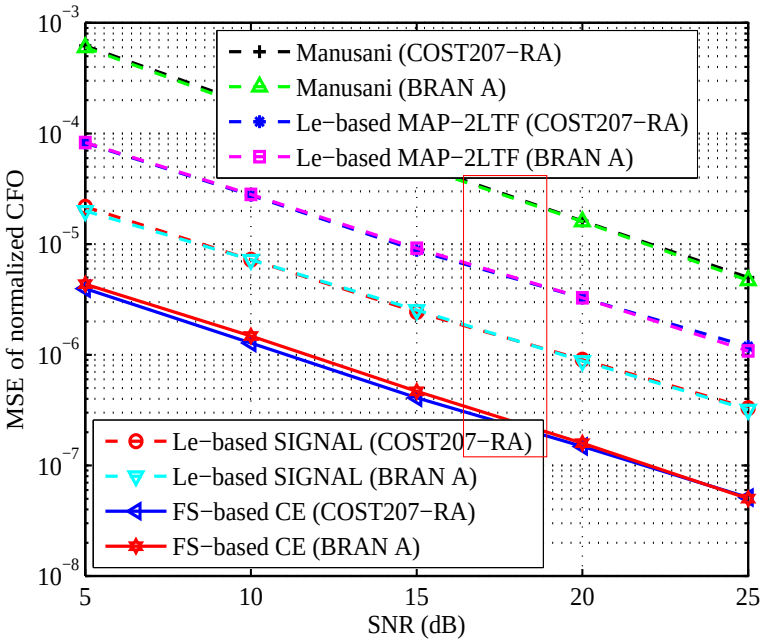

Figure 5.5. MSE of normalized CFO of algorithms in [57] (Manusani), [52] (Le-based MAP-2LTF), algorithms exploiting the SIGNAL field and channel estimation with $|\epsilon| \leq 0.6$

Figure 5.5 shows that, for every values of SNR, the proposed algorithm (solid line) is able to provide much lower MSE compared to the other ones. To illustrate this, consider the 802.11a operating mode at for example SNR=17.5 dB. The MSE provided by algorithms 1, 2, 3 and 4 is respectively: MSE(Manusani)= 3×10^{-5}; MSE(Le-based MAP-2LTF)=5×10^{-6}; MSE(Le-based SIGNAL)=1.1×10^{-6} and MSE(FS-based CE)=2.8×10^{-7}.

5.5 Conclusion

In this chapter, we proposed two CFO estimators based on the SIGNAL field as well as on the channel information provided by the RtS control frame when the CSMA/CA mechanism is triggered. The MAP criterion was also applied to enhance the estimate process. By such strategy, the two proposed frequency synchronization schemes have much better performance than the other frequency synchronization algorithms proposed in the literature. This has been validated over both the indoor and outdoor environments for the entire range of SNRs.

CHAPTER 6

Time and frequency synchronization algorithms

Contents

6.1 Introduction

In Chapter 4, we presented the symbol timing estimators that indicate the positions of ISI-free FFT windows. To determine the CFO included in received signal, frequency synchronization algorithms were investigated in Chapter 5. In both chapters, the performance of the synchronization algorithms has been improved significantly by taking advantage of the RtS control frame reception when the CSMA/CA mechanism is active. However, when the time synchronization is considered, the frequency offset has been assumed to be known and perfectly compensated by the receiver and vice versa.

In this chapter, we first propose a synchronization algorithm which considers both time and frequency synchronization based on MAP criterion. Then to enhance the accuracy of timing symbol estimation, this algorithm is followed by the fine time synchronization stage in presence of imperfect channel state information that was described in Section 4.5.

6.2 Joint MAP time and frequency synchronization

The proposed synchronization algorithm, as summarized in Figure 6.1, is performed by the receiver in two main stages: (i) coarse time synchronization using the SIGNAL field and channel estimation from the RtS control frame ("STF-based CCF"; "SIGNAL-based CCF"); (ii) joint MAP fine time synchronization and frequency offset estimation (denoted as "Joint MAP TS-FS" in Figure 6.1).

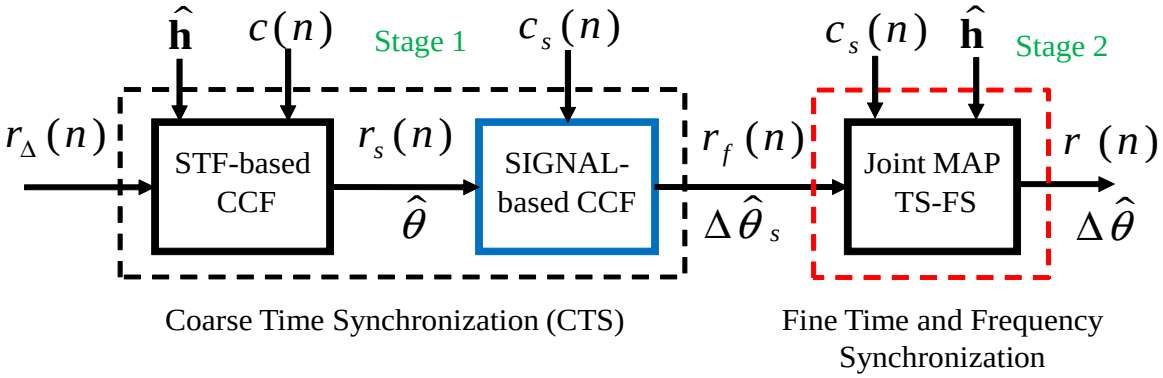

Figure 6.1. Proposed time and frequency synchronization algorithm (Joint MAP TS-FS)

6.2.1 Coarse time synchronization

The first stage estimates the symbol timing θ (see equation (2.8)) of the received signal. This is done via the coarse time synchronization stage described in Section

4.4 (denoted as "Time synchronization using Channel Estimation (CE) based on CSMA/CA mechanism"). Specifically, first, the channel information is estimated from the RtS control frame reception by equation (4.32). This channel estimation is then used as an additional information for estimating the symbol timing θ of the DATA frame according to equation (4.35). The remaining time offset is then estimated by exploiting the SIGNAL field knowledge according to equation (4.7).

The received signal $r_f(n)$ with residual time offset $\Delta\theta$ and normalized CFO ϵ reads

$$r_f(n) = \sum_{i=0}^{L-1} h(i)x(n-i-\Delta\theta)e^{j\frac{2\pi\epsilon(n-\Delta\theta)}{N}} + g(n). \tag{6.1}$$

6.2.2 Joint MAP fine time and frequency synchronization

To estimate the remaining time offset $\Delta\theta$ and the normalized CFO ϵ appearing in equation (6.1), the second stage of the proposed algorithm (see Figure 6.1) proposes a joint time and frequency synchronization approach based on the MAP criterion ("Joint MAP TS-FS"). In order to do so, we not only adapt the frequency synchronization algorithm developed in [52] to the IEEE 802.11a specifications but also make changes to the algorithm since the authors assumed that the time synchronization is known and then perfectly compensated by the receiver. Moreover, the knowledge of the SIGNAL field, as described in the previous chapter, is also taken into account in this stage.

The received signal $\mathbf{r}$ corresponding to the two LTF repetitions and the SIGNAL field can be expressed in matrix form as follows:

$$\mathbf{r} = \mathbf{\Phi}_{\Delta\theta,\epsilon}\mathbf{S}_{\Delta\theta}\mathbf{h} + \mathbf{g}, \tag{6.2}$$

where

$\mathbf{r} = [r_f(n), r_f(n+1), ..., r_f(n+2N+N_G+N_S-1)]^T$;
$\mathbf{S}_{\Delta\theta} = [\mathbf{S}_{0,\Delta\theta}; \mathbf{S}_{1,\Delta\theta}, \ldots, \mathbf{S}_{L-1,\Delta\theta}]$;
$\mathbf{S}_{l,\Delta\theta} = [x(n-l-\Delta\theta), x(n+1-l-\Delta\theta), \ldots, x(n+2N+N_G+N_S-1-l-\Delta\theta)]^T$;
$\mathbf{h} = [h(0), h(1), \ldots, h(L-1)]^T$;
$\mathbf{g} = [g(n-\Delta\theta), g(n-\Delta\theta+1), \ldots, g(n-\Delta\theta+2N+N_S+N_G-1)]^T$;
$\mathbf{\Phi}_{\Delta\theta,\epsilon} = \text{diag}\left\{e^{j\frac{2\pi\epsilon(n-\Delta\theta)}{N}}, \ldots, e^{j\frac{2\pi\epsilon(n-\Delta\theta+2N+N_S+N_G-1)}{N}}\right\}$.

Where the various $x(n)$ are the known LTF and SIGNAL samples in the time domain ($0 \leq l \leq L-1$), N the number of samples of one LTF repetition, N_S the

length of the SIGNAL field and N_G the length of its guard interval, $\mathbf{h}$ is the CIR vector and $\mathbf{g}$ is noise vector.

The remaining time offset $\Delta\theta$, the normalized frequency offset ϵ and the CIR $\mathbf{h}$ are jointly estimated according to the MAP criterion as follows:

$$\{\hat{\mathbf{h}}, \widehat{\Delta\theta}, \hat{\epsilon}\} = \arg\max_{\mathbf{h},\Delta\theta,\epsilon} \ln P(\mathbf{h}, \Delta\theta, \epsilon|\mathbf{r}), \tag{6.3}$$

where P is the *a posteriori* probability density function of $\mathbf{h}$, $\Delta\theta$ and ϵ given $\mathbf{r}$. Note that ϵ is also assumed to be uniformly distributed in the range $[-\epsilon_0, \epsilon_0]$. To solve equation (6.3), we first define a set $\mathbf{\Lambda}$ containing $2M+1$ possible time offset values; $\mathbf{\Lambda} = \{-\Delta\theta_M, \ldots, \Delta\theta_M\}$. For a given value $\Delta\theta_m \in \mathbf{\Lambda}$, the MAP-based estimations of the CFO and channel coefficients are given as follows:

$$\{\hat{\mathbf{h}}_{\Delta\theta_m}, \hat{\epsilon}_{\Delta\theta_m}\} = \arg\min_{\mathbf{h},\epsilon} f^{(m)}_{\text{MAP}}(\mathbf{h}, \epsilon), \tag{6.4}$$

where

$$f^{(m)}_{\text{MAP}}(\mathbf{h}, \epsilon) = \frac{1}{\sigma_g^2}||\mathbf{r}_{\Delta\theta_m} - \mathbf{\Phi}_{\Delta\theta_m,\epsilon}\mathbf{S}_{\Delta\theta_m}\mathbf{h}||^2 + \mathbf{h^H}\mathbf{R_h^{-1}}\mathbf{h},$$

with $\mathbf{r}_{\Delta\theta_m}$ being the received signal corresponding to the offset value $\Delta\theta_m$.

Setting the gradient vector of $f^{(m)}_{\text{MAP}}(\mathbf{h}, \epsilon)$ with respect to $\mathbf{h}^H$ to zero provides the MAP-based channel estimate

$$\widehat{\mathbf{h}}_{\Delta\theta_m} = \left[\mathbf{S}^H_{\Delta\theta_m}\mathbf{S}_{\Delta\theta_m} + \sigma_g^2\mathbf{R_h^{-1}}\right]^{-1}\mathbf{S}^H_{\Delta\theta_m}\mathbf{\Phi}^H_{\Delta\theta_m,\epsilon}\mathbf{r}_{\Delta\theta_m}. \tag{6.5}$$

Replacing (6.5) into $f^{(m)}_{\text{MAP}}(\mathbf{h}, \epsilon)$ produces the CFO estimate

$$\hat{\epsilon}_{\Delta\theta_m} = \arg\min_{\epsilon} g^{(m)}_{\text{MAP}}(\epsilon), \tag{6.6}$$

where

$$\begin{aligned} g^{(m)}_{\text{MAP}}(\epsilon) &= \mathbf{r}^H_{\Delta\theta_m}\mathbf{\Phi}_{\Delta\theta_m,\epsilon}\mathbf{S}^+_{\Delta\theta_m}\mathbf{\Phi}^H_{\Delta\theta_m,\epsilon}\mathbf{r}_{\Delta\theta_m}, \\ \mathbf{S}^+_{\Delta\theta_m} &= \mathbf{S}_{\Delta\theta_m}\left[\mathbf{S}^H_{\Delta\theta_m}\mathbf{S}_{\Delta\theta_m} + \mathbf{R_h^{-1}}\sigma_g^2\right]^{-1}\mathbf{S}^H_{\Delta\theta_m}. \end{aligned}$$

The Newton-Raphson iteration is then calculated as follows:

$$\hat{\epsilon}_{\Delta\theta_m,i+1} = \hat{\epsilon}_{\Delta\theta_m,i} - \left[\frac{\partial^2 g^{(m)}_{\text{MAP}}(\epsilon)}{\partial\epsilon^2}\right]^{-1}\frac{\partial g^{(m)}_{\text{MAP}}(\epsilon)}{\partial\epsilon}\Big|_{\hat{\epsilon}=\epsilon_i}, \tag{6.7}$$

where $\hat{\epsilon}_{\Delta\theta_m,i}$ indicates the CFO estimation at the i^{th} iteration where the starting

frequency offset $\hat{\epsilon}_{\Delta\theta_m,0}$ is initialized as described in Section 5.3.1, and

$$\begin{aligned}
\frac{\partial g^{(m)}_{\mathrm{MAP}}(\epsilon)}{\partial \epsilon} &= 2\Re\left\{\mathbf{r}^H_{\Delta\theta_m}\mathbf{G}_{\Delta\theta_m}\mathbf{\Phi}_{\Delta\theta_m,\epsilon}\mathbf{S}^+_{\Delta\theta_m}\mathbf{\Phi}^H_{\Delta\theta_m,\epsilon}\mathbf{r}_{\Delta\theta_m}\right\},\\
\frac{\partial g^2_{\mathrm{MAP}}(\epsilon)}{\partial \epsilon^2} &= 2\Re\left\{\mathbf{r}^H_{\Delta\theta_m}\mathbf{G}^2_{\Delta\theta_m}\mathbf{\Phi}_{\Delta\theta_m,\epsilon}\mathbf{S}^+_{\Delta\theta_m}\mathbf{\Phi}^H_{\Delta\theta_m,\epsilon}\mathbf{r}_{\Delta\theta_m} + \right.\\
&\qquad \left.\mathbf{r}^H_{\Delta\theta_m}\mathbf{G}_{\Delta\theta_m}\mathbf{\Phi}_{\Delta\theta_m,\epsilon}\mathbf{S}^+_{\Delta\theta_m}\mathbf{G}^H_{\Delta\theta_m}\mathbf{\Phi}^H_{\Delta\theta_m,\epsilon}\mathbf{r}_{\Delta\theta_m}\right\},\\
\mathbf{G}_{\Delta\theta_m} &= j\frac{2\pi}{N}\mathrm{diag}\left\{n-\Delta\theta_m, n-\Delta\theta_m+1, ...,\right.\\
&\qquad \left. n-\Delta\theta_m+2N+N_S+N_G-1\right\}.
\end{aligned}$$

From equations (6.5) and (6.6), the CIR estimate is obtained by

$$\widehat{\mathbf{h}}_{\Delta\theta_m} = \left[\mathbf{S}^H_{\Delta\theta_m}\mathbf{S}_{\Delta\theta_m} + \sigma_g^2\mathbf{R}^{-1}_{\mathbf{h}}\right]^{-1}\mathbf{S}^H_{\Delta\theta_m}\mathbf{\Phi}^H_{\Delta\theta_m,\hat{\epsilon}_m}\mathbf{r}_{\Delta\theta_m}. \tag{6.8}$$

Among the $2M+1$ estimates of $\widehat{\mathbf{h}}_{\Delta\theta_m}$ based on (6.5), we select those that satisfy the following conditions:

$$|\hat{h}_{\Delta\theta_m}(0)| > \beta \max_{\Delta\theta_i}|\hat{h}_{\Delta\theta_i}(0)|, \tag{6.9}$$

where β is a given threshold that is selected based on the noise level and type of channel model. Therefore, the set $\mathbf{\Lambda}$ becomes $\mathbf{\Gamma}$ given by

$$\mathbf{\Gamma} = \{\omega_0, \ldots, \omega_{M'}; \quad M^{'} \leq 2M\}. \tag{6.10}$$

Finally, the remaining time offset is estimated as

$$\Delta\widehat{\theta} = \arg\max_{\omega_{m'}}\sum_{n=0}^{L-1}|\hat{h}_{\omega_{m'}}(n)|^2. \tag{6.11}$$

6.2.3 Numerical Results

This section shows the simulation results of the proposed synchronization algorithm. As in the previous chapters, the normalized frequency offset ϵ is taken randomly according to a uniform distribution in the range $[-0.6, 0.6]$ and the symbol timing θ is also randomly distributed according to a uniform distribution. The robustness of our algorithms in various channel environments is checked via simulations following two models: COST207-RA and BRAN A. The performance of the following algorithms is compared:

i) **Canet [16]**: The ACF relied on the STF is used for the Coarse Time Synchronization (CTS) and Frequency Synchronization (FS). The CCF based on the LTF is then employed for the Fine Time Synchronization (FTS) stage;

ii) **Canet with a perfect TS** (Time Synchronization) is Canet's algorithm, assuming that the true symbol timing θ is known and perfectly compensated by the receiver;

iii) **Canet with a perfect FS** (Frequency Synchronization) is Canet's algorithm but when the true value of frequency offset ϵ is known and then perfectly compensated by the receiver;

iv) **Joint MAP TS-FS** is the algorithm proposed in this section;

v) **Joint MAP TS-FS with a perfect TS** is Joint MAP TS-FS algorithm when the true symbol timing θ is known and perfectly compensated by the receiver;

vi) **Joint MAP TS-FS with a perfect FS** is Joint MAP TS-FS algorithm when the true frequency offset ϵ is perfectly known and compensated at the receiver. Specifically, the received signal after the coarse time synchronization stage ("Stage 1" in Figure 6.1) as given by equation (6.1) is multiplied by $e^{-j\frac{2\pi\epsilon n}{N}}$. Equation (6.2) becomes

$$\mathbf{r} = \mathbf{S}_{\Delta\theta}\mathbf{h} + \mathbf{g}, \tag{6.12}$$

since $\mathbf{\Phi}_{\Delta\theta,\epsilon}$ is an identity matrix. Now, this algorithm becomes the joint time and channel estimation and equation (6.3) is reduced to

$$\{\hat{\mathbf{h}}, \widehat{\Delta\theta}\} = \arg\max_{\mathbf{h},\Delta\theta} \ln P(\mathbf{h}, \Delta\theta|\mathbf{r}). \tag{6.13}$$

To solve equation (6.13), we define a set $\mathbf{\Lambda}$ containing $2M+1$ possible time offset values; $\mathbf{\Lambda} = \{-\Delta\theta_M, \ldots, \Delta\theta_M\}$. For a given value $\Delta\theta_m \in \mathbf{\Lambda}$, the MAP-based estimation of channel coefficients deduced from equation (6.13) is given by

$$\{\hat{\mathbf{h}}_{\Delta\theta_m}\} = \arg\min_{\mathbf{h}} f^{(m)}_{\mathrm{MAP}}(\mathbf{h}), \tag{6.14}$$

where

$$f^{(m)}_{\mathrm{MAP}}(\mathbf{h}) = \frac{1}{\sigma_g^2}||\mathbf{r}_{\Delta\theta_m} - \mathbf{S}_{\Delta\theta_m}\mathbf{h}||^2 + \mathbf{h^H}\mathbf{R_h^{-1}}\mathbf{h},$$

Setting the gradient vector of $f^{(m)}_{\mathrm{MAP}}(\mathbf{h})$ with respect to $\mathbf{h}^H$ to zero provides the MAP-based channel estimate

$$\widehat{\mathbf{h}}_{\Delta\theta_m} = \left[\mathbf{S}^H_{\Delta\theta_m}\mathbf{S}_{\Delta\theta_m} + \sigma_g^2\mathbf{R_h^{-1}}\right]^{-1}\mathbf{S}^H_{\Delta\theta_m}\mathbf{r}_{\Delta\theta_m}. \tag{6.15}$$

Equations from (6.9) to (6.11) are then performed to obtain $\widehat{\Delta\theta}$.

The simulation results under the COST207-RA channel are illustrated in Figures 6.2, 6.3 and 6.4.

Figure 6.2 illustrates the MSE between the true CFO and its estimate ($E\{(\epsilon - \hat{\epsilon}_m)^2\}$) versus SNR. The analysis of the curves shows that regardless of the time synchronization being perfect or not, the MSE of our algorithm is much lower than Canet's algorithm. Indeed, at SNR=17.5 dB, MSE(Canet) $= 4.2 \times 10^{-5}$ and MSE(Joint MAP TS-FS) $= 1.6 \times 10^{-6}$. Besides, it can be observed from the figure that the two curves corresponding to our algorithm (i.e. Joint MAP TS-FS and Joint MAP TS-FS with a perfect TS) are similar showing that even if the time offset is estimated the MSE is not affected compared to a perfect time offset compensation.

Figure 6.3 measures the detection probability of arrival time of the transmitted physical packet for a given deviation with respect to its true time position (i.e., $\widehat{\theta} - \theta$) at SNR=15 dB for Canet and Joint MAP TS-FS algorithms using 7.10^4 test physical packets. The Joint MAP TS-FS algorithm provides the highest estimation accuracy of 99% when the packet arrival time is detected without time deviation (with respect to the arrival time of packet) compared to other algorithms.

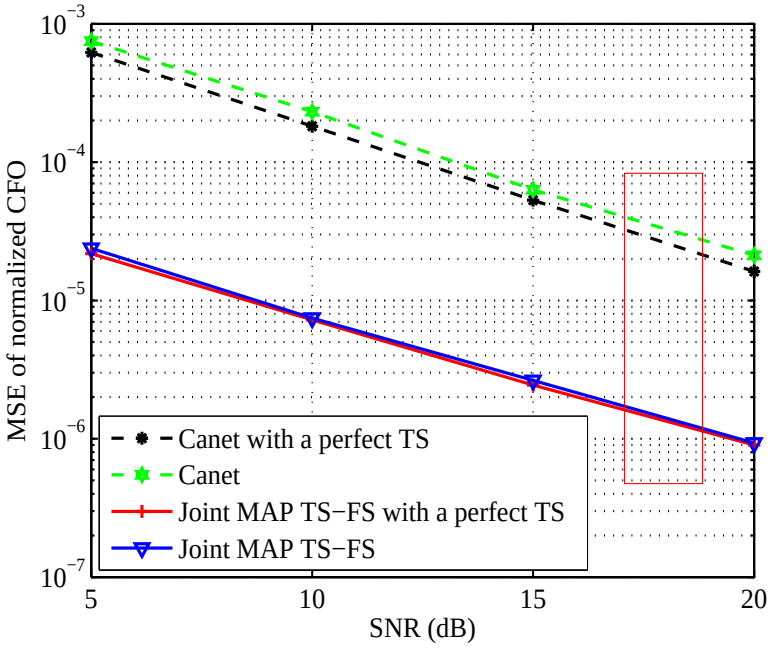

Figure 6.2. MSE of normalized CFO of Canet [16] and Joint MAP TS-FS algorithms with $|\epsilon| \leq 0.6$ under COST207-RA channel model (the rectangular box represents the operating mode of the 802.11a standard)

Figure 6.4 provides PSF versus SNR. Considered the operating mode of the IEEE 802.11a standard, for example at SNR = 17.5 dB and with no time deviation (i.e. $\hat{\theta}-$

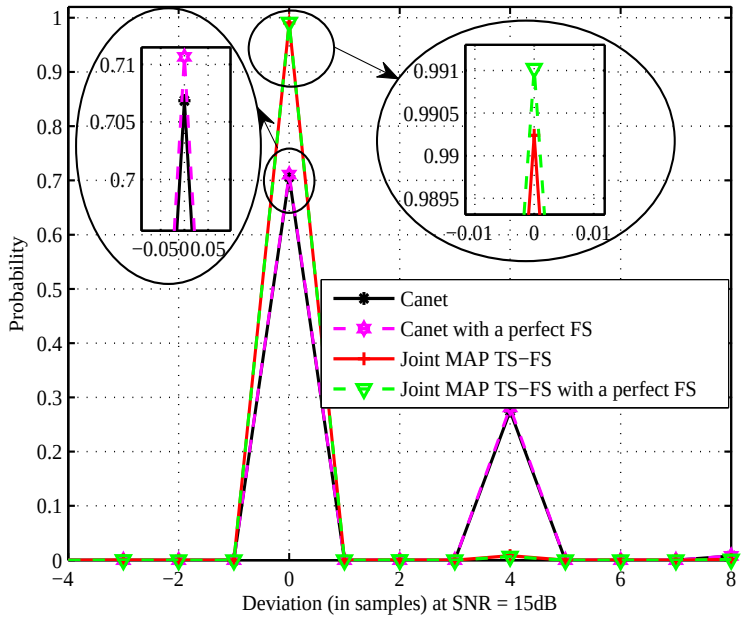

Figure 6.3. Deviation with respect to the true time position of a physical packet of for algorithms Canet [16] and Joint MAP TS-FS with $|\epsilon| \leq 0.6$ under COST207-RA channel model

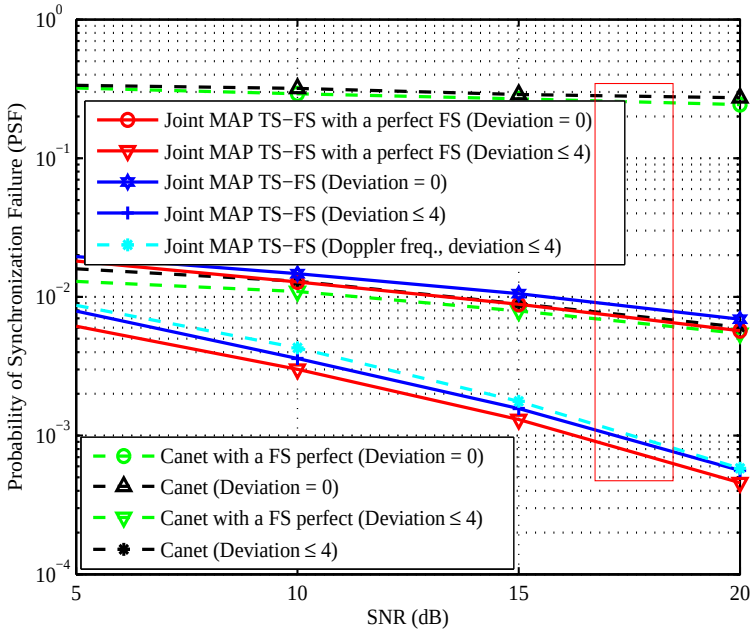

Figure 6.4. PSF of Canet [16] and Joint MAP TS-FS algorithms with $|\epsilon| \leq 0.6$ under COST207-RA channel model

$\theta = 0$; θ true value), the PSF of Canet and Joint MAP TS-FS algorithms are as follows: PSF(Canet, perfect FS) $= 2.5 \times 10^{-1}$; PSF(Joint MAP TS-FS, perfect FS) $=$

7.2×10^{-3} and PSF(Joint MAP TS-FS) $= 8.7 \times 10^{-3}$ which is close to the PSF calculated when the frequency offset is perfectly compensated. When accepting arrival packets with time deviation which do not exceed 4 samples (which can be assumed compatible with the existentce of the cyclic prefix), the PSF of both algorithms is reduced. However, the PSF of Joint MAP TS-FS algorithm is smaller than that of other algorithm. For example, at SNR = 17.5 dB, when the CFO is not perfectly compensated we obtain PSF(Joint MAP TS-FS) $= 1 \times 10^{-3}$ while PSF(Canet) $= 7 \times 10^{-3}$.

Moreover, the analysis of the PSF curves indicates that the performance in terms of PSF of the Joint MAP TS-FS algorithm in both cases (i.e., perfect or not perfect FS) is almost similar. This is explained via equation (6.8). First, if we replace $\mathbf{r}_{\Delta\theta_m} = \mathbf{\Phi}_{\Delta\theta_m,\epsilon}\mathbf{S}_{\Delta\theta_m}\mathbf{h} + \mathbf{g}$ (see equation (6.2)) into equation (6.8), we obtain

$$\begin{aligned}\widehat{\mathbf{h}}_{\Delta\theta_m} = &\left[\mathbf{S}^H_{\Delta\theta_m}\mathbf{S}_{\Delta\theta_m} + \sigma_g^2\mathbf{R}_{\mathbf{h}}^{-\mathbf{1}}\right]^{-1}\mathbf{S}^H_{\Delta\theta_m}\mathbf{I}_{\Delta\theta,\hat{\epsilon}_m}(\mathbf{S}_{\Delta\theta_m}\mathbf{h}) + \\ &\left[\mathbf{S}^H_{\Delta\theta_m}\mathbf{S}_{\Delta\theta_m} + \sigma_g^2\mathbf{R}_{\mathbf{h}}^{-\mathbf{1}}\right]^{-1}\mathbf{S}^H_{\Delta\theta_m}\mathbf{\Phi}^H_{\Delta\theta_m,\hat{\epsilon}_m}\mathbf{g},\end{aligned} \tag{6.16}$$

where $\mathbf{I}_{\Delta\theta,\hat{\epsilon}_m}$ is the diagonal matrix of size $(2N + N_G + N_S) \times (2N + N_G + N_S)$ and is given by

$$\mathbf{I}_{\Delta\theta,\hat{\epsilon}_m} = \mathrm{diag}\left\{e^{j\frac{2\pi(\epsilon-\hat{\epsilon}_m)\Delta\theta}{N}}, e^{j\frac{2\pi(\epsilon-\hat{\epsilon}_m)\Delta\theta}{N}}, \ldots, e^{j\frac{2\pi(\epsilon-\hat{\epsilon}_m)\Delta\theta}{N}}\right\}.$$

Moreover Figure 6.2 shows that at a given SNR = 17.5 dB, the MSE of the normalized CFO of our algorithm (i.e. Joint MAP TS-FS) is equal to 1.6×10^{-6}. The experimental results show that the remaining value $\Delta\theta$ is relatively small and thus $e^{j2\pi(\epsilon-\hat{\epsilon}_m)\Delta\theta/N} \approx 1$. Therefore, $\mathbf{I}_{\Delta\theta,\hat{\epsilon}_m}$ is considered as an identity matrix and equation (6.16) becomes:

$$\widehat{\mathbf{h}}_{\Delta\theta_m} = \left[\mathbf{S}^H_{\Delta\theta_m}\mathbf{S}_{\Delta\theta_m} + \sigma_g^2\mathbf{R}_{\mathbf{h}}^{-\mathbf{1}}\right]^{-1}\mathbf{S}^H_{\Delta\theta_m}(\mathbf{S}_{\Delta\theta_m}\mathbf{h}) + \mathbf{g}', \tag{6.17}$$

where $\mathbf{g}' = \left[\mathbf{S}^H_{\Delta\theta_m}\mathbf{S}_{\Delta\theta_m} + \sigma_g^2\mathbf{R}_{\mathbf{h}}^{-\mathbf{1}}\right]^{-1}\mathbf{S}^H_{\Delta\theta_m}\mathbf{\Phi}^H_{\Delta\theta_m,\hat{\epsilon}_m}\mathbf{g}$.

In the case of perfect FS, from equation (6.15), we also obtain

$$\widehat{\mathbf{h}}_{\Delta\theta_m} = \left[\mathbf{S}^H_{\Delta\theta_m}\mathbf{S}_{\Delta\theta_m} + \sigma_g^2\mathbf{R}_{\mathbf{h}}^{-\mathbf{1}}\right]^{-1}\mathbf{S}^H_{\Delta\theta_m}(\mathbf{S}_{\Delta\theta_m}\mathbf{h}) + \mathbf{g}'', \tag{6.18}$$

where $\mathbf{g}'' = \left[\mathbf{S}^H_{\Delta\theta_m}\mathbf{S}_{\Delta\theta_m} + \sigma_g^2\mathbf{R}_{\mathbf{h}}^{-\mathbf{1}}\right]^{-1}\mathbf{S}^H_{\Delta\theta_m}\mathbf{g}$.

It can be observed that equation (6.17) is equivalent to (6.18). Otherwise both cases (i.e., known by the receiver and perfectly compensated (perfect); estimated by the receiver (not perfect FS)) employ the CIR estimate (i.e. $\widehat{\mathbf{h}}_{\Delta\theta_m}$) to estimate the remaining time offset $\Delta\theta$. As a result, for our algorithm (i.e. Joint MAP TS-FS algorithm) the PSF when the CFO is not perfectly compensated is close to the one of the perfect FS.

In addition, Figure 6.4 also illustrates the performance (in terms of PSF) of our algorithm when the estimated channel $\widehat{\mathbf{h}}$ during the negotiation of the transmission medium (see Section 4.4, equation (4.32)) has been slightly modified according to the relative motion of the receiving station just when the DATA frame is transmitted. It can be observed that the presence of Doppler frequency does not impair the performance of the proposed algorithm. This testifies that our algorithm is also not effected by the Doppler frequency in this particular context since the waiting time between the control and DATA frames is reasonably small.

In conclusion, the simulation results confirmed the performance of our algorithm in the COST207-RA channel. The conclusion is similar when the BRAN A model is introduced, and our algorithm shows the best performance in terms of MSE (Figure 6.5), PSF versus SNR (Figure 6.6) as well as PSF versus deviation respect to the true time position (Figure 6.7). For instance, SNR = 17.5 dB with no deviation, PSF(Canet) $= 4.3 \times 10^{-1}$ while the PSF of our algorithm (i.e. Joint MAP TS-FS) is 5.6×10^{-3}.

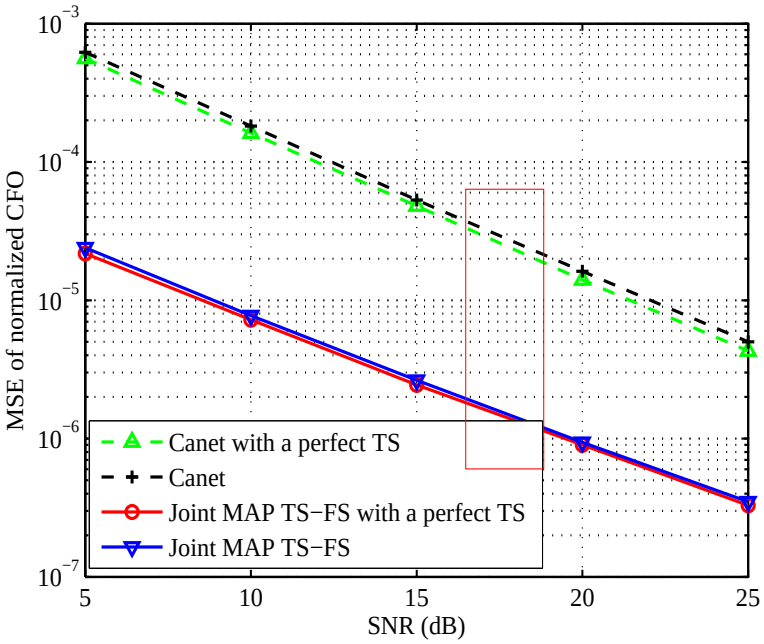

Figure 6.5. MSE of normalized CFO of Canet [16] and Joint MAP TS-FS algorithms with $|\epsilon| \leq 0.6$ under BRAN A channel model

6.3 Improved time and frequency synchronization

In the previous section, the algorithm joint MAP time and frequency synchronization has been developed. To obtain a more precise estimation of the remaining time

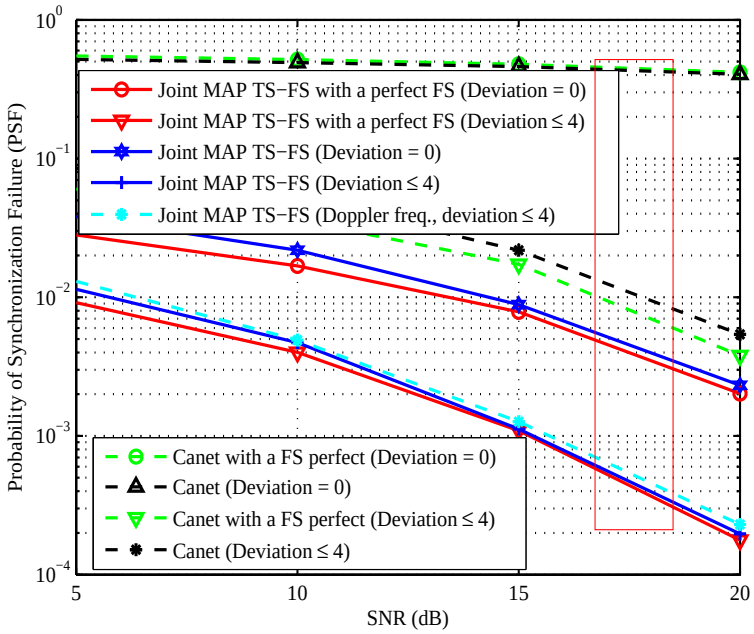

Figure 6.6. PSF of Canet [16] and Joint MAP TS-FS algorithms with $|\epsilon| \leq 0.6$ under BRAN A channel model

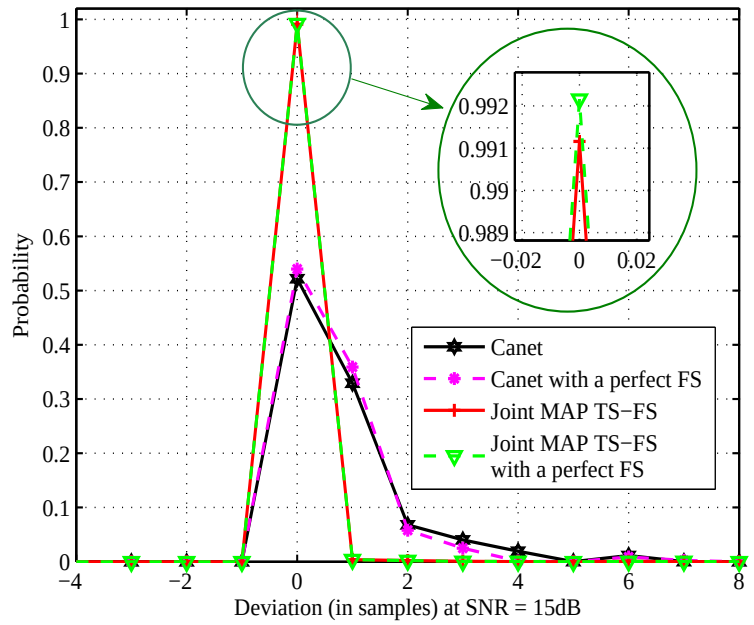

Figure 6.7. Deviation with respect to the true time position of a physical packet of for algorithms Canet [16] and Joint MAP TS-FS with $|\epsilon| \leq 0.6$ under BRAN A channel model

offset, after the second stage of the Joint MAP TS-FS algorithm (Figure 6.1), we add a third stage to further refine the fine time synchronization stage of the al-

gorithm mentioned in Section 4.5. Therefore, the new synchronization algorithm (see Figure 6.8) is performed by the receiver in three main stages: (i) coarse time synchronization using the SIGNAL field and channel estimation from the RtS control frame; (ii) joint MAP fine time synchronization and frequency offset estimation (denoted by "Joint MAP TS-FS"); and (iii) improved fine time synchronization in presence of imperfect channel state information denoted by "LTF-based timing metric". Stages 1 and 2 have been described in Section 6.2, we concentrate here on

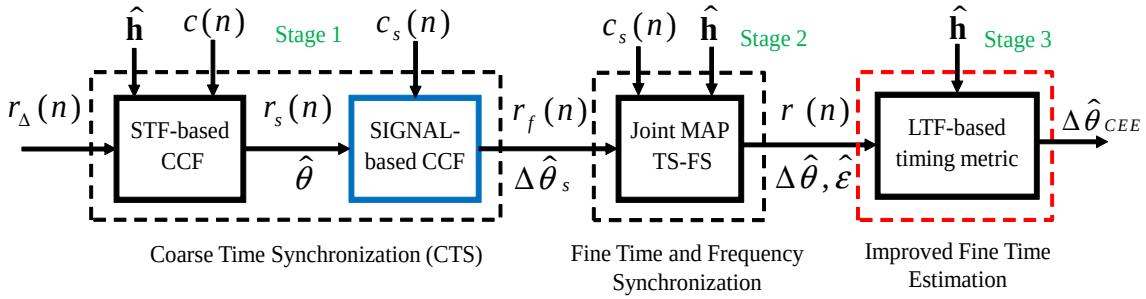

Figure 6.8. Improved fine time synchronization algorithm (Joint MAP TS-FS added TM)

the third stage. Recall that the "Joint MAP TS-FS" stage (i.e. stage 2) estimates the remaining time offset $\Delta\hat{\theta}$. The received signal at the input of third stage is then given by

$$r(n) = \sum_{i=0}^{L-1} h(i)x(n - i - \Delta\theta_{CEE}) + g(n), \tag{6.19}$$

where $\Delta\theta_{CEE} = \Delta\theta - \Delta\widehat{\theta}$ is the remaining time offset. Note that the received signal here is assumed to be free of frequency offset because the "Joint MAP TS-FS" stage discussed in Section 6.2 allows an almost perfect frequency offset compensation.

The purpose of the "LTF-based timing metric" stage is to estimate the remaining time offset $\Delta\theta_{CEE}$. This is performed according to the timing metric mentioned in Section 4.5 (Chapter 4). Therefore, the remaining time offset $\Delta\theta_{CEE}$ is estimated according to equation (4.40) as follows:

$$\Delta\hat{\theta}_{CEE} = \arg \min_{\Delta\theta_{CEE}\in\mathbf{\Lambda}} \{\widetilde{D}(\Delta\theta_{CEE})\}, \tag{6.20}$$

with

$$\begin{aligned}\widetilde{D}(\Delta\theta_{CEE}) = E[\mathbf{R}^H\mathbf{R}] - E[\mathbf{R}^H\mathbf{X}]\mu_{\mathbf{H}|\hat{\mathbf{H}}} - \mu^H_{\mathbf{H}|\hat{\mathbf{H}}}E[\mathbf{X}^H\mathbf{R}] + tr(\mathbf{\Sigma}_{\mathbf{H}|\hat{\mathbf{H}}}\mathbf{X}\mathbf{X}^H) + \\ + \mu^H_{\mathbf{H}|\hat{\mathbf{H}}}\mathbf{X}^H\mathbf{X}\mu_{\mathbf{H}|\hat{\mathbf{H}}},\end{aligned} \tag{6.21}$$

where the received signal $\mathbf{R}$ is obtained by taking the FFT function of equation (6.19).

The performance of the new synchronization scheme is evaluated on, Figures 6.9, 6.11 which provide the PSF versus SNR and Figures 6.10, 6.12 which shows the detection probability versus deviation of algorithms denoted "Joint MAP TS-FS" and "Joint MAP TS-FS added TM" in the various channels. The observation from both figures confirms that the new scheme gives a much lower PSF than that of the Joint MAP TS-FS algorithm. Indeed, in the COST207-RA, at SNR = 17.5 dB, for deviation no more than 4, when the CFO is estimated we achieve PSF(Joint MAP TS-FS added TM) $= 1.3 \times 10^{-4}$ while PSF(Joint MAP TS-FS) $= 7 \times 10^{-4}$.

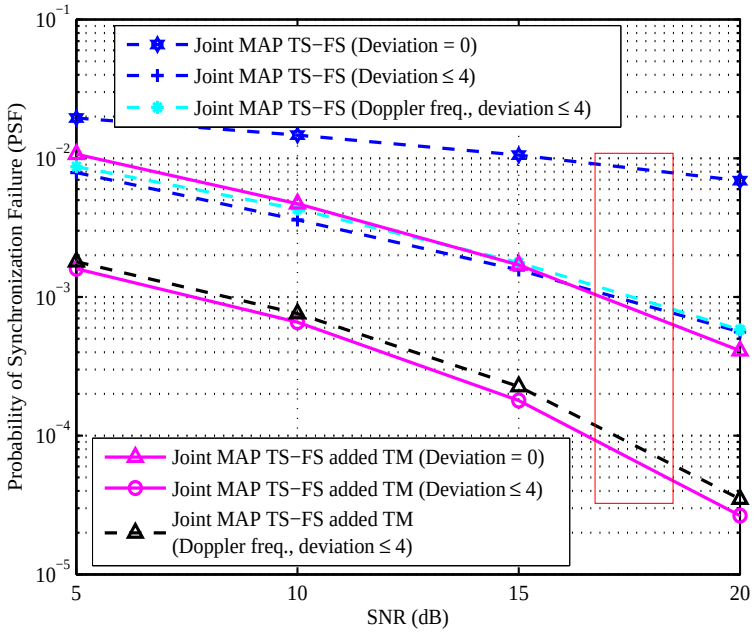

Figure 6.9. PSF of the Joint MAP TS-FS and Joint MAP TS-FS added TM algorithms with $|\epsilon| \leq 0.6$ under COST207-RA channel model

6.4 Conclusion

This chapter proposed a novel algorithm for time and frequency synchronization compliant with the IEEE 802.11a wireless communication standard when the activity of the CSMA/CA handshaking is activated. First we build a posterior function of time offset, CFO and channel coefficients based on the training sequence and SIGNAL field. Maximizing this posterior function allows to estimate jointly the time offset and CFO. Second, a timing metric in the frequency domain taking into account the imperfect channel state information was finally added. The combined approaches achieve considerable improvement measured by different terms as

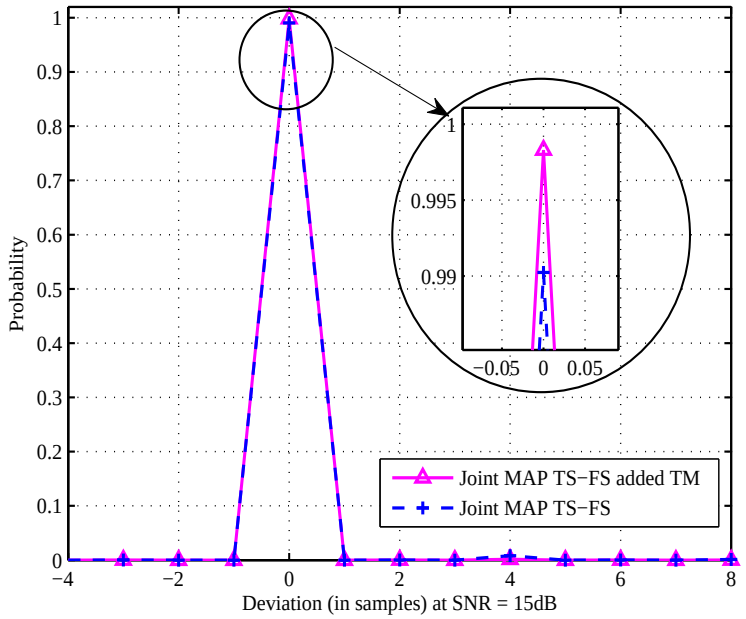

Figure 6.10. Deviation with respect to the true time position of a physical packet of the Joint MAP TS-FS and Joint MAP TS-FS added TM algorithms with $|\epsilon| \leq 0.6$ under COST207-RA channel model

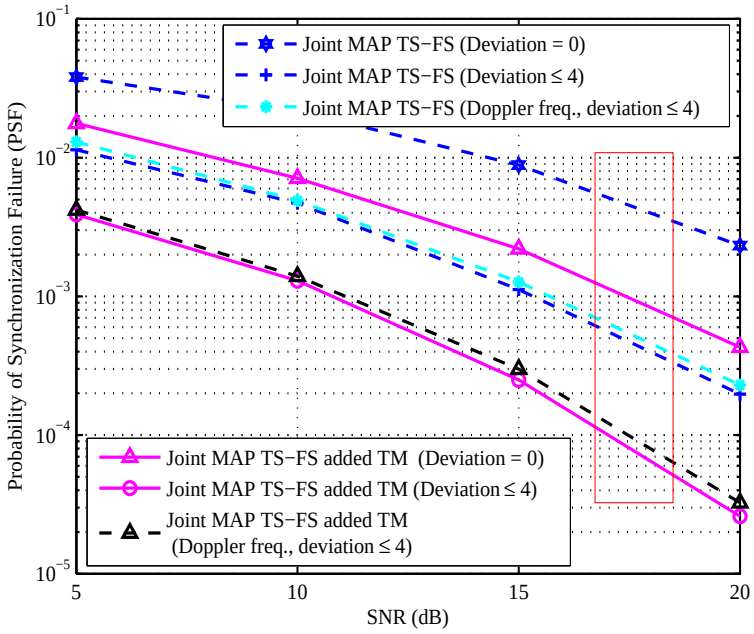

Figure 6.11. PSF of the Joint MAP TS-FS and Joint MAP TS-FS added TM algorithms with $|\epsilon| \leq 0.6$ under BRAN A channel model

probability of synchronization failure, mean square error in various channel environments.

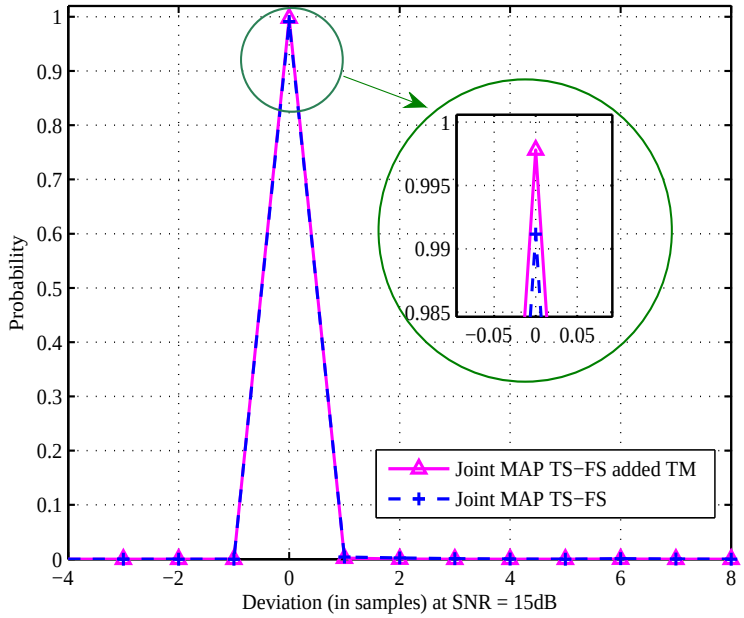

Figure 6.12. Deviation with respect to the true time position of a physical packet of the Joint MAP TS-FS and Joint MAP TS-FS added TM algorithms with $|\epsilon| \leq 0.6$ under BRAN A channel model

CHAPTER 7

Conclusions and perspectives

This thesis has focused on synchronization algorithms in practical OFDM systems. The algorithms developed in this thesis were adapted to the IEEE 802.11a standard, however they are also applicable to existing and future OFDM systems, robust to challenging mobile wireless channel conditions, and feasible for hardware real-time implementation. This thesis can be summarized via the content of each chapter below.

In Chapter 2, we presented the mathematical modeling of a general wireless communication system based on OFDM technique. The traditional wireless propagation channel models COST-207, BRAN A and their power delay profiles used in simulations were also described. Besides, the IEEE 802.11a physical packet structure as well as the functions of the various fields included in the packet were also given in this chapter.

In Chapter 3, we begun by analyzing the effects of synchronization errors on the received signal, namely the Symbol Timing Offset (STO) and the Carrier Frequency Offset (CFO), on the performance of the system via mathematical expressions. We then classified the synchronization methodologies and reviewed conventional synchronization designs for OFDM systems. Indeed, they are classified into Non Data-Aided (NDA) and Data-Aided (DA) synchronization techniques. The NDA techniques with no training sequence requirement have smaller performance but higher spectral efficiency than the DA ones. Simulations were finally realized to assess their performance.

In Chapter 4, we proposed time synchronization algorithms adapted to the wireless communication system based on the IEEE 802.11a standard. The motivation behind this work was to develop synchronization schemes taking advantages from both the NDA and DA techniques. To achieve this objective, in addition to using the preamble field as the reference sequence at the receiver, we exploited the SIGNAL field in physical packet and used it as a supplementary training sequence when the CSMA/CA medium reservation mechanism is triggered. Indeed the receiver exploits the SIGNAL field since its parts are known or predictable via the control frames RtS and CtS. Next, to take full advantage of the CSMA/CA mechanism, the channel state information obtained from the RtS control frame reception was also exploited for DATA physical packet synchronization. Finally, a new timing metric that minimizes the average of transmission error function over all channel estimation errors has been introduced to improve the fine estimation accuracy.

Inspired by the time synchronization results based on the CSMA/CA mechanism, in Chapter 5, we suggested two algorithms for the CFO estimation corresponding

to the use of the SIGNAL field and the channel information provided by the RtS frame. The MAP criterion was applied to increase the efficiency of the algorithms.

In Chapter 6, we investigated an efficient algorithm for both time and frequency synchronization. Investigations first focused on building a posterior function of the STO, CFO and channel coefficients based on the training sequence and SIGNAL field. These parameters were determined by maximizing the posterior function. To improve the timing estimation, a timing metric in frequency domain with presence of imperfect channel state information was added.

Tables 7.1, 7.2 and 7.3 summarize the methods as well as the type of data used in referred synchronization algorithms and all proposed ones in this thesis.

Globally, if one compares the performance of the proposed algorithms with the performance of the standard ones in the actual operating modes (shown as red boxes in almost all curves), one can see that the improvements certainly allow a huge extension of this operating mode towards smaller SNRs.

Constrained by the time frame of the Ph.D period, there are still some remaining and emerging synchronization problems in practical OFDM systems that have not been addressed in this thesis. A short but far from complete list of the problems that need to be investigated by future research are given below.

First, for the algorithms exploiting the SIGNAL field and channel information, the performance has just been improved under the condition that the CSMA/CA mechanism was active. I would be more interesting (and widely applicable) if we can make use of similar information without the activity of the CSMA/CA mechanism.

Second, the performance of the above algorithms was demonstrated only for the IEEE 802.11a standard system. It would be interesting to study their application under others standards as IEEE 802.11n, Long Term Evolution (LTE) 4G because each standard has its own training and header structure, a fact which can heavily impact our proposals.

Third, the metric that minimizes the average of transmission error function over all channel estimation errors has been only proposed for time synchronization. It is further possible to be exploited for frequency synchronization in estimating the integer part of the carrier frequency offset. And it is the new challenges that drive the advance of new technologies.

Finally, the performance of developed synchronization algorithms needs also to be measured in other terms as the sensitivity of frequency synchronization versus symbol timing estimation error, CFO estimation range, computational cost ...

Table 7.1. Referred and proposed algorithms for time synchronization

Stages \ Algorithms	**Canet** [16]	**LS** [94]	**MMSE** [87]	**SIGNAL-LS**	**SIGNAL-MMSE**	**SIGNAL-MAP**	**CE-SIGNAL-MAP**	**CE-SIGNAL-CEE**
Cross-correlation function using STF		**X**	**X**	**X**	**X**	**X**		
Cross-correlation function using estimated STF based on channel estimation using RTS frame							**X**	**X**
Cross-correlation function using SIGNAL				**X**	**X**	**X**	**X**	**X**
Auto-correlation function using STF	**X**							
Cross-correlation function using LTF	**X**							
Channel estimation based on LS using LTF		**X**		**X**				
Channel estimation based on MMSE using LTF			**X**		**X**			
Channel estimation based on MAP using LTF						**X**	**X**	
Timing metric using LTF in presence of channel estimation errors								**X**

Table 7.2. Referred and proposed algorithms for frequency synchronization

Algorithms / **Stages**	**Song** [84]	**Manusani** [57]	**Le-based MAP** [52]	**Le-based SIGNAL**	**FS-based CE**
Auto-correlation function using CP	**X**				
Auto-correlation function using STF		**X**	**X**	**X**	**X**
Auto-correlation function using LTF		**X**	**X**	**X**	**X**
Joint frequency offset and channel estimation based on MAP using LTF			**X**		
Joint frequency offset and channel estimation based on MAP using SIGNAL				**X**	
Metric exploiting channel estimation using RTS frame					**X**

Table 7.3. Referred and proposed algorithms for time and frequency synchronization

Algorithms / **Stages**	**Canet** [16]	**Joint MAP TS-FS**	**Joint MAP TS-FS added TM**
Auto-correlation function using STF	**X**	**X**	**X**
Auto-correlation function using LTF	**X**	**X**	**X**
Cross-correlation function using LTF	**X**		
Cross-correlation function using estimated STF based on channel estimation using RTS frame		**X**	**X**
Cross-correlation function using SIGNAL		**X**	**X**
Joint time and frequency offset estimation based on MAP using SIGNAL		**X**	**X**
Timing metric using LTF in presence of channel estimation errors			**X**

APPENDIX A

Auto-correlation and cross-correlation functions based-timing estimation comparison

In this part, we compare mathematically between the symbol timing estimations relied on auto- and cross-correlation functions.

Assuming that the received discrete baseband signal $r_\Delta(n)$ is given by

$$r_\Delta(n) = \sum_{i=0}^{L-1} h(i)x(n-i-\theta)e^{j\frac{2\pi\epsilon n}{N}} + g(n), \tag{A.1}$$

where θ is the symbol timing and ϵ is the normalized CFO.

For simplicity, the noise term $g(n)$ is ignored in the next stages, (A.1) is thus rewritten as follows:

$$r_\Delta(n) = \sum_{i=0}^{L-1} h(i)x(n-i-\theta)e^{j\frac{2\pi\epsilon(n-\theta)}{N}} \tag{A.2}$$

Let $c(n)$ be a known training sequence with period duration of N_P in general. It means that $c(n)$ may be the preamble specified by the standards or the training sequence proposed by authors.

A.1 Symbol timing estimation based on cross-correlation function

The symbol timing is estimated by

$$\hat{\theta} = \arg\max_d |Z(d)|. \tag{A.3}$$

where $Z(d)$ is the cross-correlation function between the received signal and the known sequence and given by

$$\begin{aligned} Z(d) &= \sum_{n=0}^{L_{\mathrm{W}}-1} c^*(n) r_{\Delta}(n+d) \\ &= \sum_{n=0}^{L_{\mathrm{W}}-1} \{\sum_{i=0}^{L-1} h(i) x(n-i-\theta+d) e^{j\frac{2\pi\epsilon(n+d)}{N}}\} c^*(n) \end{aligned} \tag{A.4}$$

where L_{W} is the computation window length.

If we only consider the first tap (as usual, the first tap has the biggest power), we have

$$Z(d) = \sum_{n=0}^{L_{\mathrm{W}}-1} \{h(0) x(n-\theta+d) e^{j\frac{2\pi\epsilon(n+d)}{N}}\} c^*(n) \tag{A.5}$$

It can be seen from (A.5) that when the index n is increased from 0 to L_{W}, the phase $\frac{2\pi\epsilon(n+d)}{N}$ is changed. Consequently, when n reaches a big value, the function $Z(d)$ is significantly effected by the frequency offset (i.e. ϵ).

A.2 Symbol timing estimation based on auto-correlation function

The symbol timing is estimated by

$$\hat{\theta} = \arg\max_{d} |Z(d)|. \tag{A.6}$$

where $Z(d)$ is the auto-correlation function between the received signal and itself delayed the period duration of the training sequence:

$$\begin{aligned} Z(d) &= \sum_{n=0}^{L_{\mathrm{W}}-1} r_{\Delta}^*(n+d) r_{\Delta}(n+d+N_{\mathrm{P}}) \\ &= \sum_{n=0}^{L_{\mathrm{W}}-1} \{\sum_{i=0}^{L-1} h(i) x(n-i-\theta+d) e^{j\frac{2\pi\epsilon(n+d)}{N}}\}^* \\ &\quad \{\sum_{i=0}^{L-1} h(i) x(n-i-\theta+d+N_{\mathrm{P}}) e^{j\frac{2\pi\epsilon(n+d+N_{\mathrm{P}})}{N}}\} \end{aligned} \tag{A.7}$$

Similar to Section A.1. We only consider the signal on the first tap:

$$\begin{aligned} Z(d) &= \sum_{n=0}^{L_{\mathrm{W}}-1} \{h(0) x(n-\theta+d) e^{j\frac{2\pi\epsilon(n+d)}{N}}\}^* \{h(0) x(n-\theta+d+N_{\mathrm{P}}) e^{j\frac{2\pi\epsilon(n+d+N_{\mathrm{P}})}{N}}\} \\ &= \sum_{n=0}^{L_{\mathrm{W}}-1} x^*(n-\theta+d) x(n-\theta+d+N_{\mathrm{P}}) e^{j\frac{2\pi\epsilon N_{\mathrm{P}}}{N}} \end{aligned} \tag{A.8}$$

In (A.8), the phase $\frac{2\pi\epsilon N_{\mathrm{P}}}{N}$ is independent from the index n. For the preamble as STF specified by the IEEE 802.11a standard, $N_{\mathrm{P}} = 16$ and $N = 64$, then $\frac{N_{\mathrm{P}}}{N} = 0.25$.

Consequently, the phase is reduced by a factor of 0.25. It means that when the auto-correlation function is used, the frequency offset is less effective on $Z(d)$ than the cross-correlation case.

Bibliography

[1] IEEE Standard for Local and Metropolitan Area Networks, Part 16: Air Interface for Fixed and Mobile Broadband Wireless Access Systems - Amendment 2: Physical and Medium access control layers for combined fixed and mobile operation in licensed bands and corigendum 1. URL `http://ieeexplore.ieee.org/xpl/mostRecentIssue.jsp?punumber=10676`.

[2] IEEE Standard 802.11a-1999(2003): Wireless LAN Medium Access Control (MAC) and Physical Layer (PHY) Specifications, 2003.

[3] IEEE P802.11n/D1.10 Wireless LAN Medium Access Control (MAC) and Physical Layer (PHY) specifications: Enhancements for Higher Throughput, Feb. 2007.

[4] Z. H. Abdzadeh and M. G. Shayesteh. Robust timing and frequency synchronization for OFDM systems. *Vehicular Technology, IEEE Transactions on*, 60(8):3646–3656, 2011.

[5] Z. H. Abdzadeh, M. G. Shayesteh, and M. Manaffar. An improved timing estimation method for OFDM systems. *Consumer Electronics, IEEE Transactions on*, 56(4): 2098–2105, 2010.

[6] E. Aboutanios and B. Mulgrew. Iterative frequency estimation by interpolation on Fourier coefficients. *Signal Processing, IEEE Transactions on*, 53(4):1237–1242, 2005.

[7] A. Al-Dweik, B. Sharif, and R. Shubair. Robust frequency offset estimator for OFDM with general constellation. *IET Electronic Letters*, 44:980–981, 2008.

[8] A. Al-Dweik, B. Sharif, and R. Shubair. Iterative frequency offset estimator for OFDM systems. *IET Communications*, 4:2008–2019, 2010.

[9] C. R. Athaudage. BER sensitivity of OFDM systems to time synchronization error. In *Communication Systems, 2002. ICCS 2002. The 8th International Conference on*, volume 1, pages 42–46. IEEE, 2002.

[10] A. B. Awoseyila, C. Kasparis, and B. G. Evans. Improved preamble-aided timing estimation for OFDM systems. *Communications Letters, IEEE*, 12(11):825–827, 2008.

[11] A. B. Awoseyila, C. Kasparis, and B. G. Evans. Robust time-domain timing and frequency synchronization for OFDM systems. *Consumer Electronics, IEEE Transactions on*, 55(2):391–399, 2009.

[12] M. Baker. LTE-Advanced physical layer. Technical report, 2009. URL `http://www.3gpp.org/ftp/workshop/2009-RIMT-Adveval/pdf/REV-09-r1.pdf`. Technical Report.

[13] V. M. Baronkin, Y. V. Zakharov, and T. C. Tozer. Maximum likelihood single tone frequency estimation in a multipath channel. *Communications, IEE Proceedings-*, 148(6):400–404, 2001. ISSN 1350-2425. doi: 10.1049/ip-com:20010632.

[14] N. Benvenuto and S. Tomasin. On the comparison between OFDM and single carrier modulation with a DFE using a frequency-domain feedforward filter. *Communications, IEEE Transactions on*, 50(6):947–955, 2002. ISSN 0090-6778. doi: 10.1109/TCOMM.2002.1010614.

[15] R. N. Braithwaite. Crest factor reduction for OFDM using selective subcarrier degradation. Technical report.

[16] M. J. Canet, V. Almenar, J. Marin-Roig, and J. Valls. Time synchronization for the IEEE 802.11a/g WLAN standard. In *Personal, Indoor and Mobile Radio Communications, 2007. PIMRC 2007. IEEE 18th International Symposium on*, pages 1–5, 2007. doi: 10.1109/PIMRC.2007.4394066.

[17] S. Chang and B. Kelley. Time synchronisation for OFDM-based WLAN systems. *Electronics Letters*, 39(13):1024–1026, 2003.

[18] N. Chen, M. Tanaka, and R. Heaton. OFDM timing synchronisation under multipath channels. In *Vehicular Technology Conference, 2003. VTC 2003-Spring. The 57th IEEE Semiannual*, volume 1, pages 378–382. IEEE, 2003.

[19] S. Chen and C. Zhu. ICI and ISI analysis and mitigation for OFDM systems with insufficient cyclic prefix in time-varying channels. *Consumer Electronics, IEEE Transactions on*, 50(1):78–83, 2004.

[20] P. Chevillat, D. Maiwald, and G. Ungerboeck. Rapid training of a voiceband data-modem receiver employing an equalizer with fractional-T spaced coefficients. *Communications, IEEE Transactions on*, 35(9):869–876, 1987.

[21] W. L. Chin and S. G. Chen. On the analysis of combined synchronization error effects in OFDM Systems. In *Vehicular Technology Conference, 2009. VTC Spring 2009. IEEE 69th*, pages 1 –5, april 2009. doi: 10.1109/VETECS.2009.5073724.

[22] Y. S. Cho, J. Kim, W. Y. Yang, and C. G. Kang. *MIMO-OFDM Wireless Communications with MATLAB*. John Wiley & Sons, 2010.

[23] F. Classen and H. Meyr. Frequency synchronization algorithms for OFDM systems suitable for communication over frequency selective fading channels. In *Vehicular Technology Conference, 1994 IEEE 44th*, pages 1655–1659 vol.3, 1994. doi: 10.1109/VETEC.1994.345377.

[24] W. Cochran, J. Cooley, D. Favin, H. Helms, R. Kaenel, W. Lang, G. Jr. Maling, D. Nelson, C. Rader, and P. Welch. What is the fast Fourier transform? *Audio and Electroacoustics, IEEE Transactions on*, 15(2):45 – 55, Jun. 1967. ISSN 0018-9278. doi: 10.1109/TAU.1967.1161899.

[25] J. W. Cooley and J. W. Tukey. An algorithm for the machine calculation of complex fourier series. *Mathematics of Computation*, 19(90):pp. 297–301, 1965. ISSN 00255718. URL `http://www.jstor.org/stable/2003354`.

[26] A. J. Coulson. Maximum likelihood synchronization for OFDM using a pilot symbol: algorithms. *Selected Areas in Communications, IEEE Journal on*, 19(12):2486–2494, 2001. ISSN 0733-8716. doi: 10.1109/49.974613.

[27] A. Czylwik. Synchronization for single carrier modulation with frequency domain equalization. In *Vehicular Technology Conference, 1998. VTC 98. 48th IEEE*, volume 3, pages 2277–2281. IEEE, 1998.

[28] A. Doufexi, S. Armour, M. Butler, A. Nix, D. Bull, J. McGeehan, and P. Karlsson. A comparison of the HIPERLAN/2 and IEEE 802.11a wireless LAN standards. *Communications Magazine, IEEE*, 40(5):172–180, May 2002. ISSN 0163-6804. doi: 10.1109/35.1000232.

[29] M. Ergen and P. Varaiya. Throughput analysis and admission control for IEEE 802.11 a. *Mobile networks and Applications*, 10(5):705–716, 2005.

[30] Norme ETSI. Channel models for HIPERLAN/2 in different indoor scenarios. Technical report, 1998. URL `https://www.zotero.org/wayne.hanwei/items/itemKey/R72HREIN`.

[31] K. Fazel and S. Kaiser. *Multi-carrier and spread spectrum systems: from OFDM and MC-CDMA to LTE and WiMAX*. John Wiley and Sons, 2008.

[32] M. Gast. 802.11 Wireless Networks: The Definitive Guide, (Definitive Guide). 2005.

[33] F. R. Gfeller and W. Hirt. Method for improved wireless optical communication and frames for use in a wireless optical communication system, Nov. 2003. US Patent 6,643,469.

[34] L. Hanzo, C. H. Wong, and M. S. Yee. *Adaptive wireless transceivers: Turbo-Coded, Turbo-Equalised and Space-Time Coded TDMA, CDMA and OFDM systems*. John Wiley & Sons, 2002.

[35] M. Heinrich, M. Marc, and F. Stefan. *Digital Communication Receivers: Synchronization, Channel Estimation, and Signal Processing*. John Wiley & Sons, Inc., New York, NY, USA, 1997. ISBN 0471502758.

[36] S. R. Herlekar, C. Zhang, H. C. Wu, A. Srivastava, and Y. Wu. OFDM performance analysis in the phase noise arising from the hot-carrier effect. *Consumer Electronics, IEEE Transactions on*, 52(3):757–765, 2006.

[37] G. Holland, N. Vaidya, and P. Bahl. A rate-adaptive MAC protocol for multi-hop wireless networks. In *Proceedings of the 7th annual international conference on Mobile computing and networking*, pages 236–251. ACM, 2001.

[38] T. Hwang, C. Yang, G. Wu, S. Li, and G. Y. Li. OFDM and Its Wireless Applications: A Survey. *Vehicular Technology, IEEE Transactions on*, 58(4):1673–1694, 2009. ISSN 0018-9545. doi: 10.1109/TVT.2008.2004555.

[39] S. Jagannathan, H. Aghajan, and A. Goldsmith. The effect of time synchronization errors on the performance of cooperative MISO systems. In *Global Telecommunications Conference Workshops, 2004. GlobeCom Workshops 2004. IEEE*, pages 102–107. IEEE, 2004.

[40] W. C. Jakes. Microwave mobile communications. 1975.

[41] J. Jansons, A. Ipatovs, and E. Petersons. Estimation of Doppler Shift for IEEE 802.11 g Standard. In *Baltic Conference Advanced Topics in Telecommunication, University of Rostock*, pages 73–82, 2009.

[42] L. Jian, L. Guoqing, and G. B. Giannakis. Carrier frequency offset estimation for OFDM-based WLANs. *Signal Processing Letters, IEEE*, 8(3):80 –82, march 2001. ISSN 1070-9908. doi: 10.1109/97.905946.

[43] Y. Kang, S. Kim, D. Ahn, and H. Lee. Timing estimation for OFDM systems by using a correlation sequence of preamble. *Consumer Electronics, IEEE Transactions on*, 54(4):1600–1608, 2008.

[44] S. M. Kay. *Fundamentals of Statistical signal processing, Volume 2: Detection theory*. Prentice Hall PTR, 1998.

[45] T. Keller and L. Hanzo. Adaptive multicarrier modulation: A convenient framework for time-frequency processing in wireless communications. *Proceedings of the IEEE*, 88(5):611–640, 2000.

[46] D. Kim and G. L. Stuber. Residual ISI cancellation for OFDM with applications to HDTV broadcasting. *Selected Areas in Communications, IEEE Journal on*, 16(8): 1590–1599, 1998.

[47] J. J. Kim, Y. J. Ryu, H. S. Oh, and D. S. Han. Frame selection algorithm with adaptive FFT input for OFDM systems. In *Communications, 2002. ICC 2002. IEEE International Conference on*, volume 1, pages 187–191. IEEE, 2002.

[48] S. Kim, D. Chong, S. Y. Kim, and S. Yoon. A Novel Periodogram-Based Frequency Offset Estimation Method for OFDM Systems.

[49] S. Kinjo. An MMSE channel estimation algorithm based on the conjugate gradient method for OFDM systems. In *The 23rd International Technical Conference on Circuits/Systems, Computers and Communications*, 2008.

[50] M. Kornfeld. DVB-H-the emerging standard for mobile data communication. In *Consumer Electronics, 2004 IEEE International Symposium on*, pages 193–198. IEEE, 2004.

[51] T. L. Kung and K. K. Parhi. Frequency domain symbol synchronization for OFDM systems. In *Electro/Information Technology (EIT), 2011 IEEE International Conference on*, pages 1–5, 2011. doi: 10.1109/EIT.2011.5978592.

[52] H. N. Le and N. T. Le. Pilot-aided joint CFO and doubly-selective channel estimation for OFDM transmissions. *Broadcasting, IEEE Transactions on*, 56(4):514–522, 2010. ISSN 0018-9316. doi: 10.1109/TBC.2010.2055673.

[53] J. Lei and T. S. Ng. Periodogram-based carrier frequency offset estimation for Orthogonal Frequency Division Multiplexing applications. In *Global Telecommunications Conference, 2001. GLOBECOM'01. IEEE*, volume 5, pages 3070–3074. IEEE, 2001.

[54] D. Li, Y. Li, H. Zhang, and L. Wang. Cross ambiguity function based integer frequency offset estimation for OFDM systems. In *Wireless Communications and Networking Conference (WCNC), 2012 IEEE*, pages 1065–1069. IEEE, 2012.

[55] Z. Li, A. Das, A. K. Gupta, and S. Nandi. Full auto rate MAC protocol for wireless ad hoc networks. *Communications, IEE Proceedings-*, 152(3):311–319, 2005. ISSN 1350-2425. doi: 10.1049/ip-com:20041022.

[56] R. Love, R. Kuchibhotla, A. Ghosh, R. Ratasuk, B. Classon, and Y. Blankenship. Downlink control channel design for 3GPP LTE. In *Wireless Communications and Networking Conference, 2008. WCNC 2008. IEEE*, pages 813–818. IEEE, 2008.

[57] S. K. Manusani, R. S. Kshetrimayum, and R. Bhattacharjee. Robust time and frequency synchronization in OFDM based 802.11a WLAN systems. In *India Conference, 2006 Annual IEEE*, pages 1–4, 2006. doi: 10.1109/INDCON.2006.302775.

[58] H. Minn, M. Zeng, and V. K. Bhargava. On timing offset estimation for OFDM systems. *Communications Letters, IEEE*, 4(7):242–244, 2000. ISSN 1089-7798. doi: 10.1109/4234.852929.

[59] H. Minn, V. K. Bhargava, and K. B. Letaief. A robust timing and frequency synchronization for OFDM systems. *Wireless Communications, IEEE Transactions on*, 2(4):822–839, 2003.

[60] P. H. Moose. A technique for Orthogonal Frequency Division Multiplexing frequency offset correction. *Communications, IEEE Transactions on*, 42(10):2908–2914, 1994. ISSN 0090-6778. doi: 10.1109/26.328961.

[61] M. Morelli and U. Mengali. An improved frequency offset estimator for OFDM applications. In *Communication Theory Mini-Conference, 1999*, pages 106–109. IEEE, 1999.

[62] Y. Mostofi and D. C. Cox. Analysis of the effect of timing synchronization errors on pilot-aided OFDM systems. In *Signals, Systems and Computers, 2003. Conference Record of the Thirty-Seventh Asilomar Conference on*, volume 1, pages 638–642. IEEE, 2003.

[63] Y. Mostofi and D. C. Cox. Mathematical analysis of the impact of timing synchronization errors on the performance of an OFDM system. *Communications, IEEE Transactions on*, 54(2):226–230, 2006.

[64] R. V. Nee and R. Prasad. *OFDM for wireless multimedia communications*. Artech House, Inc., 2000.

[65] M. Pätzold and J. Wiley. *Mobile fading channels*. John Wiley, 2002.

[66] J. P. Pavon and S. Choi. Link adaptation strategy for IEEE 802.11 WLAN via received signal strength measurement. In *Communications, 2003. ICC'03. IEEE International Conference on*, volume 2, pages 1108–1113. IEEE, 2003.

[67] F. Peng and W. E. Ryan. Low-complexity soft demapper for OFDM fading channels with ICI. In *Wireless Communications and Networking Conference, 2006. WCNC 2006. IEEE*, volume 3, pages 1549–1554. IEEE, 2006.

[68] P. Piantanida, S. Sadough, and P. Duhamel. On the outage capacity of a practical decoder accounting for channel estimation inaccuracies. *Communications, IEEE Transactions on*, 57(5):1341–1350, 2009.

[69] T. Pollet. BER sensitivity of OFDM systems to carrier frequency offset and Wiener phase noise. *IEEE Trans. Commun.*, 43(2), 1995.

[70] B. Y. Prasetyo, F. Said, and A. H. Aghvami. Fast burst synchronisation technique for OFDM-WLAN systems. *Communications, IEE Proceedings-*, 147(5):292–298, 2000. ISSN 1350-2425. doi: 10.1049/ip-com:20000612.

[71] J. Proakis. *Digital Communications*. McGraw-Hill Science/Engineering/Math, 4 edition, August 2000. ISBN 0072321113.

[72] T. S. Rappaport. *Wireless communications: principles and practice*, volume 2. Prentice Hall PTR New Jersey, 1996.

[73] U. Reimers. Digital video broadcasting. *Communications Magazine, IEEE*, 36(6): 104–110, 1998.

[74] G. Ren, Y. Chang, H. Zhang, and H. Zhang. Synchronization methods based on a new constant envelope preamble for OFDM systems. *IEEE Transactions on Broadcasting*, 51(1):139–143, 2005.

[75] G. Ren, Y. Chang, H. Zhang, and H. Zhang. An efficient frequency offset estimation method with a large range for wireless OFDM systems. *Vehicular Technology, IEEE Transactions on*, 56(4):1892–1895, 2007.

[76] M. Ruan. *Timing and Frequency Synchronization in Practical OFDM Systems*. PhD thesis, 2009. URL `http://hdl.handle.net/1885/49339` `http://digitalcollections.anu.edu.au/handle/1885/49339`.

[77] B. Sadeghi, V. Kanodia, A. Sabharwal, and E. Knightly. Opportunistic media access for multirate Ad-hoc networks. In *Proceedings of the 8th annual international conference on Mobile computing and networking*, pages 24–35. ACM, 2002.

[78] M. Sandell, J. J. Van de Beek, and P. O. Borjesson. Timing and frequency synchronization in OFDM systems using the cyclic prefix. In *in Proc. Int. Symp. Synchronization*, pages 16–19, 1995.

[79] H. Sari, G. Karam, and I. Jeanclaude. Transmission techniques for digital terrestrial tv broadcasting. *Communications Magazine, IEEE*, 33(2):100–109, Feb 1995. ISSN 0163-6804. doi: 10.1109/35.350382.

[80] T. M. Schmidl and D. C. Cox. Low-overhead, low-complexity [burst] synchronization for OFDM. In *Communications, 1996. ICC '96, Conference Record, Converging Technologies for Tomorrow's Applications. 1996 IEEE International Conference on*, volume 3, pages 1301–1306 vol.3, 1996. doi: 10.1109/ICC.1996.533620.

[81] T. M. Schmidl and D. C. Cox. Robust frequency and timing synchronization for OFDM. *Communications, IEEE Transactions on*, 45(12):1613–1621, December 1997. ISSN 0090-6778. doi: 10.1109/26.650240. URL `http://dx.doi.org/10.1109/26.650240`.

[82] C. Shin, J. G. Andrews, and E. J. Powers. An efficient design of doubly selective channel estimation for OFDM systems. *Wireless Communications, IEEE Transactions on*, 6(10):3790–3802, 2007.

[83] H. C. So, Y. T. Chan, Q. Ma, and P. C. Ching. Comparison of various periodograms for sinusoid detection and frequency estimation. *Aerospace and Electronic Systems, IEEE Transactions on*, 35(3):945–952, 1999.

[84] H. K. Song, Y. H. You, J. H. Paik, and Y. S. Cho. Frequency-offset synchronization and channel estimation for OFDM-based transmission. *Communications Letters, IEEE*, 4(3):95 –97, march 2000. ISSN 1089-7798. doi: 10.1109/4234.831036.

[85] M. Speth, F. Classen, and H. Meyr. Frame synchronization of OFDM systems in frequency selective fading channels. In *Vehicular Technology Conference, 1997, IEEE 47th*, volume 3, pages 1807 –1811 vol.3, may 1997. doi: 10.1109/VETEC.1997.605870.

[86] M. Speth, S. A. Fechtel, G. Fock, and H. Meyr. Optimum receiver design for wireless broad-band systems using OFDM. I. *Communications, IEEE Transactions on*, 47 (11):1668–1677, 1999.

[87] V. Srivastava, C. K. Ho, P. H. W. Fung, and S. Sun. Robust MMSE channel estimation in OFDM systems with practical timing synchronization. In *Wireless Communications and Networking Conference, 2004. WCNC. 2004 IEEE*, volume 2, pages 711–716. IEEE, 2004.

[88] H. Steendam and M. Moeneclaey. Sensitivity of Orthogonal Frequency-Division Multiplexed systems to carrier and clock synchronization errors. *Signal processing*, 80(7):1217–1229, 2000.

[89] G. L. Stuber, J. R. Barry, S. W. Mclaughlin, Y. Li, M. A. Ingram, and T. G. Pratt. Broadband MIMO-OFDM wireless communications. *Proceedings of the IEEE*, 92 (2):271–294, 2004.

[90] Ph. J. Tourtier, R. Monnier, and P. Lopez. Multicarrier modem for digital HDTV terrestrial broadcasting. *Signal processing: Image communication*, 5(5):379–403, 1993.

[91] J. J. Van de Beek, M. Sandell, M. Isaksson, and P. O. Borjesson. Low-complex frame synchronization in OFDM systems. In *Universal Personal Communications. 1995. Record., 1995 Fourth IEEE International Conference on*, pages 982 –986, nov 1995. doi: 10.1109/ICUPC.1995.497156.

[92] J. J. Van de Beek, M. Sandell, and P. O. Borjesson. ML estimation of time and frequency offset in OFDM systems. *Signal Processing, IEEE Transactions on*, 45 (7):1800–1805, 1997.

[93] H. L. Van Trees and K. L. Bell. *Bayesian bounds for parameter estimation and nonlinear filtering/tracking*. IEEE press, 2007.

[94] K. Wang, M. Faulkner, and J. Sing. Timing synchronization for 802.11a WLANs under multipath channels. In *Vehicular Technology Conference, 2008. VTC 2008-Fall. IEEE 68th*, pages 1–5, 2003. doi: ATNAC'03.

[95] S. Wang and A. Abdi. Joint singular value distribution of two correlated rectangular Gaussian matrices and its application. *SIAM J. Matrix Anal. Appl.*, 29 (3):972–981, October 2007. ISSN 0895-4798. doi: 10.1137/060652907. URL `http://dx.doi.org/10.1137/060652907`.

[96] Y. C. Wu, K. W. Yip, T. S. Ng, and E. Serpedin. Impacts of multipath fading on the timing synchronization of IEEE802.11a wireless LANs. *Presented at IEEE ICC'02*, 2002.

[97] Y. C. Wu, K. W. Yip, T. S. Ng, and E. Serpedin. Maximum-likelihood symbol synchronization for IEEE 802.11 a WLANs in unknown frequency-selective fading channels. *Wireless Communications, IEEE Transactions on*, 4(6):2751–2763, 2005.

[98] Y. Yao and G. B. Giannakis. Blind carrier frequency offset estimation in SISO, MIMO, and multiuser OFDM systems. *Communications, IEEE Transactions on*, 53(1):173–183, 2005.

[99] S. Younis. *Synchronization Algorithms and Architectures for Wireless OFDM Systems.* PhD thesis, 2012. URL `https://theses.ncl.ac.uk/dspace/bitstream/10443/1417/1/Younis12.pdf`.

[100] T. Yucek, R. M. Tannious, and H. Arslan. Doppler spread estimation for wireless OFDM systems. In *Advances in Wired and Wireless Communication, 2005 IEEE/Sarnoff Symposium on*, pages 233–236. IEEE, 2005.

[101] H. K. Yun, S. Iickho, Y. Seokho, and R. P. So. An efficient frequency offset estimator for OFDM systems and its performance characteristics. *IEEE Transactions on Vehicular Technology*, 50:1307–1312, 2001.

[102] X. Zeng and A. Ghrayeb. A blind carrier frequency offset estimation scheme for OFDM systems with constant modulus signaling. *Communications, IEEE Transactions on*, 56(7):1032–1037, 2008.

[103] Y. Zhang, J. Zhang, and M. Xia. Joint timing synchronization and channel estimation for OFDM systems via MMSE criterion. In *Vehicular Technology Conference, 2008. VTC 2008-Fall. IEEE 68th*, pages 1–4, 2008. doi: 10.1109/VETECF.2008.239.

Résumé en Français

Le problème de la synchronisation en temps et en fréquence dans un système de transmission OFDM (Orthogonal Frequency Division Multiplexing) sans fil de type IEEE 802.11a est étudié. Afin d'améliorer la synchronisation de trame entre les stations mobiles, bien que des solutions aient déjà été proposées pour compenser les décalages en temps et en fréquence, nous avons développé une nouvelle approche conforme à la norme IEEE 802.11a. Cette approche exploite non seulement les informations habituellement spécifiées par la norme à savoir les séquences d'apprentissage mais également d'autres sources d'informations disponibles au niveau de la couche physique et par ailleurs connues par l'émetteur et le récepteur qui les exploitera. Tenant compte des informations fournies par les protocoles réseaux, nous avons montré que les différents sous-champs du champ SIGINAL de la trame physique, identifié comme séquence de référence, sont connus ou prédictibles à partir des deux trames de contrôle RTS (Request to Send) et CtS (Clear to Send) lorsque le mécanisme de réservation de support CSMA/CA (Transporteur Sense Multiple Access avec évitement de collision) est activé conjointement à des algorithmes d'adaptation de débit binaire sur le canal. De plus, la trame RTS reçue permet au récepteur d'estimer le canal avant d'entamer l'étape de synchronisation. Tenant compte de la connaissance sur le champ SIGNAL et de l'information sur le canal de transmission, nous avons développé plusieurs algorithmes conjoints de synchronisation temporelle et fréquentielle et d'estimation de canal compatible avec la norme 802.11a. Les résultats de simulation montrent une amélioration conséquente des performances en termes de probabilité d'échec de synchronisation en comparaison avec les algorithmes existants.

Titre en Anglais

ROBUST TIME AND FREQUENCY SYNCHRONIZATION IN 802.11a COMMUNICATION WIRELESS SYSTEM

Résumé en Anglais

Time and frequency synchronization problem in the IEEE 802.11a OFDM (Orthogonal Frequency Division Multiplexing) wireless communication system is investigated. To enhance the frame synchronization between mobile stations, although solutions to compensate time and frequency offsets have already been proposed, we developed a new approach conform to the IEEE 802.11a standard. This approach exploits not only the reference information usually specified by the standard such as training sequences but also additional sources of information available at the physical layer further known by both the transmitter and receiver to be then exploited. According to the knowledge protocol, we showed that the parts of the identified SIGNAL field considered as a reference sequence of the physical frame are either known or predictable from the RtS (Request to Send) and CtS (Clear to Send) control frames when the CSMA/CA (Carrier Sense Multiple Access with Collision Avoidance) mechanism is triggered jointly to bit-rate adaptation algorithms to the channel. Moreover the received RtS control frame allows the receiver to estimate the channel before synchronization stage. According to the knowledge of the SIGNAL field and the channel information, we developed multistage joint time\frequency synchronization and channel estimation algorithms conform to the standard. Simulation results showed a strongly improved performance in terms of synchronization failure probability in comparison with the existing algorithms.

Mots-Clefs

IEEE 802.11a	**OFDM**	**RtS**	**Time Synchronization**
Communications	**CSMA/CA**	**CtS**	**Frequency Synchronization**

Discipline

SIGNAUX ET IMAGES

LABORATOIRE DE TRAITEMENT ET TRANSPORT DE L'INFORMATION – L2TI – EA3043